THESIS FOR THE DEGREE OF DOCTOR OF PHILOSOPHY

# The Release, Distribution, and Implications of Alkalis in Chemical Looping Combustion of Biomass

IVAN GOGOLEV

Department of Space, Earth and Environment

CHALMERS UNIVERSITY OF TECHNOLOGY

Gothenburg, Sweden 2022

**The Release, Distribution, and Implications of Alkalis in Chemical Looping Combustion of Biomass**

IVAN GOGOLEV
ISBN: 978-91-7905-715-2



Department of Space, Earth and Environment
Division of Energy Technology
Chalmers University of Technology
SE-412 96 Gothenburg
Sweden
Telephone + 46 (0)31-772 5252

Printed by Chalmers Reproservice
Gothenburg, Sweden 2022

# The Release, Distribution, and Implications of Alkalis in Chemical Looping Combustion of Biomass

IVAN GOGOLEV
Division of Energy Technology
Department of Space, Earth and Environment
Chalmers University of Technology

## Abstract

Chemical looping combustion (CLC) of biomass is a promising technology for power generation with a potential net negative $CO_2$ footprint. Like other fluidized bed biomass conversion technologies, biomass CLC may be susceptible to alkali-induced agglomeration, fouling, and corrosion. The mechanisms, distribution, and implications of alkali release in CLC systems presents a significant knowledge gap that is critical for upscaling and commercialization of biomass CLC.

To investigate gas-phase alkali release in CLC, a CLC-specific surface ionization detector (SID) measurement system was developed. This system was validated in Papers V and VI against two independent alkali measurement techniques. Alkali emissions were measured in four experimental campaigns using three different CLC pilots, four oxygen carriers (OC), and nine different biomass fuels. The SID-based emissions measurements showed that up to 17% of the fuel alkalis are released to the gas phase of the fuel reactor (FR), and up to 7% to the air reactor (AR). Thermodynamic modelling of alkali release, and chemical analysis of flue gas alkalis indicated that gaseous FR alkalis are dominated by KOH(g) and KCl(g). FR alkali emissions levels were found to rise with temperature and steam concentration. Two key alkali release processes were identified: 1) sublimation of KCl(s) to KCl(g), and 2) decomposition of alkali salts, such as $K_2CO_3$, to yield KOH(g). It was determined that higher temperature accelerates both of these processes, while steam enables and accelerates the second path. AR emissions were independent of temperature and other operating parameters within the performed tests. Experimental evidence suggests that AR emissions occur via carryover of char from the FR to AR. Ash-bound and OC-bound carryover mechanisms were also proposed, but could not be experimentally validated. Modelling of alkali release and AR fly ash chemical analyses suggest that AR emissions are essentially KCl-free. Alkali retention in condensed phases was found to be >77%, with OC alkali uptake accounting for approx. 30%. A balance on potassium in the 10 kW pilot indicated that up to 60% of fuel alkalis can be elutriated from the FR as solid ash particles, while AR fly ash accounted for up to 3% of fuel alkalis.

Biomass CLC experiments indicate that alkali release behavior does not constrain the fuel conversion and carbon capture performance of CLC systems. Furthermore, CLC technology offers inherent advantages for conversion of high alkali biomass. The key advantage is that the low corrosion potential of the AR flue gases should allow for higher steam temperatures, and thus more efficient operation of the main process heat exchangers in the AR. Further work is needed to evaluate long-term effects of alkali release on OC performance.

**Keywords**: chemical looping combustion, alkali release, biomass, carbon capture

# ACKNOWLEDGEMENTS

I would like to thank Professor Anders Lyngfelt, Professor Tobias Mattisson, and an associate Professor Carl Linderholm for creating the opportunity for my participation in the ash chemistry project, and for creating a truly impressive experimental research infrastructure at the Energiteknik laboratory.

I would like to thank Professor Lyngfelt for his feedback on my work and papers, for his trust and respect. Despite facing several difficult situations on my PhD journey, I found Professor Lyngfelt's support to be unwavering. Thank you for your patience!

I would like to thank Associate Professor Carl Linderholm for his efforts in helping me find my way at the division and for his feedback on my scientific work. Thank you for trying to understand my viewpoints and personality traits.

I would like to express a special thank you to Associate Professor Pavleta Knutsson for joining my supervision team. Thank you for providing me the much-needed support and motivation. Thank you for the scientific and career development discussions.

I would like to thank Dr. Dan Gall for his initial guidance on using the SID instrumentation. It has been a pleasure to work with Dan in the lab and while co-authoring publications.

I would like to thank Dr. Amir Soleimanisalim for being the best office mate, colleague, and collaborator. Working with Amir has been a pleasure and a privilege.

I would like to thank Ulf Stenman for his dedication to helping me and other PhD students achieve success in our experimental work. Ulf is a true professional and a wonderful colleague.

I would like to thank Rustan Hvitt for his support in fabrication of experimental equipment, for always being there to help, and for being a wonderful colleague.

I would like to thank the very important dynamic duo, Marie Iwanow and Katarina Bergkvist, for providing endless support and guidance in pretty much everything. You truly create a professional, caring, and supportive environment at Energiteknik.

I would also like to thank my colleagues Sofia, Jesper, Matthias, Patrick, Daofeng, the three Viktors, Fredrick, Ivana, Nasrin, Felicia, Xiaoyun, Marianne and other members of the CLC and Energiteknik family for your collaboration and companionship.

I would like to thank my parents for raising me to value education and to have the confidence to pursue my dreams. Thank you for supporting me throughout my PhD and for accepting my temporary relocation abroad.

Last but most, I would like to sincerely thank my sambo Maria Kandaurova. Thank you for being brave and taking on the challenge of moving to Sweden. Thank you for your support and care throughout the difficult moments.

I would like to acknowledge Natural Sciences and Engineering Research Council of Canada for the generous NSERC PGS-D scholarship that supported me in my PhD studies.

I would like to acknowledge the funding from the Swedish Research Council, project “Biomass combustion chemistry with oxygen carriers”, contract 2016-06023, and the Swedish Energy Agency (grant number P43936-1) via the OxyCar-FBC project, which is a project performed within the framework of ERA-NET Bioenergy. Rebuild of 10 kW unit was supported by Carl Tryggers Stiftelse, contract CTS 14:285.

# List of Publications Included in the Thesis

This thesis is based on the following six appended papers:

I. Gogolev, Ivan, Carl Linderholm, Dan Gall, Matthias Schmitz, Tobias Mattisson, Jan BC Pettersson, and Anders Lyngfelt. "Chemical-looping combustion in a 100 kW unit using a mixture of synthetic and natural oxygen carriers–Operational results and fate of biomass fuel alkali." *International Journal of Greenhouse Gas Control* 88 (2019): 371-382.

II. Gogolev, Ivan, Amir H. Soleimanisalim, Carl Linderholm, and Anders Lyngfelt. "Commissioning, performance benchmarking, and investigation of alkali emissions in a 10 $kW_{th}$ solid fuel chemical looping combustion pilot." *Fuel* 287 (2021): 119530.

III. Gogolev, Ivan, Toni Pikkarainen, Juho Kauppinen, Carl Linderholm, Britt-Marie Steenari, and Anders Lyngfelt. "Investigation of biomass alkali release in a dual circulating fluidized bed chemical looping combustion system." *Fuel* 297 (2021): 120743.

IV. Gogolev, Ivan, Amir H. Soleimanisalim, Daofeng Mei, and Anders Lyngfelt. "Effects of temperature, operation mode, and steam concentration on alkali release in chemical looping conversion of biomass– experimental investigation in a 10 kWth pilot." *Energy & Fuels* (2022).

V. Gogolev, Ivan, Toni Pikkarainen, Juho Kauppinen, Markus Hurskainen, and Anders Lyngfelt. "Alkali emissions characterization in chemical looping combustion of wood, wood char, and straw fuels." *Fuel Processing Technology* 237 (2022): 107447.

VI. Gall, Dan, Jan Viljanen, Ivan Gogolev, Thomas Allgurén, and Klas Andersson. "Alkali monitoring of industrial process gas by surface ionization – calibration, assessment, and comparison to in-situ laser diagnostics." *Energy & Fuels* 35, no. 24 (2021): 20160-20171.

# Paper I-VI Contribution Summary

| Author/Coauthor | Paper I | | | | | | | | Paper II | | | | | | | | Paper III | | | | | | | |
|---|---|---|---|---|---|---|---|---|---|---|---|---|---|---|---|---|---|---|---|---|---|---|---|---|
| | Experimental Design | Experimental Setup | Experiment Execution | Data Collection | Data Proc. & Eval. | Manuscript Authorship | Manuscript Review | Manuscript Editing | Experimental Design | Experimental Setup | Experiment Execution | Data Collection | Data Proc. & Eval. | Manuscript Authorship | Manuscript Review | Manuscript Editing | Experimental Design | Experimental Setup | Experiment Execution | Data Collection | Data Proc. & Eval. | Manuscript Authorship | Manuscript Review | Manuscript Editing |
| **Ivan Gogolev** | p | p | p | p | p | p | p | p | p | p | p | p | p | p | p | p | s | p | p | p | p | p | p | p |
| Carl Linderholm | s | s | s | | | s | | s | | | | | | s | | s | | | | | | | | s |
| Dan Gall | s | s | s | s | | | | | | | | | | | | | | | | | | | | |
| Matthias Schmitz | | | s | | | | | | | | | | | | | | | | | | | | | |
| Tobias Mattisson | | | | | | | | s | | | | | | | | | | | | | | | | |
| Jan Pettersson | | | | | | | | s | | | | | | | | | | | | | | | | |
| Anders Lyngfelt | s | | | | | | | s | | | | | s | s | | s | | | | | | | | s |
| Amir Soleimani Salim | | | | | | | | | | | s | | | | | | | | | | | | | |
| Toni Pikkarainen | | | | | | | | | | | | | | | | | p | | | s | | | | |
| Juho Kauppinen | | | | | | | | | | | | | | | | | s | | | s | | | | |
| Britt-Marie Steenari | | | | | | | | | | | | | | | | | | | | | | | s | |

| Author/Coauthor | Paper IV | | | | | | | | Paper V | | | | | | | | Paper VI | | | | | | | |
|---|---|---|---|---|---|---|---|---|---|---|---|---|---|---|---|---|---|---|---|---|---|---|---|---|
| | Experimental Design | Experimental Setup | Experiment Execution | Data Collection | Data Proc. & Eval. | Manuscript Authorship | Manuscript Review | Manuscript Editing | Experimental Design | Experimental Setup | Experiment Execution | Data Collection | Data Proc. & Eval. | Manuscript Authorship | Manuscript Review | Manuscript Editing | Experimental Design | Experimental Setup | Experiment Execution | Data Collection | Data Proc. & Eval. | Manuscript Authorship | Manuscript Review | Manuscript Editing |
| **Ivan Gogolev** | p | p | p | p | p | p | p | p | p | p | p | p | p | p | p | p | s | p | p | p | p | s | s | s |
| Anders Lyngfelt | s | | | | | | s | | | | | | | | s | | | | | | | | | |
| Amir Soleimani Salim | s | | s | | | | s | | | | | | | | | | | | | | | | | |
| Daofeng Mei | | | s | | | | s | | | | | | | | | | | | | | | | | |
| Toni Pikkarainen | | | | | | | | | p | | | | | | s | | | | | | | | | |
| Juho Kauppinen | | | | | | | | | | p | p | p | p | | s | | | | | | | | | |
| Markus Hurskainen | | | | | | | | | | | | | s | | s | | | | | | | | | |
| Dan Gall | | | | | | | | | | | | | | | | | p | p | p | p | p | p | p | p |
| Jan Viljanen | | | | | | | | | | | | | | | | | p | p | p | p | s | s | s | |
| Thomas Allguren | | | | | | | | | | | | | | | | | s | | s | | | | s | |
| Klas Andersson | | | | | | | | | | | | | | | | | s | | | | | | s | |

**LEGEND:**

p - primary contributor
s - supporting contributor

## Other related contributions that are not included in this thesis:

- Ivan Gogolev and Anders Lyngfelt. "Biomass chemical looping combustion – the interdependence of alkali release, performance, and operability." 6th International Conference on Chemical Looping (2022), Zaragoza, Spain

- Ivan Gogolev and Anders Lyngfelt. "Fate and operational implications of alkalis in chemical looping combustion of biomass – summary and discussion of recent pilot experiment results." The 24th Fluidized Bed Conversion Conference (2022), Gothenburg, Sweden

- Ivan Gogolev, Carl Linderholm, Dan Gall, Matthias Schmitz, Tobias Mattisson, Jan BC Pettersson, and Anders Lyngfelt. "Chemical-looping combustion in a 100 kW unit using a mixture of synthetic and natural oxygen carriers – operational results and fate of biomass fuel alkali." 5th International Conference on Chemical Looping (2018), Park City, Utah, USA

- Daofeng Mei, Ivan Gogolev, Fredrik Hildor, Anders Lyngfelt, Tobias Mattisson. "Investigation of LD-Slag oxygen carrier for CLC and OCAC in a 10 kW unit using high-volatile biomass." 6th International Conference on Chemical Looping (2022), Zaragoza, Spain

- Amir H. Soleimanisalim, Fredrik Hildor, Daofeng Mei, Ivan Gogolev, Tobias Mattisson. "Selection of oxygen carrier for chemical looping gasification of biomass." The 24th Fluidized Bed Conversion Conference (2022), Gothenburg, Sweden

# Table of Contents

1. Introduction ..... 1
1.1 Motivation ..... 1
1.2 Aim and scope of this thesis ..... 2
1.3 Contribution of the published papers to this thesis ..... 3
1.4 Outline of this thesis ..... 4
2. Background ..... 5
2.1 Chemical Looping Combustion (CLC) Principle ..... 5
2.2 Chemical Looping Combustion Fuels ..... 6
2.2.1 Gaseous Fuels ..... 6
2.2.2 Solid Fuels ..... 6
2.2.3 Biomass Solid Fuels ..... 8
2.3 Oxygen Carriers ..... 9
2.3.1 Manufactured Materials ..... 9
2.3.2 Low-Cost Materials ..... 10
2.3.3 Oxygen Carriers for Chemical Looping with Oxygen Uncoupling (CLOU) ..... 10
2.4 Ash-Related Issues in Thermal Conversion of Biomass ..... 11
2.4.1 Alkali Release and Retention in Biomass Thermal Conversion ..... 12
2.4.2 Implications of Gaseous Alkali Release ..... 13
2.4.3 Implications of Alkali Retention ..... 14
2.5 The State of Knowledge of Alkali Release in CLC of Biomass ..... 14
2.6 Chemical Looping Gasification (CLG) and Oxygen Carrier Aided Combustion (OCAC) ..... 15
3. Experimental Setup ..... 16
3.1 CLC Pilot Systems ..... 16
3.1.1 100 kW Solid Fuels CLC Pilot (Chalmers) ..... 17
3.1.2 10 kW Solid Fuels CLC pilot (Chalmers) ..... 18
3.1.3 Dual Circulating Fluidized Bed (D-CFB) CLC pilot (VTT, Finland) ..... 19
3.2 Fuels and Oxygen Carriers ..... 20
3.3 Reactor Gas Analysis ..... 22
3.4 Alkali Measurement System ..... 22
3.4.1 Surface Ionization Detector (SID) Alkali Measurement System ..... 23
3.4.2 Impactor-based Alkali Measurements ..... 27
3.4.3 Collinear Photofragmentation and Atomic Absorption Spectroscopy (CPFAAS) ..... 27
3.5 Thermodynamic Modelling ..... 28

4. Data Processing and Analysis ..... 29
4.1 CLC Performance Data and Calculations ..... 29
4.1.1 Carbon Capture Efficiency ..... 29
4.1.2 Oxygen Demand and Gas Conversion Efficiency ..... 30
4.1.3 Circulation Index ..... 30
4.2 Alkali Emissions Data and Calculations ..... 31
5. Main Results ..... 33
5.1 Development of the SID-based alkali measurement technique ..... 33
5.2 Investigation of alkali release and distribution in CLC operation ..... 37
5.2.1 Alkali Emissions vs. Fuel Alkali Content ..... 37
5.2.2 Distribution of Gas-phase Alkalis in a CLC system ..... 39
5.2.3 Origin of AR Alkali Emissions ..... 39
5.2.4 Effect of Operating Temperature on AR and FR Alkali Emissions ..... 42
5.2.5 Effect of Chemical Looping Gasification (CLG) and Oxygen Carrier Aided Combustion (OCAC) Modes on Alkali Release ..... 43
5.2.6 Effect of Steam on Alkali Release in CLC ..... 47
5.2.7 FR Alkali Emissions Speciation ..... 47
5.2.8 Alkali Retention in Condensed Phases ..... 53
5.3 Interdependence of CLC process performance and alkali release ..... 55
6. Discussion ..... 58
6.1 RQ1 – Alkali release and distribution in chemical looping ..... 58
6.2 RQ2 – Interdependence of CLC performance and alkali release ..... 61
6.3 RQ3 – Advantages of CLC technology for processing biomass fuels ..... 63
6.4 Key limitations and remaining research gaps ..... 64
6.4.1 AR Alkali Levels, Origin, and Speciation ..... 64
6.4.2 Long-term Effects of Alkalis on OC Performance ..... 64
7. Conclusions ..... 66
Nomenclature ..... 68
References ..... 69

CHAPTER 1

# 1. Introduction

## 1.1 Motivation

Despite the increasing awareness of global warming and over two decades of effort to combat climate change, greenhouse gas emissions in the 2000's grew faster than in the 1990's[1]. The Paris Agreement of 2015 is the latest and most extensive pledge to combat climate change. At current, 197 countries - parties to the Paris Agreement, are committed to take action in order to limit global warming to well below 2 $^{o}$C above the pre-industrial era average temperatures. The possible pathways to achieving this ambitious global goal were assessed by the Intergovernmental Panel for Climate Change (IPCC) and were outlined in the Sixth Assessment Report [2]. There, the majority of the scenarios designed to meet the 2 $^{o}$C target heavily rely on large-scale implementation of negative emissions technologies (NETs) in the second half of this century. Therefore, intensive research to support the development and implementation of NETs technologies is a crucial and pressing issue.

Many NETs technologies have been proposed in the recent years. These include direct air capture methods, reforestation and afforestation, enhanced weathering of minerals to capture $CO_2$ from the atmosphere, bioenergy with carbon capture and storage (BECCS), as well as many others. Although there is no clear winner amongst the current NETs technologies, BECCS is considered to be a promising lower cost option [1]. Successful, and commercially viable implementation of BECCS requires low-cost and robust fuel conversion and carbon capture technologies.

Chemical looping combustion (CLC) is a novel technology that allows thermal conversion of fuels with inherent carbon capture [3]. In CLC, oxygen is separated from air and is delivered to the fuel by an oxygen carrier (OC) material that is circulated between two interconnected reactors. Most of the CLC schemes are based on two interconnected fluidized bed reactors, although alternative designs based on moving bed [4], packed bed [5], and rotary reactor designs [6] have been proposed. In all CLC schemes fuel conversion is accomplished by oxygen

supplied with the OC. The resulting fuel reactor flue gas consist primarily of $CO_2$ and water, and is nitrogen free, thus avoiding costly gas separation. In comparative studies evaluating different carbon capture technologies, CLC has consistently been reported to have lower energy and cost penalties than competing carbon capture technologies [7–10].

CLC technology, primarily in the interconnected dual-fluidized bed configuration, has been extensively studied over the past decade. The CLC principle has been successfully demonstrated for gaseous, liquid, and solid fuels such as coal [11]. CLC of biomass, however, has not yet been extensively explored [12]. Since fluidized bed reactors are the technology of choice for biomass combustion [13], biomass should be well suited for the CLC process. In fact, the few pilot demonstrations of biomass CLC have shown promising results [14–20]. These initial investigations, however, primarily looked at short-term operation, with the reactors not extensively optimized specifically for biomass fuel operation.

Experience from contemporary biomass technologies of fluidized bed combustion (FBC) and circulating fluidized bed combustion (CFBC) shows that biomass presents significant operational challenges that stem from the high alkali content of biomass fuels. The first major issue is the onset of bed agglomeration that typically results from formation of sticky alkali-silicate melts that form within the bed material [21–26]. The second detrimental issue is the deposition of alkali chlorides, alkali sulphates, and other species that form on heat exchange surfaces of the flue gas convection pass. These deposits cause fouling and corrosion of the heat exchange surfaces and result in lower steam cycle thermal efficiency due to impeded heat transfer [22,24,27–30].

Like FBC and CFBC technologies, CLC reactors could be challenged with alkali-induced fouling, corrosion, and bed material agglomeration issues. Furthermore, the nature of the CLC process can introduce additional issues. The reactivity of the oxygen carrier may be affected by biomass alkalis, thus having a great impact on the CLC process. The two-reactor nature of the CLC process also needs to be carefully considered. At the onset of the work presented in this thesis, it was not clear how the alkalis are released and partitioned in a CLC reactor system.

## 1.2 Aim and scope of this thesis

The work presented in this thesis was structured to address key research questions pertaining alkali release in chemical looping conversion of biomass fuels. The key research questions were:

*RQ1 - How are alkalis released/retained and distributed in the CLC process?*

*RQ2 - What is the interdependence between alkali release/retention and the key process control parameters in a CLC system?*

*RQ3 - What are the operational advantages and/or disadvantages of CLC technology for processing alkali-containing biomass?*

At the inception of the work presented herein, there was no published literature on the fate or implications of alkalis in chemical looping processes. The posed research questions were explored experimentally at the pilot scale. The scope of the work in this thesis consisted of:

- Progressive development of a surface ionization detector (SID)-based measurement system capable of online measurement of flue gas alkali emissions from the two flue gas streams of a CLC system
- Validation of the SID-based system against an in-situ laser-based and an impactor-based alkali measurement methods, as well as against mass balances on alkalis based on solids sampling and analyses
- four experimental investigations of alkali release in CLC systems at different design and operating conditions:
    - three different CLC pilots of different scale and design
    - nine different biomass fuels
    - four different oxygen carriers
    - various operating temperatures
    - various system circulation rates
    - three pilot operating modes
        - chemical looping combustion (CLC)
        - chemical looping gasification (CLG)
        - oxygen carrier aided combustion (OCAC)
- Performance evaluation of fuel conversion and carbon capture efficiency of the CLC pilots
- Thermodynamic modelling of alkali release speciation and fuel-OC interactions in CLC
- Design, development, and construction of supplementary experimental infrastructure

## 1.3 Contribution of the published papers to this thesis

Paper I of the thesis establishes the methodology for the SID-based online measurement of alkali emissions in CLC systems. This paper presents the first data set on fuel reactor alkali emissions in CLC systems and provides an initial insight into how alkali emissions are partitioned between the air and fuel reactors.

Paper II further establishes the alkali emissions measurement methodology, which is applied in a new CLC pilot system that is specifically designed for high-volatiles biomass fuels. The paper also provides a first look at the interplay between reactor performance in terms of fuel conversion and carbon capture efficiency and operational issues stemming the biomass alkali species.

Paper III establishes how gas-phase alkali emissions in CLC operation compare to alkali emissions in OCAC operation. This paper analyses how fuel decomposition and the reactor

atmosphere influence the alkali release, and how ash formation and oxygen carriers influence the retention of alkali materials in the reactor system.

Paper IV establishes how operating temperatures affect alkali release in CLC, CLG, and OCAC operating modes. The paper also validates the previously observed difference in emissions between CLC and OCAC operation, showing that this difference is caused by the steam-rich atmosphere in CLC operation. Furthermore, Paper IV establishes a detailed potassium balance over the entire CLC pilot system, providing a more detailed understanding on the partitioning and fate of condensed-phase alkali species.

Paper V uses impactor-based alkali measurement to establish speciation of the gas-phase alkalis in CLC operation. The measurements also provide insight into how alkali species condense and form particulates in the flue gases. Thermodynamic modelling performed in Paper V supports interpretation of impactor-based alkali speciation analysis and provides insight on how fuel interactions with the OC affect alkali retention in condensed phases.

Paper VI provides an important validation for the SID-based alkali measurement system via comparison of the SID technique to an in-situ laser-based alkali emissions measurement technique. Furthermore, Paper VI highlights several factors that influence the performance of the SID-based measurement system and establishes key sources of uncertainty in SID-based measurements.

## 1.4 Outline of this thesis

This thesis is based on the six appended papers (Papers I - VI) and this introductory essay. Chapter 2 of the thesis introduces the working principle of CLC and covers background theory on alkali release in thermal conversion of biomass fuels. Chapter 3 discusses the experimental methodology and equipment used in the experiments that make up the work presented in Papers I - VI. Chapter 4 explains the data acquisition, data processing, and calculation procedures used to derive the experimental findings. Chapter 5 presents and discusses the main findings of Papers I - VI. Chapter 6 organizes the main results into an overall scheme of alkali release and distribution in CLC systems, and discusses how the observed alkali release behavior is advantageous for processing alkali-containing biomass in the CLC process. Chapter six also highlights important research limitations that need to be addressed in follow-up research. Chapter 7 outlines the main conclusions of this thesis with respect to the main research questions.

CHAPTER 2

# 2. Background

The following sub-sections provide the background on CLC and related phenomena. Theory of alkali release, largely from conventional fluidized bed combustion and gasification studies, is also summarized to set the stage for extending the concepts to the CLC technology context.

## 2.1 Chemical Looping Combustion (CLC) Principle

A simplified schematic of the CLC process is shown in Figure 1. The CLC principle relies on cyclical oxidation and reduction of a metal oxide material, the oxygen carrier (OC), circulated between two interconnected reactors.

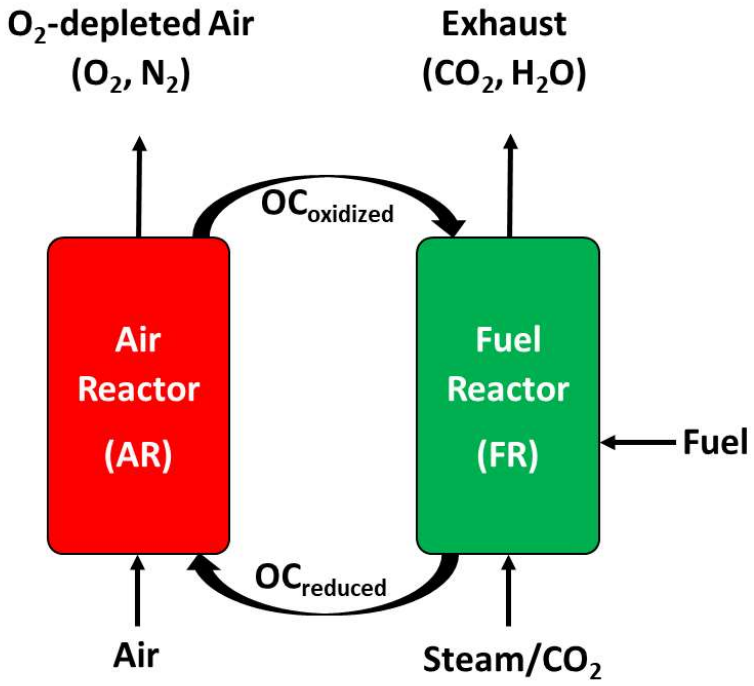


***Figure 1 – Simplified process diagram for chemical looping combustion of solid fuels***

In the CLC process, the oxygen carrier (OC) material, typically a metal oxide, is oxidized by air in the air reactor (AR), and is reduced by the fuel in the fuel reactor (FR). In this process scheme, oxygen is transferred by the OC from the air in the AR to the fuel in the FR, while nitrogen is rejected in the AR. Thus, fuel in the FR is converted with oxygen from the oxygen carrier, resulting in a nitrogen-free flue gas. This avoids the costly separation of $CO_2$ from nitrogen that is required in post-combustion $CO_2$ capture systems. The reduction and oxidation of the oxygen carrier can be represented by the reactions below:

$$\text{Fuel} + a\text{Me}_x\text{O}_y \rightarrow b\text{CO}_2 + c\text{H}_2\text{0} + a\text{Me}_x\text{O}_{y-1} \quad \text{(R 1)}$$

$$a\text{Me}_x\text{O}_{y-1} + 0.5a\text{O}_2 \rightarrow a\text{Me}_x\text{O}_y \quad \text{(R 2)}$$

The OC reduction in the FR (Reaction R 1) is typically mildly endothermic, while OC oxidation (Reaction R 2) in the AR is highly exothermic. CLC systems are designed to recover the majority of the process heat from the AR flue gas. Minor heat recovery from the FR flue gas is also possible. The net heat release in a CLC system is equivalent to conventional fuel combustion. The two-reactor scheme essentially separates the combustion reaction into two separate steps - each involves the OC and occurs in a separate reactor. The CLC process is most typically implemented in a dual-fluidized bed arrangement. Description of such systems is covered in Chapter 3.

## 2.2 Chemical Looping Combustion Fuels

### *2.2.1 Gaseous Fuels*

CLC was initially developed and demonstrated with gaseous fuels [3]. Gaseous fuel, typically methane or syngas, is introduced at the bottom of the fuel reactor as the fluidizing gas. As the fuel gas makes its way through the OC bed, it reacts with the solid oxygen carrier and is converted to $CO_2$ and $H_2O$. Fuel conversion of gaseous fuels in CLC is typically quite high and can reach nearly 100% with highly reactive oxygen carriers such as nickel [31] and calcium manganite [32]. Fuel conversion primarily relies on the properties of the oxygen carrier and the contact between the fuel and the oxygen carrier. Thus, the fluidization regime and bed height have a significant impact on fuel conversion.

### *2.2.2 Solid Fuels*

For solid fuels, the fuel conversion process is more complex and involves in-situ gasification of the fuel char. The OC bed of the FR is typically fluidized by $CO_2$ or steam, with the solid fuel fed directly into the bottom section of the reactor bed by means of a screw-feeder or pneumatic transport. As the fuel enters the reactor bed, it is rapidly heated and undergoes the following staged conversion process:

1. Drying – water content is removed by evaporation from the fuel particles
2. Devolatilization – the fuel's volatile content is released in the vapor phase, leaving behind solid char and most of the fuel's inorganic content
3. Gasification – char is gasified by reacting with the $CO_2$ or steam fluidizing medium, leaving behind fuel ash. The main gasification reactions are [33]:

$$C_{(s)} + H_2O_{(g)} \rightarrow CO_{(g)} + H_{2(g)} \quad \text{(R 3)}$$

$$CO_{(g)} + H_2O_{(g)} \rightarrow CO_{2(g)} + H_{2(g)} \quad \text{(R 4)}$$

$$C_{(s)} + CO_{2(g)} \rightarrow 2CO_{(g)} \quad \text{(R 5)}$$

4. Oxidation – volatiles released in devolatilization, as well as the char gasification products are oxidized by reacting with the oxygen carrier material, as per reaction R 1.

Of these process steps, steps 1 through 3 are sequential, but step 4 occurs concurrently with the others. A simplified visualization of the staged conversion process is presented in Figure 2.

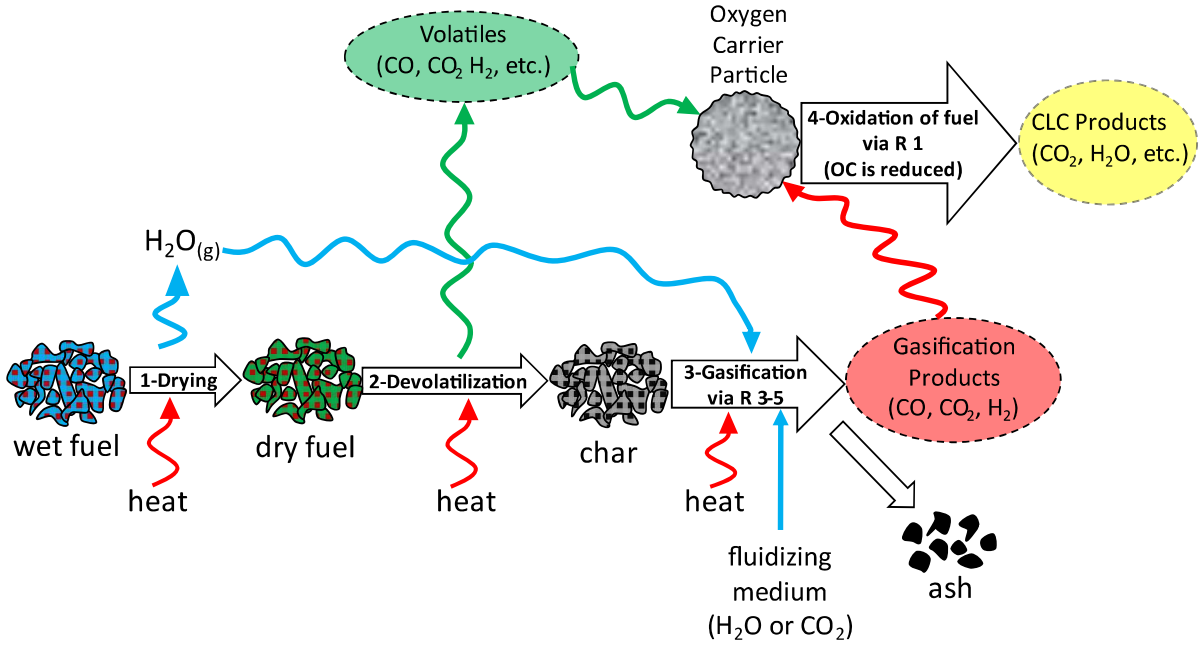


***Figure 2 – Solid fuel staged conversion process steps in chemical looping combustion***

Solid fuel use in CLC presents challenges that arise largely from the fuel's composition. Typical composition ranges of several solid fuels are presented in the Table 1.

***Table 1 – Proximate analysis of selected solid fuels from Phyllis 2 database****[34]*

| | Fossil Fuels | | | Biomass Fuels | | |
|---|---|---|---|---|---|---|
| **Property** | **Lignite Coal** | **Petroleum Coke** | **Finnish Peat** | **Pine Sawdust** | **Wheat Straw** | **Rice Husk** |
| **Moisture content (wt.% a.r.)** | 13.40 | 0.32 | 9.80 | 13.67 | 15.10 | 11.20 |
| **Ash content (wt.% a.r.)** | 3.32 | 0.40 | 6.77 | 1.15 | 7.60 | 18.29 |
| **Volatile matter (wt.% a.r.)** | 42.61 | 17.24 | 65.49 | 69.45 | 62.32 | 48.31 |
| **Fixed carbon (wt.% a.r.)** | 40.68 | 82.04 | 17.95 | 15.73 | 14.98 | 22.20 |
| **Lower heating value (MJ/kg)** | 20.15 | 36.10 | 20.70 | 16.46 | 13.60 | 10.70 |

For fossil fuels, such as coal and coke, the relatively high fixed carbon content presents a challenge. For such fuels, char gasification is often the slowest and rate limiting step of the thermal conversion sequence outlined above [12,33]. Slow gasification can cause unconverted char elutriation into the FR's flue-gas stream, or carryover of char from the FR to the AR. Char elutriation in the FR causes incomplete fuel conversion and can overwhelm the downstream flue-gas clean-up system. In larger pilot scale studies with fuels such as coal and petroleum coke, elutriated fuel fractions were reported to range from 5% to 50%, depending greatly on the fuel type, fuel size, fuel residence time, oxygen carrier material, and other operating parameters [12]. Char carryover to the AR leads to char combustion, and consequentially the release of uncaptured $CO_2$ from the AR. To mitigate such undesirable effects several reactors have been designed to have either a dedicated or integrated carbon stripper section in the FR. Both approaches rely on elutriating the char from the OC and reintroducing it back to the FR, thus giving the char more time to convert and gasify.

### *2.2.3 Biomass Solid Fuels*

Biomass conversion in CLC differs from that of other solid fuels. Biomass has a much higher volatile content than that of solid fossil fuels such as coal and coke. Depending on the type, biomass volatiles content is typically in the range of 63-85 wt.% on dry fuel basis, while coals typically contain 18-43 wt.% [13,35]. Due to the high volatiles content, on average, approximately 50-75% of the biomass fuel's mass is released in the devolatilization stage [35]. While this may not be an issue in conventional fluidized-bed combustion where biomass burns in the reactor bed as well as the reactor freeboard in the presence of excess air, in CLC, combustion of the released volatile species depends on effective contact with the oxygen carrier material. Depending on where the volatiles are released, their conversion can vary. Volatiles released at the bottom of the FR have a greater chance of achieving full oxidation as they make their way up through the OC bed. Volatiles released in the top portion of the bed have less time for contact [33]. Although higher OC inventory or lower fuel feeding rate can improve contact between the released volatiles and the OC material, in practice, full oxidation of the volatiles typically does not occur. Achieving full conversion requires downstream injection of pure oxygen in order to complete the oxidation. This oxygen injection step is often called "oxy-polishing" [12]. For similar operating conditions, fuels with higher volatiles content

tend to require more supplemental oxygen to complete the oxidation of the produced gaseous species [12].

Biomass char conversion is also different from other solid fuels. Biomass contains less fixed carbon and therefore produces less char [35]. Biomass char is also more reactive than that of fossil fuels due to several factors. Biomass char tends to be more porous, with larger pore sizes. This increases the char's reactivity due to higher active surface area and improved diffusion [13]. Further, and perhaps more significantly, biomass tends to contain a significantly higher levels of alkalis (K and Na), compared to fossil-based solid fuels. Alkalis act as catalysts for char gasification, thus increasing the rate of char conversion [13,36,37].

## 2.3 Oxygen Carriers

Oxygen carrier materials constitute the cornerstone of chemical looping combustion technology. Selection of an oxygen carrier is quite complex and is highly dependent on the application. Nevertheless, the following parameters are considered critical:

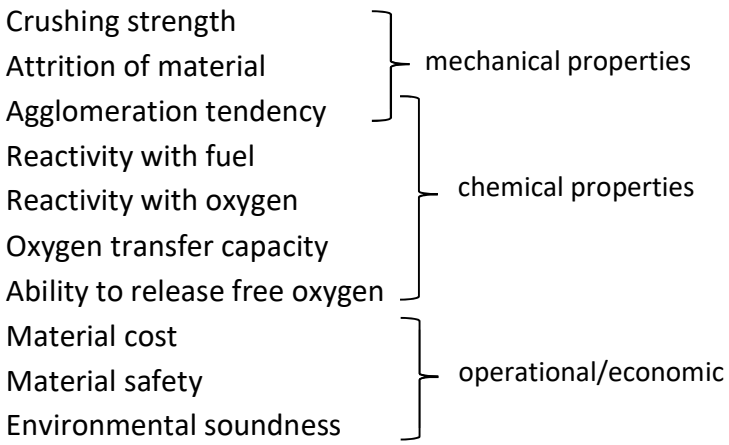


To date, it is estimated that over 1000 potential OC materials have been investigated. At the highest level, these materials can be divided into high-performing manufactured materials, and the less effective low-cost materials.

### *2.3.1 Manufactured Materials*

Manufactured oxygen carriers are typically based on oxides of Ni, Fe, Mn, and Cu supported on inert materials such as $Al_2O_3$. These materials were primarily developed for CLC of gaseous fuels and optimized for high conversion of $CH_4$. Further to single oxide oxygen carriers, multiple mixed-oxide and combined-oxide oxygen carriers have been successfully developed for CLC. Mixed-oxide oxygen carriers are based on physical combination of different metal oxides in one oxygen carrier material. Combined oxide oxygen carrier materials are made by chemically combining two or more metal oxides or by forming materials with a perovskite

structure. The advantage of these manufactured materials is that their properties can be tailored, but the major disadvantage is their high cost. Due to high cost, manufactured oxygen carriers are primarily suited for use with gaseous fuels, where the oxygen carrier lifetime in the CLC system can justify the investment. Use of manufactured oxygen carriers with solid fuels is cost prohibitive, as solid fuel CLC is often accompanied with significant ash formation. Ash formation can contaminate or deactivate oxygen carriers and limit their useful lifetime [38].

### *2.3.2 Low-Cost Materials*

Low cost oxygen carriers are materials which have oxygen carrying properties but are either naturally occurring, such as manganese ore, iron ore, and ilmenite, or are low-cost industrial by-products, such as industrial slags. In all cases, these materials contain naturally occurring metal oxides, along with other inorganic matter that exhibits oxygen carrying behavior. The major disadvantage of such materials is that their properties are set, and their reactivity towards methane is generally quite low. This makes most low-cost oxygen carriers a poor choice for CLC with gaseous fuel. However, the reactivity of these same materials with CO and $H_2$ is generally much higher. Since solid fuel conversion invariably relies on gasification of char to CO and $H_2$, low-cost materials can be sufficiently reactive with solid fuels [39,40]. The low cost of these materials, when compared to manufactured oxygen carriers, also makes them the only economically justifiable choice for CLC with solid fuels, where effects of fuel ash can greatly limit the oxygen carrier's useful lifetime. Ilmenite, a naturally occurring titanium-iron oxide ($FeTiO_3$) is by far the most widely used low-cost material which has been extensively and successfully tested in CLC operation with solid fuels [12].

### *2.3.3 Oxygen Carriers for Chemical Looping with Oxygen Uncoupling (CLOU)*

Some oxygen carrier materials have the ability to release molecular oxygen in conditions typical of the FR. Chemical looping combustion operation with such oxygen carriers is a subset of CLC technology called chemical looping with oxygen uncoupling (CLOU) [41]. Three metal oxide systems that show oxygen release appropriate for the CLOU process are the $Mn_2O_3/Mn_3O_4$, $CuO/CuO_2$ and $CoO_4/CoO$ systems. These oxide systems have been used to create manufactured CLOU oxygen carriers, but are also present in some naturally occurring materials. For example, several manganese ores exhibit CLOU behavior [42–44]. In the CLOU process, gaseous oxygen is released from the OC in the FR. This enables the fuel to be directly oxidized by the free oxygen, instead of reacting with the solid oxygen carrier. Although useful for all fuel types, the CLOU process is especially beneficial for solid fuel conversion. Whereas in non-CLOU CLC, char conversion is often rate-limited by the slow gasification step, in the CLOU process, char can be converted directly to combustion products by reacting with the free oxygen released by the oxygen carrier. The CLOU process partially or fully eliminates the slow char gasification step [12,16]. Experimental studies have shown that CLOU is able to accelerate the rate of fuel conversion by a factor of 45 for petroleum coke and by a factor of

60 for bituminous coal, when compared to the conversion rates of these fuels in a non-CLOU CLC process [17]. The improved fuel reactivity observed in the CLOU process also realizes the benefit of a much-reduced OC inventory [17]. This is because in non-CLOU operation, gaseous fuel components (the volatile fuel fraction and the gasification products) require adequate contact time with the OC to reach a reasonable conversion level. This is typically achieved by increasing bed material height, and thus inventory levels. In the CLOU process, the gaseous fuel components react in contact with the OC (gas-solid reaction), but have the additional benefit of reacting with the molecular oxygen released by the CLOU oxygen carrier. Contact of the free oxygen with the gaseous fuel fraction is much more efficient, and thus, less OC inventory is required. In fact, conversion of volatiles by free molecular oxygen can occur above the bed of the fuel reactor.

## 2.4 Ash-Related Issues in Thermal Conversion of Biomass

In conventional thermal fuel conversion processes, such as combustion and gasification, biomass fuels are known to cause issues that stem from their inorganic fraction. Biomass inorganic content can vary greatly from <1 wt.% for woody biomass, to as high as 40 wt.% for green house residues. The inorganic (ash) content of several selected fuels is shown in Table 1. Ash analysis, showing distribution of the most common inorganic species (shown in oxide form) for several biomass fuels and a fossil fuel is presented in Table 2, reproduced from reference [21].

***Table 2 – Ash composition for selected biomass and fossil fuels (wt.% of ash basis)*** *[21]*

| Fuel | $SiO_2$ | $Al_2O_3$ | $Fe_2O_3$ | Mn | MgO | CaO | $Na_2O$ | $K_2O$ | $TiO_2$ | $P_2O_5$ | $SO_3$ |
|---|---|---|---|---|---|---|---|---|---|---|---|
| **Wood pellets** | 4.3 | 1.3 | 1.5 | 5.9 | 8.5 | 55.9 | 0.6 | 16.8 | 0.1 | 3.9 | 1.3 |
| **Demolition wood pellets** | 20.4 | 3.5 | 2.2 | 0.3 | 7.5 | 27.5 | 4.8 | 10.5 | 2.5 | 11.1 | - |
| **Pepper plant residue** | 12.6 | 4.9 | 2 | 0.2 | 7.4 | 32.2 | 0.9 | 24.6 | 0.5 | 5.2 | - |
| **Greenhouse residue** | 28.4 | 3.9 | 18.4 | 0.3 | 5.7 | 25.8 | 0.8 | 9.7 | 0.8 | 3.8 | - |
| **Sunflower pellets** | 2.9 | 0.6 | 0.8 | 0.1 | 21.6 | 21.6 | 0.24 | 22.8 | 0.1 | 15.2 | 14 |
| **Olive cake pellets** | 12.8 | 2.9 | 3 | 0.1 | 4.9 | 17.5 | 3.9 | 47.9 | 0.2 | 6 | 1.1 |
| **Wheat straw** | 53.1 | 3.6 | 1.2 | - | 3 | 17.7 | 4.5 | 30 | - | 4.1 | - |
| **Sewage sludge** | 38.3 | 0.8 | 12.5 | - | 2.8 | 9.1 | 2.2 | 2.2 | 0.8 | 15.4 | 1.1 |
| **Bituminous Coal** | 59.7 | 20.3 | 7 | < 0.01 | 1.9 | 1.8 | 1 | 2.3 | 0.9 | 0.1 | 1.3 |

*Fuels ashed at 815 °C*

Ash forming species in biomass fuels can be grouped by their volatility. Elements like Ca, Si, Mg, Fe, and Al are known to be non-volatile. K, Na, S, Cl are known to be highly volatile, along with some heavy metals like Zn, Cd, and Pb [45,46]. Ash formed from biomass conversion is typically categorized as bottom ash or fly ash [22,28]. In fluidized bed systems, bottom ash is formed primarily from non-volatile species that are left over after char conversion [45,46]. Bottom ash particles are generally large, and depending on composition, can be sticky due to melt formation [22]. The majority of the bottom ash stays in the bed, where it either interacts with the bed material or remains as separate ash particles.

Fly ash, the ash that is present in the flue gas, has two main origins that are typically grouped by particle size. Fine fly ash with a particle diameter <1 μm is typically formed via condensation of volatile species that are released to the gas phase during fuel conversion. For biomass, the most relevant species are K, Cl and S, whereas Na and heavy metals typically have a minor contribution [22,45]. From these, gas-phase species particles initially form through nucleation of small primary particles that further grow through condensation, coagulation, and agglomeration. Coarse fly ash with a particle size >1 μm arise from entrainment and stripping of smaller or fragmented bottom ash particles from the bed. These fly ash particles are primarily composed of the non-volatile species, although volatile species can condense on their surface [22,28,45–47].

### *2.4.1 Alkali Release and Retention in Biomass Thermal Conversion*

From the many inorganic species present in biomass fuels, K, Na, and Cl are considered highly problematic as their release is associated with fouling and corrosion of heat exchange equipment [21,22,27], and bed material agglomeration [21,27,35,48,49]. Alkalis, K and Na, are present in biomass in three primary forms: 1) salts, 2) organically-associated form, and 3) excluded minerals. Alkali species present as excluded minerals arise mostly from contamination of fuel during fuel preparation and processing. In combustion processes this form of alkali species tends to be quite inert and does not have significant implications for thermal conversion [22]. Alkali salts and organically-associated alkalis, however, are known to be releasable and reactive during the fuel conversion process. From these forms, alkali salts are estimated to account for up to 90% of the biomass alkalis [50–52]. Alkali salts are originally present in dissolved form in plant fluids. Once the plant is harvested and the biomass begins to dry, the water soluble components begin to precipitate as phosphates, carbonates, sulphates, chlorides, and nitrates [53–56]. The release and reactivity behavior of K and Na is considered to be equivalent [22,57,58]. For this reason, and because the abundance of K in biomass far exceeds that of Na, further discussion is based on release and transformations of the K species. The transformations discussed below are equivalent for Na.

Alkali species are released in different proportions during thermal conversion of biomass. As biomass fuel is introduced into a reacting system (e.g., boiler, gasifier), it is heated and undergoes a staged decomposition process. As the fuel particle temperature rises, devolatilization starts to occur. This step is common to combustion and gasification processes. At the devolatilization stage about <10% of K is released at temperatures below 700 $^{o}$C. This release is associated with decomposition of the organic structure and release of organically-associated K [50,59]. Since the K release in the devolatilization step is quite small, most of the K species remain trapped in the char fraction as char-bound K, as K-salts, such KCl, $K_2CO_3$ and $K_2SO_4$, and as silicates [50,59–63].

Further fuel decomposition differs for combustion and gasification. In combustion, char is oxidized to $CO_2$, while in gasification the char is gasified to CO and $H_2$. In both processes, the

high temperature release occurs >700 $^{o}$C and is dominated by sublimation of KCl to the gas phase. The amount of KCl fraction in the char depends on the original fuel, with annual biomass typically containing more KCl, and on release of Cl. Several studies estimate that up to 75% of the fuel's Cl can be released at lower temperatures in the devolatilization stage through formation of $HCl_{(g)}$ [50,64]. After KCl evaporation, further release of K occurs through devolatilization of char-bound K and decomposition of K carbonates, sulphates, and silicates, listed decreasing order of significance [50,61,63–66].

Throughout the fuel conversion process gas-phase release of K is counteracted by competing formation of K-silicates. At high temperatures K readily reacts with Si and Al to form potassium silicate or aluminosilicate species [22,59]. Silicate species remain in condensed form at temperatures below 1200 $^{o}$C, but start to decompose releasing K to the gas phase at higher temperatures [50]. Both, the release, and retention of K, can have detrimental effects on the thermal conversion system's operation.

### *2.4.2 Implications of Gaseous Alkali Release*

Alkali species released to the gas-phase are known to cause fouling and corrosion of heat exchange equipment in contact with the flue gases [21,22,27,28,67]. In biomass fluidized bed boilers used for steam production, steam superheaters are operated at temperatures of approximately 400-600 $^{o}$C, while typical combustion temperatures are maintained in the range of 800-900 $^{o}$C [21,28]. Deposition of gaseous alkali species occurs as the flue gas begins to cool in the vicinity of the heat exchangers. Alkali salts condense onto the surface of the heat exchanger, forming a sticky coating. Further deposition occurs via further condensation of gaseous alkali species or by impaction of fly ash and other condensed species [21,27,28]. The deposits insulate the steam tubes and impede heat transfer, leading to lower overall heat extraction, and consequently lower boiler thermal efficiency.

Extreme deposit growth requires installation of soot blowers that are used to clean the deposits off the steam tubes without having to take the boiler offline. Soot blower equipment, however, is costly to install and operate. Depending on the species present in the deposits, severe corrosion of steam tube materials can occur. Of the possible species, KCl is known to be especially detrimental as it causes severe high temperature corrosion [22,27,68]. In extreme cases corrosion permanently damages the steam tube material, requiring boiler shutdown to replace the compromised tube packs. KCl-induced corrosion is typically dealt with by addition of sulfur (S) to the fuel. In the boiler, S reacts with KCl to form $K_2SO_4$ and HCl. Although these species also participate in corrosion, they are significantly less aggressive than KCl. Sulfur is typically added to the process by co-firing with sulfur-containing fuel (e.g., sewage sludge), addition of elemental sulfur, or addition of sulfur containing species (e.g., ammonium sulfate) to the flue gas of the boiler [21,69].

### *2.4.3 Implications of Alkali Retention*

Alkali species that are trapped within the bottom ash fraction can also be problematic for boiler or gasifier operation. Alkali silicate species that form by reaction of alkalis with $SiO_2$ have a melting point of approximately 700 $^oC$ [23]. Since typical biomass-fueled furnaces operate at around 800-900 $^oC$, alkali silicates form sticky melts. Once significant amounts of these melts are formed, the bed material particles start to stick together and form agglomerates. With continued operation, severe agglomeration of the bed material leads to defluidization and shut down of the process units [21,35,48]. Agglomeration can be dealt with, to some extent, by reducing combustion temperatures to limit the formation of the sticky melts. This strategy, however, results in lower thermal efficiency of the steam cycle. In practice, mitigating or limiting agglomeration is managed by continuous replacement of bed material (i.e., removal of old material with makeup of fresh material). Large scale commercial boilers operated with agglomeration-prone fuels can require continuous material replacement of up to a third of the boiler inventory per day of operation [33]. Other methods to mitigate agglomeration involve adding aluminum-containing materials such as kaolin, or other clay minerals. Aluminum readily reacts with alkali silicates to reform them to aluminosilicates that have a much higher melting point. Another strategy involves using alternative bed materials such as olivine, dolomite, blast furnace slag, feldspar and others [69].

## 2.5 The State of Knowledge of Alkali Release in CLC of Biomass

At the onset of the work presented in this thesis, the fate of alkalis in CLC was largely unexplored, with only several pilot-scale studies reporting qualitative observations on the interaction of alkalis with OC materials. Gu et al. reported alkali deposit formation on the surface of the iron ore OC in 1 kW CLC operation with wood sawdust fuel. In this study, the alkali deposit was found to have no effect on the oxygen carrier reactivity [70]. In a similar investigation at 500 W scale, Mendiara et al. found no alkali deposition or alkali effect on reactivity of iron ore OC [17]. Other results on alkali interaction with oxygen carriers were reported from studies using ilmenite oxygen carrier in oxygen carrier aided combustion (OCAC) [71] and in gasification [72]. Both studies showed that that ilmenite can capture potassium. This property was attributed to ilmenite's $TiO_2$ fraction that can form stable potassium titanate compounds within the ilmenite OC particles. The few reported interaction results made it clear that alkalis can affect the OC, and in turn, the OC can influence alkali behavior. Thus OC-alkali interactions should be considered when evaluating oxygen carrier materials for use in CLC of biomass.

How alkalis are released and partitioned within a CLC system operated with biomass was untested prior to the work presented in this thesis. However, consideration of the nature of the CLC process led to the expectation that in CLC most of the alkali release to the gas phase should occur in the fuel reactor. This expectation was based on the knowledge that alkali

release in thermal conversion is known to occur during fuel decomposition, and the fact that fuel decomposition occurs primarily in the FR.

## 2.6 Chemical Looping Gasification (CLG) and Oxygen Carrier Aided Combustion (OCAC)

Research in the area of CLC has led to development of multiple related technologies [73,74]. Two such technologies are chemical looping gasification (CLG) and oxygen carrier aided combustion (OCAC). Although CLG and OCAC technologies were not the focus of this thesis, experiments in CLG and OCAC operation modes in Papers III and IV provided valuable insight into alkali release behavior in CLC systems. As such, CLG and OCAC operating principles are briefly explained.

The CLG process is used for gasification of solid fuels. CLG is essentially identical to the CLC process for solid fuels, but the extent of oxygen delivery by the OC is limited such that the solid fuel is gasified to CO and $H_2$, but does not oxidize further to $CO_2$ and $H_2O$. CLG operation can be achieved in a CLC unit by greatly limiting the OC circulation with respect to fuel flow, or by limiting the $O_2$ concentration of the AR. Both strategies result in limited delivery of oxygen to the fuel in the FR and create conditions for gasification of the solid fuel.

The OCAC process is a conventional fluidized bed combustion process that is typically carried out in a fluidized bed biomass boiler. In OCAC, however, an OC material is used as the bed material instead of silica sand. In operation, the active OC material acts as a buffer for oxygen concentration in the bed, eliminating oxygen-poor bed material zones which occur with sand beds. This oxygen concentration buffering ability of OC materials allows the boiler to be operated at lower excess air values and improves boiler emissions performance.

CHAPTER 3

# 3. Experimental Setup

The work presented in this thesis is based on four experimental CLC campaigns conducted in three different pilot systems. The following sections provide an overview of the CLC pilots, the oxygen carriers and fuels, and the alkali measurement system used in the campaigns.

## 3.1 CLC Pilot Systems

Three different CLC pilot reactor systems were used in the experimental work presented in this thesis. Schematics for these systems are presented in Figures 3 to 5. The key features of the reactors are summarized in Table 3.

***Table 3 – Key features of the CLC pilots used in the experimental investigations***

| **CLC Pilot** | **Nominal Duty** | **System OC Inventory** | **AR Configuration** | **FR Configuration** | **Reactor Connections** | **Special Features** | **Heating** |
|---|---|---|---|---|---|---|---|
| 100 kW (Chalmers)<br><br>**Paper I** | 100 kW | 150-250 kg | High velocity riser with cyclone | Circulating fluidized bed | Loop Seals | Circulation riser, carbon stripper | Oven |
| 10 kW (Chalmers)<br><br>**Paper II & IV** | 10 kW | 25-40 kg | High velocity riser with cyclone | Bubbling fluidized bed | Loop Seals | Volatiles distributor | Oven |
| D-CFB (VTT, Finland)<br><br>**Paper III & V** | 60 kW | 50-60 kg | Circulating fluidized bed | Circulating fluidized bed | L-valves | | External wall heat tracing |

### *3.1.1 100 kW Solid Fuels CLC Pilot (Chalmers)*

The 100 kW CLC pilot shown in Figure 3 was used in experiments presented in Paper I. The fuel reactor in this system has a circulating fluidized bed (CFB) design with a 5 m tall main riser. The oxygen carrier travels through the FR's main riser section and is then returned to the bottom of the FR riser via a cyclone (CY2) and a loop seal (LS2). This design allows for control of internal FR material circulation and improved contact between the fuel's gaseous components and the OC material. Material from the FR eventually overflows and travels by gravity to the circulation riser (CR) via a loop seal (LS3). The CR transports the OC material to the carbon stripper (CS), where residual unconverted char particles are gasified or elutriated, and recirculated back to the FR. From the CS, the OC material is gravity-fed to the AR via a loop seal (LS4). In the AR, the OC is oxidized and transported back to the FR via a cyclone (CY1) and a loop seal (LS1). The CR is implemented to make the system more compact. Without the circulation riser, the overall height of the system would be several meters taller, since the OC needs to be gravity-fed from the FR to the carbon stripper (CS), and from the CS to the AR. Solid fuel is fed into the system with a screw feeder (not shown) to the top of the LS2 loop seal. The entire reactor system is located in an electrically heated oven that maintains the reactor temperature. Excess heat from the AR is removed with a mantle cooler that uses ambient air as the heat transport medium. The 100 kW reactor system is described in more detail in a study by Markström et al. [75].

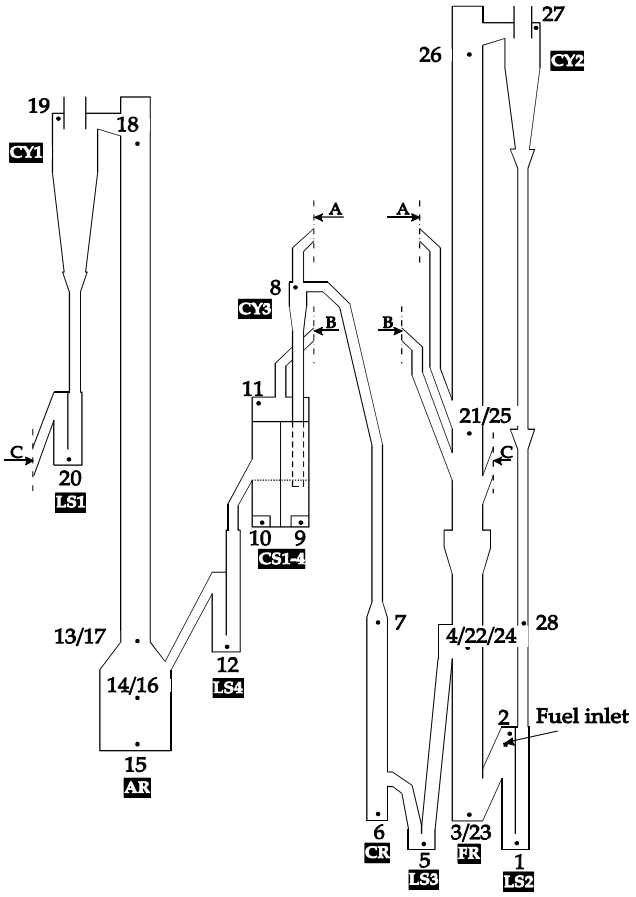


***Figure 3 – Simplified schematic of the 100 kW CLC pilot for solid fuels*** *[76]*

### *3.1.2 10 kW Solid Fuels CLC pilot (Chalmers)*

The 10 kW CLC pilot shown in Figure 4 is a newly designed and built CLC pilot system that was commissioned with the experiments presented in Paper II. This pilot system consists of a high velocity riser AR, and a bubbling fluidized bed FR. OC particles from the FR are fed by gravity to the AR via the lower loop seal (LLS). Oxidized OC particles are transported from the AR to the FR up the AR riser via the AR cyclone and the upper loop seal (ULS). Solid fuel is gravity-fed into the FR from a fuel hopper. The reactor is installed in an electrically heated oven that maintains the reactor temperature. The bubbling fluidized bed FR was specially designed for operation with high-volatiles solid fuels, such as biomass. The FR internals include a volatiles distributor, which is essentially a perforated internal baffle. The volatiles distributor is meant to help in contacting the fuel volatiles with the bed material by forcing the released volatiles through small gas distribution holes. A more detailed description of this pilot system, the details of the volatiles distributor, as well as description of the auxiliary equipment (fuel feeding system, flue gas filtration) can be found in Paper II.

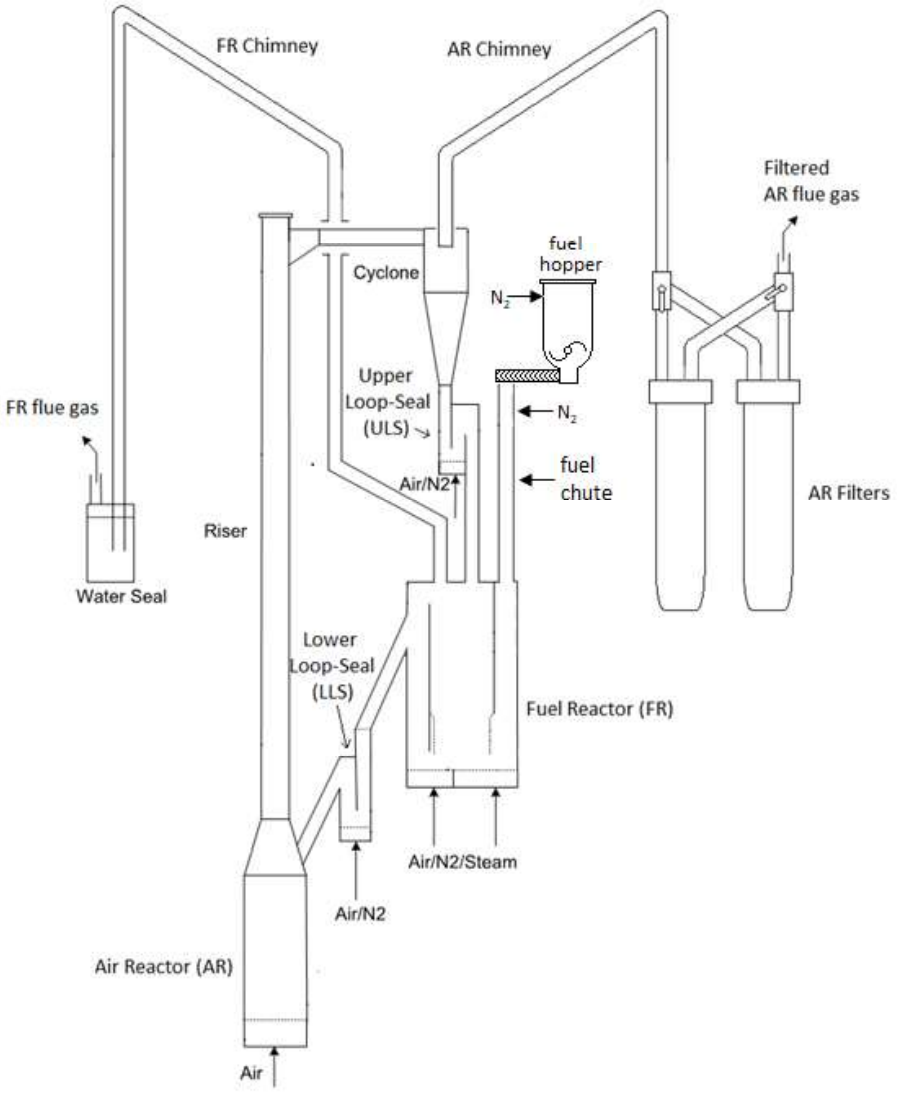


***Figure 4 – Simplified schematic of the new 10 kW CLC pilot for solid fuels*** [77]

### *3.1.3 Dual Circulating Fluidized Bed (D-CFB) CLC pilot (VTT, Finland)*

The dual circulating fluidized bed (D-CFB) CLC pilot shown in Figure 5 was used in experiments presented in Paper III. This system is located at the VVT research institute's Bioruukki piloting center in Espoo, Finland. In this system, both the FR and the AR, have a circulating fluidized bed (CFB) design. OC material from the FR is transported up the FR riser and is gravity-fed to the AR via the FR cyclone and the return leg which connects the bottom of the FR cyclone to the bottom of the AR. The oxidized OC material is transported up the AR riser and is gravity-fed to the bottom of the FR riser via the FR cyclone and a return leg. The AR and FR return legs act as L-valves and use nitrogen fluidization to minimize gas mixing between the AR and the FR. The D-CFB pilot is equipped with the capability to feed solid fuels to both the AR and the FR from two independent solid fuel feeding systems. Unlike the 100 kW and 10 kW CLC pilots described above, the D-CFB pilot is heated with electrical heat tracing which is installed locally on each reactor section. This results in higher temperature difference between the AR and FR. A more detailed description of this system is provided in Paper III.

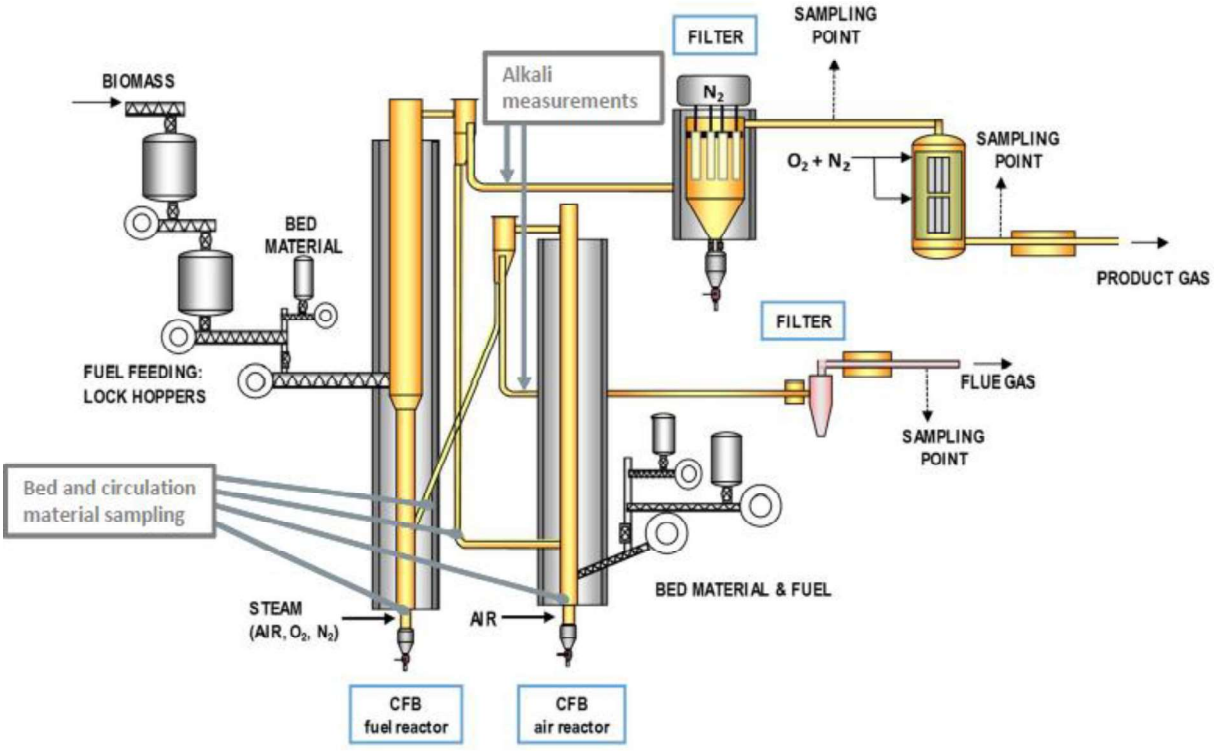


***Figure 5 – Simplified schematic of the 60 kW D-CFB CLC pilot for solid fuels (VTT, Finland)****[78]*

## 3.2 Fuels and Oxygen Carriers

The fuels and oxygen carrier materials used in experiments presented in Papers I through V are summarized in Table 4.

***Table 4 – Summary of fuels and oxygen carrier materials used in Papers I-V***

| Paper | Pilot System | OC Material | Fuels Tested |
|---|---|---|---|
| **Paper I** | 100 kW Pilot | **Ilmenite** ($FeTiO_3$)<br>mixed with<br>**Calcium Manganite**<br>($CaMn_{0.775}Ti_{0.125}Mg_{0.1}O_{3-\delta}$) | Black Pellets (BP)<br>Swedish Wood Char (SWC)<br>German Wood Char (GWC)<br>Straw Pellets Mix (SPM) |
| **Paper II** | 10 kW Pilot | **Ilmenite** ($FeTiO_3$) | Black Pellets (BP)<br>Pine Forest Residues (PFR)<br>Straw Pellets Mix (SPM) |
| **Paper III & V** | 60 kW D-CFB Pilot | **Ilmenite** ($FeTiO_3$)<br>**Braunite** | Wood Pellets (WP)<br>Wood Char (WC)<br>Straw Pellets (SP-1) |
| **Paper IV** | 10 kW Pilot | **LD Slag**<br>(Linz–Donawitz steel slag) | Black Pellets (BP)<br>Pine Forest Residues (PFR)<br>Straw Pellets (SP-2) |

*§Note: δ is the perovskite structure oxygen deficiency factor*

In Table 4, calcium manganite is a synthetic perovskite material with its elemental composition defined by its chemical formula. This material was mixed with ilmenite in different proportions throughout the experimental campaign in Paper I (see Paper I for details). Ilmenite oxygen carrier is an iron-titanium ore, consisting primarily of the mineral ilmenite ($FeTiO_3$) and some other impurities. Braunite is a manganese-silicate ore which consists of >70 wt. % $Mn_2O_3$ and $Mn_3O_4$. LD Slag is a waste slag material of the Linz-Donawitz steel making process with no defined chemical formula. The actual elemental compositions of ilmenite, braunite, and LD Slag are presented in Table 5.

*Table 5 – Elemental composition of ilmenite, braunite, and LD Slag oxygen carriers*

| Element | Unit | Ilmenite | Braunite | LD Slag |
|---|---|---|---|---|
| Ti | wt.% | 27.36 | 0.020 | 0.70 |
| P | wt.% | 0.004 | 0.030 | 0.24 |
| S | wt.% | 0.026 | 0.13 | n/a |
| Cr | wt.% | 0.051 | 0.010 | 0.37 |
| Fe | wt.% | 35.89 | 11.0 | 16.0 |
| Si | wt.% | 0.76 | 2.50 | 5.0 |
| V | wt.% | 0.11 | <0.01 | 1.9 |
| Ca | wt.% | 0.15 | 3.50 | 33.0 |
| Mg | wt.% | 2.23 | 0.89 | 5.0 |
| Al | wt.% | 0.34 | 0.25 | 0.64 |
| Mn | wt.% | 0.23 | 55.0 | 2.3 |
| K | wt.% | 0.017 | 0.020 | 0.037 |
| Na | wt.% | 0.052 | 0.22 | 0.032 |
| Zn | wt.% | 0.012 | 0.010 | 0.0006 |
| Ni | wt.% | 0.018 | 0.010 | 0.004 |
| Cu | wt.% | 0.007 | 0.040 | 0.0006 |
| Co | wt.% | 0.012 | 0.020 | 0.0004 |
| Sr | wt.% | 0.003 | 0.12 | n/a |
| Zr | wt.% | 0.017 | 0.020 | n/a |
| Nb | wt.% | 0.005 | <0.0001 | n/a |
| Pb | wt.% | <0.0001 | 0.010 | 0.00003 |
| Cl | wt.% | <0.01 | 0.030 | n/a |
| O (remainder) | wt.% | 32.7 | 26.2 | ~34.7 |

The fuels used in the experiments of Papers I through III are presented in Table 6 along with the fuels' composition and heating values.

*Table 6 – Biomass fuel composition and key properties*

| | Unit | Black Pellets (BP) | Swedish Wood Char (SWC) | German Wood Char (GWC) | Pine Forest Residues (PFR) | Straw Pellet Mix (SPM) | Wood Pellets (WP) | Wood Char (WC) | Straw Pellets 1 (SP-1) | Straw Pellets 2 (SP-2) |
|---|---|---|---|---|---|---|---|---|---|---|
| **Moisture** | wt.% a.r. | 6.90 | 3.90 | 5.10 | 9.20 | 7.85 | 7.50 | 4.10 | 8.10 | 8.8 |
| **Ash** | wt.% a.r. | 0.30 | 5.50 | 2.80 | 1.82 | 4.09 | 0.460 | 14.0 | 5.51 | 7.9 |
| **Volatiles** | wt.% a.r. | 74.2 | 16.7 | 15.7 | 80.0 | 74.6 | 78.4 | 18.7 | 69.3 | 67.5 |
| **Fixed C** | wt.% a.r. | 18.7 | 73.9 | 76.4 | 9.0 | 13.5 | 13.7 | 63.2 | 17.1 | 15.8 |
| **H** | wt.% a.r. | 5.6 | 3.30 | 3.00 | 5.69 | 5.84 | 5.64 | 2.21 | 5.24 | 6.1 |
| **C** | wt.% a.r. | 49.8 | 78.7 | 81.2 | 46.9 | 45.9 | 46.9 | 73.0 | 43.2 | 42.0 |
| **N** | wt.% a.r. | 0.09 | 0.360 | 0.480 | 0.347 | 0.377 | 0.160 | 0.960 | 0.580 | 0.70 |
| **O** | wt.% a.r. | 37.4 | 12.1 | 12.5 | 36.0 | 40.2 | 39.4 | 5.75 | 37.2 | 43.0 |
| **K** | mg/kg fuel a.r. | 460 | 2585 | 4400 | 2080 | 5730 | 404 | 3115 | 13730 | 11000 |
| **Na** | mg/kg fuel a.r. | <53 | <270 | <110 | 27 | 157 | 244 | 229 | 123 | 260 |
| **Cl** | mg/kg fuel a.r. | <100 | <100 | - | - | 900 | 26.0 | 101 | 3320 | 1700 |
| **S** | mg/kg fuel a.r. | <120 | <300 | 180 | 400 | 1080 | 93.0 | 288 | 1010 | 1080 |
| **Si** | mg/kg fuel a.r. | <530 | 2060 | 12000 | - | 9770 | 88.0 | 378 | 9210 | 19000 |
| **Ca** | mg/kg fuel a.r. | 820 | 5900 | 12000 | - | 4260 | 994 | 47000 | 3360 | 7700 |
| **LHV** | MJ/kg a.r. | 18.6 | 29.8 | 30.0 | 18.0 | 16.8 | 17.3 | 26.1 | 15.8 | 15.1 |

## 3.3 Reactor Gas Analysis

All three CLC pilot systems described above were equipped with online gas analyzers to measure the gas composition of the AR and FR flue gases. The gas analysis systems for each reactor consist of a gas conditioning system and a gas analyzer. The gas conditioning system condenses the moisture from the sampled gas, so water does not affect the analyzer operation. FR flue gas sampling on the 100 kW and 10 kW CLC pilots also includes additional filtration and condensers which clean the sampled gas from particles and excess water. The FR flue gas analyzers measure concentration of $CO_2$, CO, $CH_4$, $H_2$ and $O_2$, while the AR flue gas analyzers measure $CO_2$, CO and $O_2$ concentration. Gas analysis of the flue gas is the key process measurement that allows for calculating critical operation performance parameters of carbon capture efficiency and gas conversion efficiency. More details on the gas analysis (analyzer model, measurement principle, measurement range, uncertainty, sampling rates) are provided in Papers I through V.

## 3.4 Alkali Measurement System

There are several methods for measuring gas-phase alkali emissions. Offline measurement methods include gravimetric sampling of condensed alkali particles with impactors or filters, followed with subsequent ex-situ analyses of the collected particles. These methods are useful for speciation of the collected alkalis but can only quantify average emissions over extended measurement periods. Online methods include optical-based methods such as excimer laser induced fragmentation fluorescence (ELIF)[79], tunable diode laser absorption spectroscopy (TDLAS)[80], inductively-coupled plasma optical emission spectroscopy (ICP-OES)[81], molecular beam mass spectroscopy (MBMS)[82] and thermal methods such as volatility tandem mobility analysis (VTDMA)[83]. ELIF and TDLAS are in-situ techniques and are not suitable for alkali measurements in CLC since the AR and FR flue gas streams are typically laden with oxygen carrier fines. The ICP-EOS technique is extractive, but is complex and impractical for implementation in a CLC pilot. The VTDMA technique is also extractive but is complex and involves long stable operation periods which are difficult to maintain in experimental CLC campaigns.

The surface ionization detector (SID) is another online extractive alkali measurement technology that has been successfully implemented for alkali emission measurements in bench-scale experiments [51,84] and industrial scale investigations [72,83]. Experience from these studies shows that the SID technique is relatively easy to implement and allows for sensitive measurement of total alkali species that contain K and Na [51]. For these reasons the SID technology was chosen as the main alkali measurement methodology for the investigations presented in Papers I through V. In Paper V, impactor-based alkali measurements were also carried out concurrently with SID measurements. In Paper VI, the SID technique was validated vs. the collinear photofragmentation and atomic absorption spectroscopy (CPFAAS) technique. The following subsections provide a detailed overview of

the SID technique and brief overviews of the impactor-based and CPFAAS alkali measurement methodologies.

### *3.4.1 Surface Ionization Detector (SID) Alkali Measurement System*

A schematic of the entire SID-based alkali measurement system, as implemented in experiments presented in Papers II-V, is shown in Figure 6. This system consists of three main sub-systems: the sampling and dilution system, the SID instrument, and the calibration system.

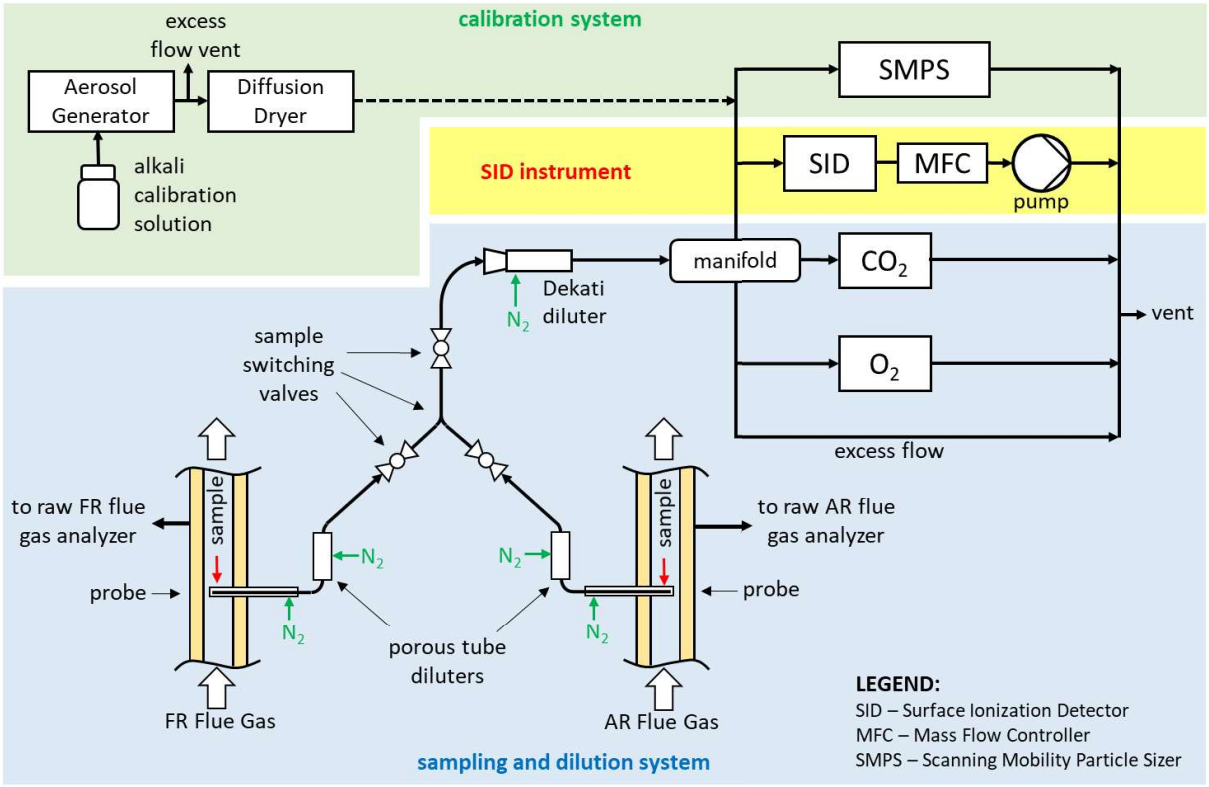


***Figure 6 – SID calibration system, SID instrument, and sampling and dilution system simplified schematic diagram***

## *Surface Ionization Detector (SID) Instrument*

The SID implemented in the experiments covered in this thesis was developed based on previously implemented SID designs [85], but includes several modifications. A simplified diagram of the SID is presented in Figure 7.

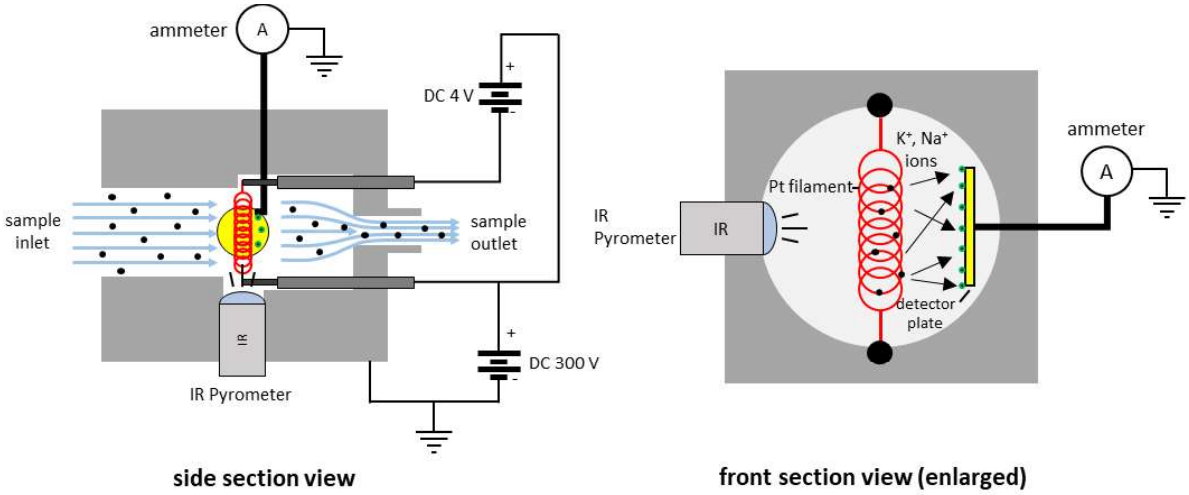


***Figure 7 – Surface ionization detector (SID) instrument side and front section view schematic***

The SID implemented in this work is a straight path flow-through device. The sample flow path is cylindrical with an inner diameter of 25 mm. A 0.2 mm diameter platinum filament formed into a loose coil is installed in the flow path of the sample. This filament is resistively heated and positively biased with DC 300 V. A metal detector plate is installed adjacent to the coil and is connected to highly sensitive ammeter capable of measuring current down to the picoampere level. An infrared pyrometer is installed opposite the coil for monitoring of the filament temperature.

In operation, gas containing condensed alkali aerosol flows through the SID, passing by the Pt filament. The sample flow is drawn by a pump at the outlet of the SID instrument. The flow is controlled by an electronic mass flow controller (MFC) set to 0.5 $L_n$/min. The Pt filament is maintained at 1100 $^oC$ with the temperature monitored by the IR pyrometer. Flowing alkali particles in the vicinity of the hot filament melt on the surface of the platinum. Surface ionization on platinum selectively ionizes $K^+$ and $Na^+$ cations, which are then pushed away from the Pt filament due to its DC 300 V positive bias. $K^+$ and $Na^+$ ions that impact the collector plate induce a current which is measured by the ammeter. The current measured by the ammeter can be directly correlated to the alkali concentration in the sample. The SID is capable of detecting alkalis in condensed and gaseous form. However, direct sampling of flue gas (typically at 900 $^oC$ or more), results in uncontrolled condensation of alkali onto the walls of the sampling lines that lead to the SID instrument. To minimize such losses, the sample drawn from the flue gas has to be conditioned to induce controlled nucleation of alkalis in the sample flow. The setup of the SID-based alkali measurement system for use in CLC underwent significant and progressive development from the prototype used in experiments presented

in Paper I to the fully developed modular SID-based measurement system used in experiments presented in Papers IV.

### *Sampling and Dilution System*

The sampling and dilution system was designed to be able to sample flue gas from both, the FR and AR reactors. However, only one reactor, either the AR or the FR, can be sampled at a time. Switching the system from one reactor to the other requires manual manipulation of the sample switching valves. During sampling, the sample is drawn from the flue gas of the reactors with a specially designed sample probe. A schematic of the sample probe is shown in Figure 8.

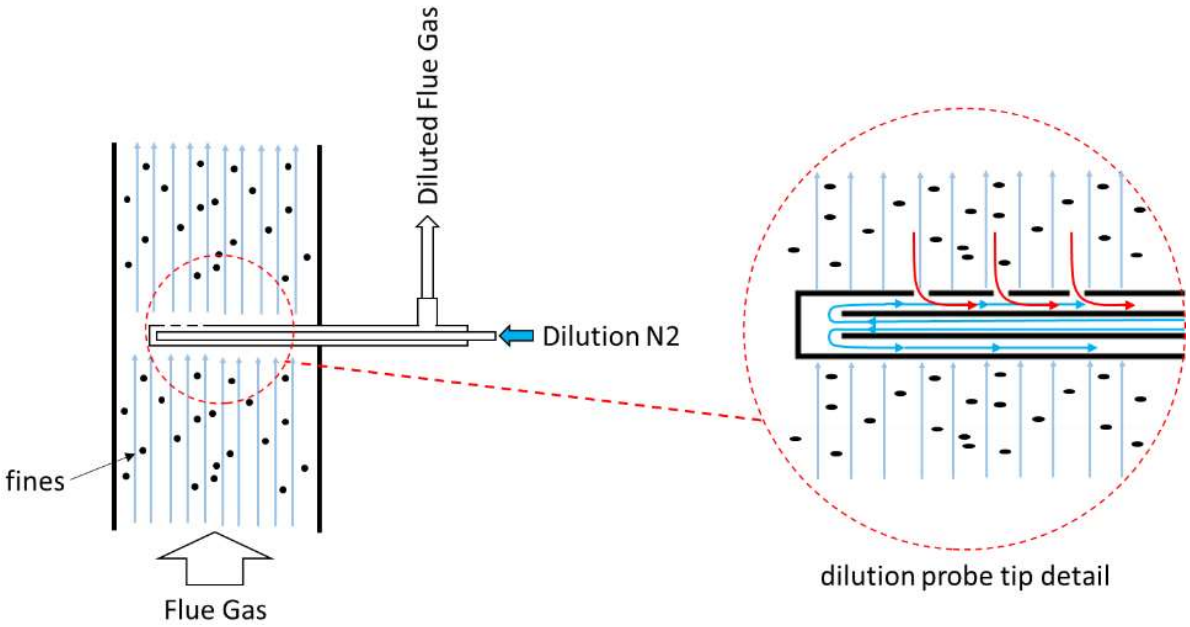


***Figure 8 – Alkali sampling probe schematic***

The probe is designed to simultaneously sample and dilute the flue gas. Dilution nitrogen is delivered to the probe tip via a 3 mm outer diameter tube installed in the center of the 10 mm inner diameter probe body. The sample is sucked from the flue gas through three 1 mm holes. Once the sample enters the probe body it is mixed with the dilution nitrogen and travels out of the probe in the annular space of the probe. The sample probe is mounted to protrude into the center of the flue gas flow and is oriented such that the sample suction direction opposes the flue gas flow direction. This is done in order to minimize ingress of solid fly ash and elutriated oxygen carrier fines.

The diluted sample leaving the sampling probe travels to a porous tube diluter to undergo further dilution by nitrogen. The porous tube diluter was installed immediately outside of the insulation of the flue gas chimney, such that the hot flue gas sample is cooled and diluted from process conditions of approx. 900-1000 $^{o}$C down to approx. 30 $^{o}$C. A schematic of the porous tube diluter is shown in Figure 9.

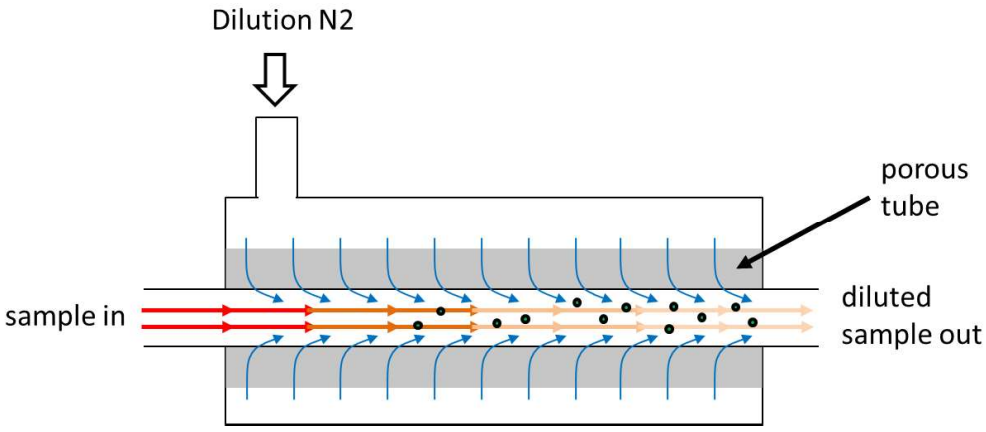


***Figure 9 – Porous tube diluter schematic***

Nitrogen in the porous tube diluter flows inward into the sample path through a porous tube. As the sample travels through the diluter, it is diluted and cooled, and the residual alkalis present in the sample nucleate to form solid particles. From the porous tube diluter, the sample proceeds to the final stage of dilution that is carried out in the Dekati diluter. The Dekati diluter is essentially a venturi device that uses nitrogen as the motive gas and a dilution medium. The venturi suction of this diluter is responsible for creating stable sample suction from the process, through the probe and the porous tube diluter. The Dekati diluter expels the diluted sample to the distribution manifold where the flow is split between the SID detector, the $CO_2$ analyzer (LICOR LI-850), and the trace $O_2$ analyzer (Alpha Omega Instruments 3000-Y230BTP).

The targeted overall dilution ratio of the system is approximately 50 to 500 times. The dilution ratio has to be adjusted during the sampling campaigns to account for a wide range of alkali emission rates such that the diluted sample alkali concentration is within the calibrated measurement range of the SID detector. In order to control dilution, the nitrogen flows to the sampling probe and the porous tube diluter are controlled by electronic mass flow controllers. Directly setting the dilution rate of the system is not possible since there is no direct measurement of the suction flow, which tends to be unstable due to probe plugging and process pressure variations. Accurate determination of the dilution ratio is critical for recalculating the measured alkali emissions back to raw flue gas basis. When sampling the FR, dilution is tracked using $CO_2$ as a tracer gas. $O_2$ is used as the tracer gas when sampling the AR. In both cases, the sampling dilution ratio is calculated by dividing the raw flue gas concentration of the tracer gas (reported by the main process analyzers) by the diluted sample concentration of the tracer gas (reported by the $CO_2$ and trace $O_2$ analyzers of the SID measurement system). Details on data processing and calculation of raw flue gas alkali emissions are provided in Chapter 4.

### *SID Calibration System*

Calibration of the SID is carried out by generating a polydisperse aerosol of solid KCl of different mass concentrations, and sampling it simultaneously with the SID detector and the

scanning mobility particle sizer (SMPS) (TSI SMPS 3082 & CPC 3750). Comparison of the SID signal against the aerosol's mass concentration, reported by the SMPS, establishes the SID's calibration curve. In the calibration system an aerosol of fine aqueous droplets is generated by an aerosol generator (TSI 3073) using a 0.005 M solution of KCl in deionized water. From the aerosol generator the aqueous aerosol flows through a diffusion dryer. In the dryer the fine aqueous aerosol nucleates into solid KCl particles. The resulting solid KCl aerosol is fed to the SID and the SMPS. The aerosol's mass concentration is controlled by a pressure setting on the aerosol generator. Calibration of the SID system is typically carried out at the start and end of each measurement campaign day.

### *3.4.2 Impactor-based Alkali Measurements*

A cascade impactor alkali measurement system was used in the experimental study presented in Paper V. The cascade impactor is a flow-through device for sampling particles from an exhaust flow. The cascade impactor consists of multiple impactors in series. Each impactor consists of an internal flow channel that forces the sample flow through a sharp directional change around an impaction surface. Large particles with high inertia are unable to make this flow direction change and end up hitting the impaction surface, where they are collected. Smaller particles of lower inertia are able to make the directional change and flow through to the next impactor stage. In a cascade impactor, the stages are designed and arranged such that each consecutive stage traps progressively smaller particles. Since impactors physically collect particles, they allow for gravimetric and chemical analyses of the collected, size-classified particles. In Paper V, cascade impactor measurements were used for determination of particle mass concentration and mass size distribution in the 60 kW D-CFB CLC pilot flue gas. Chemical analysis of the collected particles was then used to establish the speciation of condensed alkali species collected from the pilot's flue gases. Furthermore, cascade impactor alkali measurements performed in tandem with SID alkali measurement provided a basis for validation of the SID technique. A detailed description of the cascade impactor system is available in Paper V.

### *3.4.3 Collinear Photofragmentation and Atomic Absorption Spectroscopy (CPFAAS)*

Collinear photofragmentation and atomic absorption spectroscopy (CPFAAS) is an in-situ laser diagnostic technique capable of measuring gaseous alkali emissions. In experiments presented in Paper VI, CPFAAS was used in tandem with the SID-based alkali measurement system for measurement of gaseous alkalis in a propane flame doped with alkali solutions. Although this investigation did not specifically address alkali emission in CLC, the work presented in Paper VI was important for validating SID-based alkali measurement methodology – the key analytical method used in investigation alkali release in the CLC experiments presented in Papers I through V.

## 3.5 Thermodynamic Modelling

Thermodynamic modelling was used in Paper V to investigate the speciation of gaseous alkalis released in fuel conversion at CLC conditions, and to determine possible interactions between the fuel and the oxygen carriers. Furthermore, thermodynamic modelling results were instrumental for interpretation of impactor sample chemical analyses. Thermodynamic modelling was carried out in FactSage 7.2 software. This thermodynamic modelling software is based on Gibbs free energy minimization in a mass balance constrained system. The model assumes ideal mixing and is not constrained by mass transport or chemical reaction kinetics. In reality, the lack of transport and chemical kinetic limitations and perfect elemental mixing are highly unlikely since biomass is a highly heterogeneous and multi-phase fuel. However, as demonstrated in several studies by other researchers [59,61,86], thermodynamic modelling provides relevant qualitative information about alkali speciation. A detailed description of the thermodynamic modelling methodology is provided in Paper V.

CHAPTER 4

# 4. Data Processing and Analysis

Data and results from the investigations presented in Papers I through V can be divided into two categories:

1. Data relevant to general CLC system performance
2. Data relevant to alkali investigation

The following sections discuss the data and relevant calculations for both categories.

## 4.1 CLC Performance Data and Calculations

Although the work presented in this thesis is primarily focused on alkali-specific issues in CLC, this work is invariably tied to efforts to develop biomass CLC technology for efficient carbon capture from thermal conversion of biomass. As such, Papers I-IV also evaluate the fuel conversion and carbon capture efficiency of the pilot systems, and perhaps even more importantly, the performance of different combinations of OC materials and biomass fuels. Key performance parameters for CLC operation that are discussed below are all based on the online analysis of FR and AR flue gas composition and process measurements of flow and pressure. Reactor gas analysis was covered in Section 3.3.

### *4.1.1 Carbon Capture Efficiency*

Carbon capture efficiency is arguably the most important parameter in evaluating CLC system performance. There are several ways to calculate carbon capture efficiency of a CLC system, but the most practical method is to calculate the oxide oxygen efficiency. Oxide oxygen efficiency is accepted as a direct equivalent of carbon capture efficiency but is conveniently calculated solely based on measurements of the AR gas composition. Oxide oxygen efficiency is defined as the ratio of the oxygen used for oxidation of the OC in the AR, to the total oxygen consumed in the AR. It is calculated as follows:

$$\eta_{oo}[\%] = 100 * \frac{0.2099 - (1+d)x_{O2,AR} - (1+d)x_{CO2,AR}}{0.2095 - (0.9996+d)x_{O2,AR} - 0.2095x_{CO2,AR}} \quad \text{(Eq.1)}$$

Where:

$$d = \frac{\dot{Q}_{dilution\ N2}}{\dot{Q}_{air}} \quad \text{(Eq. 1.1)}$$

In the definition above, $d$ is the ratio of the dilution nitrogen flow introduced into the AR to the AR's fluidizing air flow. The origin of this dilution nitrogen varies for different pilot systems, but typically comes from nitrogen purge gas used for purging pressure taps and from nitrogen used as the fluidization gas in loop seals. Coefficients in Eq. 1 also account for the fact that air fed into the AR contains 400 ppm of $CO_2$.

### *4.1.2 Oxygen Demand and Gas Conversion Efficiency*

Oxygen demand is another critical parameter in evaluating CLC operation as it reflects the extent of fuel conversion. Oxygen demand is defined as the ratio of the additional oxygen required to fully oxidize the flue gas of the fuel reactor, to the stoichiometric oxygen required for complete fuel conversion. Essentially, oxygen demand represents an amount of oxygen that is lacking to complete the fuel conversion. Oxygen demand is calculated as follows:

$$\Omega_{OD}[\%] = 100 * \frac{0.5x_{CO,FR} + 2x_{CH_4,FR} + 0.5x_{H_2,FR}}{\Phi_o(x_{CO_2,FR} + x_{CO,FR} + x_{CH_4,FR})} \quad \text{(Eq. 2)}$$

Here $\Phi_o$ is the molar ratio [mol $O_2$ required for combustion/kg fuel] / [mol C/kg fuel].

Gas conversion efficiency is a closely related parameter which indicates the completeness of gas conversion which occurs in the fuel reactor. Gas conversion efficiency is defined as:

$$\eta_{g.c.}[\%] = 100\% - \Omega_{OD} \quad \text{(Eq. 3)}$$

It should be noted, that $\Omega_{OD}$ and $\eta_{g.c.}$ parameters do not account for the potential unconverted fuel that escapes with the fuel reactor flue gas as unconverted char. Char loss is typically accounted for separately. Higher order hydrocarbon species (C2, C3, etc.) are also not accounted for, but have been shown from previous CLC operation to be minimal.

### *4.1.3 Circulation Index*

Oxygen carrier circulation is the most important control variable for CLC system operation. Oxygen carrier circulation essentially sets the oxygen carrier residence time in different parts of the CLC system and thus directly affects oxygen transport rates, times available for reaction, in-bed mixing, and other aspects of operation. Circulation cannot be directly controlled but can be manipulated by changing reactor fluidization flows and system inventory. Direct determination of system circulation is very challenging and is system specific. For this reason,

circulation is typically monitored by tracking a proxy variable called the circulation index (CI). This parameter was used in the study presented in Paper II. CI for the 10 kW CLC pilot is calculated as a product of the AR riser pressure drop and the air flow rate of the AR.

$$CI = \triangle P_{AR\ riser}\ \dot{Q}_{AR\ air} \quad \text{(Eq. 4)}$$

## 4.2 Alkali Emissions Data and Calculations

Data collected for calculation of alkali emissions measured from the SID consists of the amperage signal measured by the SID, the FR raw flue gas $CO_2$ concentration measured by the main process gas analyzer, the diluted sample $CO_2$ and $H_2O$ concentrations measured by the LICOR $CO_2$ analyzer, the AR raw flue gas $O_2$ concentration measured by the main process gas analyzer, and the $O_2$ concentration measured by the Alpha Omega trace $O_2$ analyzer. Aside from the SID signal, all other data is used solely for the determination of the dilution ratio that is used to correct the alkali concentration measured by the SID. Before calculation of the dilution ratios, the diluted $CO_2$ and $O_2$ sample concentrations are analyzed to eliminate values which are clearly outside the measurement range of the instruments. Eliminating such values helps improve the integrity of the final calculated alkali concentrations. The dilution ratio for FR alkali measurements is calculated as follows:

$$DR_{FR} = \frac{CO_{2\ FR\ undiluted\ (dry\ basis)}}{CO_{2\ diluted\ sample\ (dry\ basis)}} \quad \text{(Eq. 5)}$$

In Eq. 5, the undiluted $CO_2$ concentration is reported on dry basis by the main process analyzer. The diluted sample $CO_2$ concentration, however, is reported on wet basis by the LICOR instrument and must be recalculated to dry basis using the diluted sample $H_2O$ measurement reported by the LICOR analyzer.

For alkali measurements in the AR reactor, $O_2$ is used as a tracer gas for determining the dilution ratio. The dilution ratio for AR alkali measurements is calculated as follows:

$$DR_{AR} = \frac{O_{2\ AR\ undiluted\ (dry\ basis)}}{O_{2\ diluted\ sample\ (wet\ basis)}} \quad \text{(Eq. 6)}$$

In Eq. 6, the undiluted $O_2$ concentration is reported on dry basis by the main process gas analyzer. The diluted concentration is reported on wet basis by the Alpha Omega trace $O_2$ analyzer. Since the AR flue gas contains very little moisture, the diluted sample $H_2O$ content is insignificant. For this reason, the wet basis oxygen concentration of the diluted sample is used in Eq. 6.

Once the dilution ratio of the alkali measurements is calculated, the undiluted raw flue gas concentration is calculated as follows:

$$K_{eq}\left[\frac{mg_{K\_eq}}{m_n^3}\right] = A_{SID}\ C_{SID}\ DR\ (\frac{298\ K}{273\ K}) \quad \text{(Eq. 7)}$$

In Eq. 7, $K_{eq}$ is the alkali concentration reported in potassium equivalents in units of mg of potassium equivalents per $m^3_n$, $A_{SID}$ is the SID signal in units of nanoamperes (nA), $C_{SID}$ is the SID calibration constant in units of mg K/(nA $m^3_n$), $DR$ is the dimensionless dilution ratio, and the last factor is temperature correction factor required for calculation on the basis of $m^3_n$.

The alkali concentration values obtained from the calculation in Eq. 7 are carefully reviewed and outlier values that can result from dilution system instability or from transient events, such as switching the sampling between reactors, are removed to minimize erroneous data. Once the final raw flue gas concentrations are obtained, the mass flowrate of gas-phase alkalis can be calculated as the product of the alkali flue gas concentration and the flue gas flowrate. The flue gas flowrates of both reactors are not measured directly and have to be calculated on the basis of a nitrogen balance. For each reactor, the main gas analyzers report the concentration of CO, $CO_2$, $CH_4$, $H_2$, and $O_2$. It is assumed that the remainder of the dry gas fraction is composed of $N_2$.This assumption has been validated in prior operation by directly measuring the $N_2$ concentration in the reactor flue gases with a micro gas chromatograph instrument. Thus, the dry basis nitrogen mole fraction can be calculated as:

$$x_{N_2(dry)} = 1 - (x_{CO} + x_{CO_2} + x_{CH_4} + x_{H_2} + x_{O_2}) \quad \text{(Eq. 8)}$$

The input of $N_2$ to each reactor is known as it consists of the loop seal fluidization nitrogen, purge nitrogen, and for the AR, the nitrogen that comes in with the fluidizing air. For each reactor system these flows are measured or can be calculated. The fluidization steam input to the FR is also measured on each reactor system. Thus, knowing the flow rate and concentration of $N_2$ is each reactor and knowing the steam input rate into the FR, reactor flow rates can be calculated as follows:

$$\dot{F}_{AR} = \frac{\sum \dot{F}_{N_2,AR}}{x_{N_{2(dry),AR}}} \quad \text{(Eq. 9)}$$

$$\dot{F}_{FR} = \frac{\sum \dot{F}_{N_2,FR}}{x_{N_{2(dry),FAR}}} + \dot{F}_{steam,FR} \quad \text{(Eq. 10)}$$

The molar flowrates of Eq. 9 and 10, are easily converted to volume basis, using the ideal gas law.

CHAPTER 5

# 5. Main Results

The results summarized in this chapter cover the experimental work presented in Papers I through VI. The results are divided into several key topics:

1) Development of the SID-based alkali measurement system
2) Investigation of alkali release and distribution in CLC operation
3) Investigation of the interdependence of CLC process performance and alkali release

## 5.1 Development of the SID-based alkali measurement technique

Investigation of alkali release and partitioning in CLC systems was contingent on the development of a robust alkali emissions measurement method. The SID principle was chosen as it is relatively simple to implement, can provide online measurements of alkali release, and has been demonstrated for alkali emissions measurements in large-scale operation [72,83]. However, at the onset of this work it was known that CLC pilot operation is often less stable than industrial scale equipment. CLC pilots often exhibit reactor pressure fluctuations, and typically have significant elutriation of fine ash and bed material particles to the flue gases of the AR and the FR. For this reason, the development of a stable sampling and dilution system was a focal point for the design of the SID alkali measurement system. The basis for the SID system's design was a SID instrument that was used primarily for lab-scale investigations [85]. This design, however, had to be reworked and augmented to make a new SID system that is more robust and suitable for CLC operation. The key developments of the SID-based alkali system is outlined below.

### *Paper I (100 kW campaign):*

**New SID instrument** – A new custom-designed SID instrument was developed. To improve SID signal stability, the new SID was designed with a straight laminar flow path and an electronically controlled sample suction facilitated by a mass flow controller followed by a

sample suction pump. The implemented flow control is critical for maintaining stable instrument sample flow despite pressure fluctuations in the reactor system.

**New sampling and flow conditioning system** – A new sampling system was developed. This system consisted of a custom-built sample probe with an integrated dilution tip, a porous wall-flow diluter, a Dekati ejector diluter, and a flow distribution manifold. The sample probe and the porous diluters were equipped with mass flow controllers for precise control of dilution nitrogen. The ability to precisely control nitrogen dilution improved the sample dilution stability, which is critical for measurement stability.

**FR sample dilution tracking capability** – A trace $CO_2$ analyzer was implemented, allowing for accurate tracking of the sample dilution ratio during FR flue gas sampling by means of a $CO_2$ balance over the undiluted and diluted sample $CO_2$ concentration.

### *Paper II and III (10 kW commissioning campaign, and 60 kW D-CFB campaign)*

**Modularized and portable system** - The SID system developed for the experiments presented in Paper I was re-built into a modular and transportable system shown in Figure 10. This system consists of two modules. Module 1 (left in Figure 10) consists of the SID instrument, along with its auxiliary components, as well as an on-board calibration system. Module 2 (right in Figure 10) consists of the sampling, dilution, and dilution tracking systems. The sampling system was designed to allow easy switching between sampling of the AR and FR flue gases using a valve control panel.

**AR sample dilution tracking capability** - A trace $O_2$ analyzer was implemented, allowing for accurate tracking of the sample dilution ratio during AR flue gas sampling by means of an $O_2$ balance over the undiluted and diluted sample $O_2$ concentration.

### *Paper IV (10 kW LD Slag campaign)*

Particle handling capability – The LD slag oxygen carrier used in experiments presented in Paper IV exhibited high attrition, creating lots of fine particles in the AR and FR flue gases. This resulted in rapid plugging of the flow orifice of the Dekati diluter and malfunction of the SID mass flow controller. To address this issue, the system was modified to have particle trap upstream of the SID instrument. The sample suction was changed to be pump-driven and controlled by a rotameter set to choked flow conditions. Filters were added upstream of the SID and main sampling pumps in order to protect pump operation. This design modification allowed for relatively steady sampling of the particle-laden flue gases.

***Figure 10 – Modular SID alkali measurement system, as setup on the D-CFB pilot***

The SID measurement system described above proved to be effective in responding to and measuring alkali emissions during stable CLC operation and during transient operational events such as fuel feed startup and shutdown. This was first demonstrated in Paper I, and later confirmed in Papers II, III and IV. However, fast transient events, such as switching the sampling between the AR and the FR proved to cause signal instability. Since the occurrence of such signal instability could not be resolved at the operational level, removal of unstable measurement data was integrated into the SID data processing routine.

### *5.1.1 Validation of the SID-based measurements*

Beyond proving the SID system's effectiveness, the validity of the SID-based alkali measurements was evaluated in two separate experimental investigations. The investigation presented in Paper VI compared the SID alkali measurement methodology to an independent in-situ laser diagnostic method called collinear photofragmentation and atomic absorption spectroscopy (CPFAAS). CPFAAS is capable of measuring KOH and KCl concentrations in clean gas environments. The measurements using both systems, SID and CPFAAS, were performed in a propane gas burner facility. During experiments, various aqueous alkali solutions (KCl and NaCl), along with varying amounts of HCl and $SO_2$ were injected into a propane flame. HCl and $SO_2$ were added to induce changes in sulfation of the alkali chloride salts. The experiments showed that SID and CPFAAS measurements are in good agreement (within 10% of each other) when measuring KCl. The experiments also showed that the SID measures KCl and NaCl equivalently, but that the SID's response to $K_2SO_4$ is much weaker than to KCl. Additional SID calibration experiments established that the SID instrument has a different response to different potassium salts. Figure 11 from Paper VI shows the difference in SID's response to a few different alkali compounds.

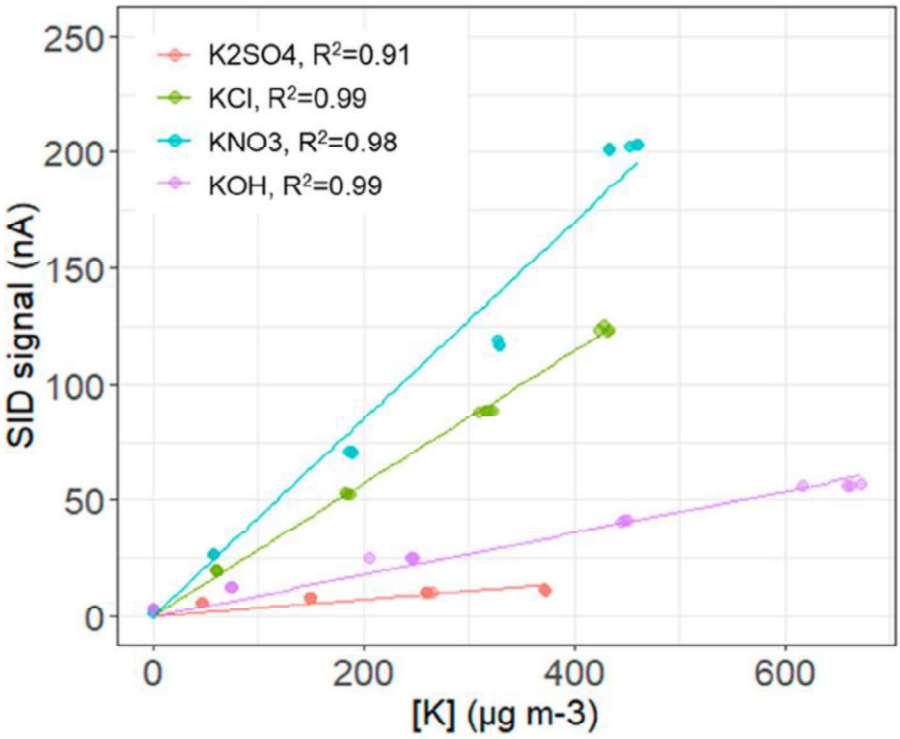


***Figure 11 – SID response to different potassium species*** *[87]*

The implication from these findings is that a SID signal measured in CLC pilot experiments is influenced by the speciation of the gaseous alkalis. Alkali emissions measurements in Papers I through III are reported in mass units of $KCl_{eq}$. This unit is used since KCl solution is used for SID calibration. The unit reflects the amount of detected alkalis, with the assumption that all detected alkalis are in the form of KCl. The unit of $KCl_{eq}$ is sufficient for comparison of relative alkali release, but not appropriate for quantifying total alkali release. Since the actual alkali speciation of the flue gas samples in CLC operation is not known, a given SID signal may be a result of different amounts various alkali species. As discussed later in Section 5.2.7, Study V established that KCl and KOH are the major gaseous species released in CLC of biomass. Thus, when attempting to quantify the total alkalis released, it is more appropriate to express the SID measurement results as a range. In this range, the minimum corresponds to alkali amounts assuming all alkalis are in the form of KCl, while the maximum corresponds to alkali amounts assuming that all alkalis are in the form of KOH. The actual amount of alkalis, K and Na, should be within this range. This approach was applied in Paper IV and to the results presented in this chapter. Studies I-III used $KCl_{eq}$ basis for estimation of total alkali release since the dependency of the SID signal was not yet established at the time of the experiments. Further to the response to different alkali species, calibration experiments in Paper VI established the influence of the SID sample flow, the Pt filament temperature, and the filament bias voltage on the accuracy of the SID signal. The effects and typical deviations of these parameters were used to determine that the SID system's inherent measurement uncertainty is +/- 1.9%.

Another validation of the SID measurement principle was conducted in Paper V, where SID results were compared to cascade impactor alkali measurements. Paper V concluded that SID

and impactor-based alkali measurements are in good agreement for CLC tests that exhibited high gaseous alkali concentrations in the FR flue gases. The validations in Paper VI and V, reinforce the validity of the SID-based alkali emissions measurement methodology.

## 5.2 Investigation of alkali release and distribution in CLC operation

Alkali emissions were measured with the SID-based alkali measurement system in four experimental campaigns presented in Papers I through V. The main observations and findings are summarized in the following sub-sections.

### *5.2.1 Alkali Emissions vs. Fuel Alkali Content*

The choice of fuel in CLC operation is perhaps the most significant parameter for biomass CLC operation. Figure 12 summarizes the average FR alkali emissions collected in the experiments presented in Papers I-IV. The results have been recalculated to basis of mg $KCl_{eq}$/kg fuel, in order to make the results comparable between the different pilot scales used in the experiments. Fuels are listed in order of increasing alkali content. Each fuel's alkali content, in units of mg alkali per kg fuel, is shown below the fuel labels.

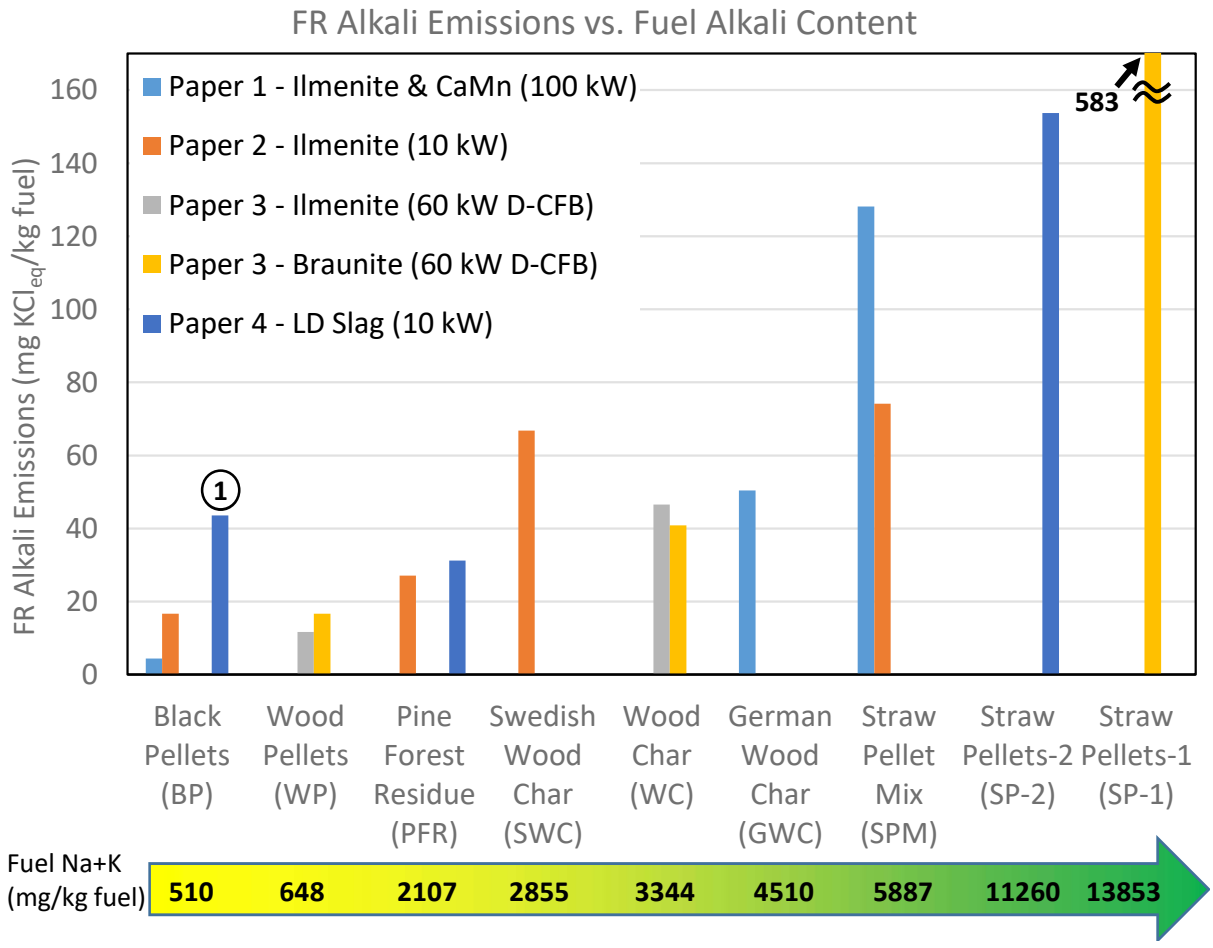


***Figure 12 - Average FR alkali emissions (Papers I – IV)***

Figure 12 clearly shows that FR alkali emissions grow with increasing fuel alkali content. Only one point of deviation to this trend is present in the results (marked with a numbered circle). This deviation is likely a result of significant SID calibration issues experienced on the day of operation when the data for BP fuel operation in Paper IV was collected. AR alkali emissions for CLC operation in experiments presented in Papers I through IV are presented in Figure 13.

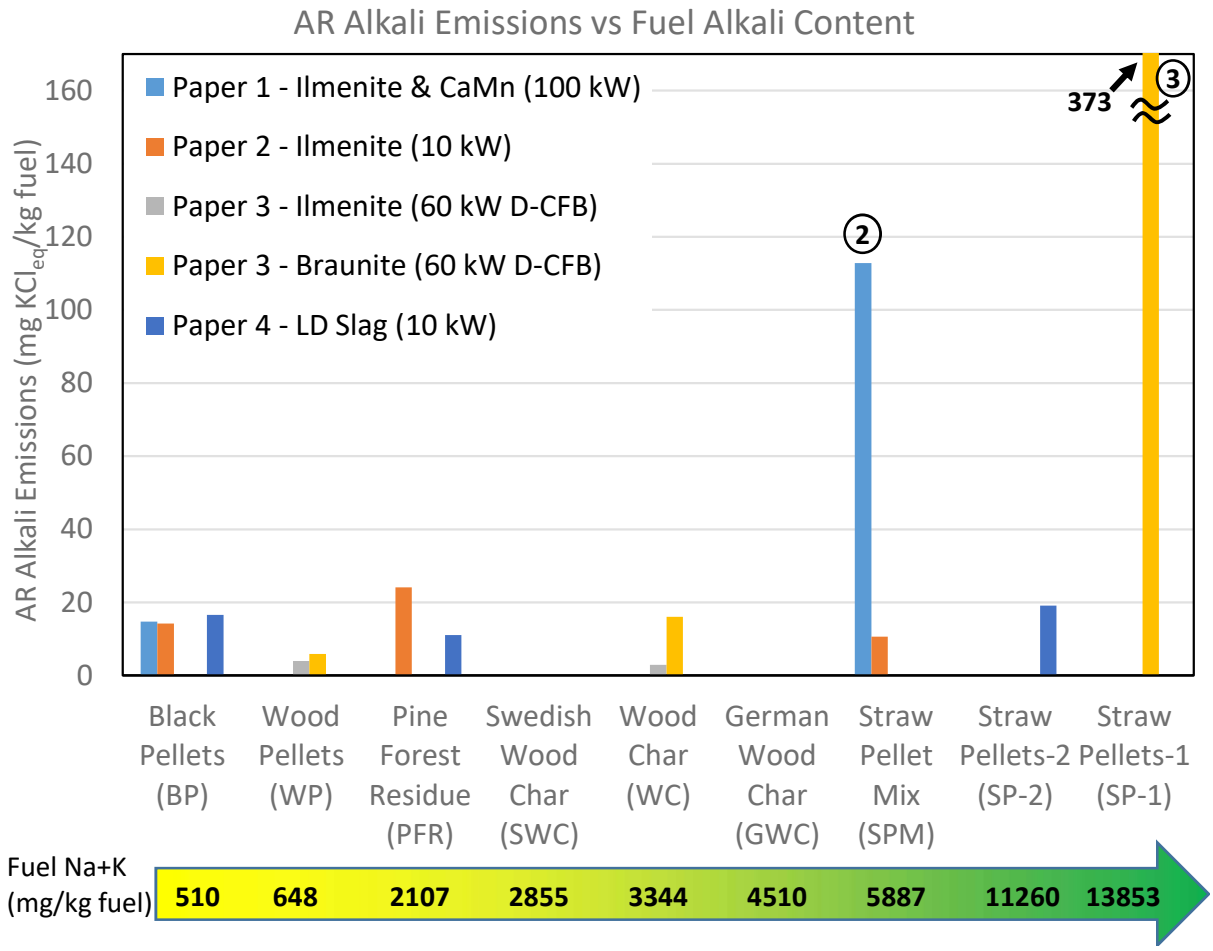


***Figure 13 - Average AR alkali emissions (Papers I – IV)***

Results presented in Figure 13 include two clear outliers, marked with numbered circles. Outlier #2, for SPM fuel operation in Paper 1, is most likely caused by error in estimating the dilution ratio of the SID sampling system. At the time of the experiments presented in Paper I, the SID sampling system did not yet have the capability to track AR sample dilution ratio by means of an $O_2$ balance. Dilution ratio of the sample was roughly estimated on the basis of sample suction and dilution flow, and was subject to significant error. Outlier #3, for SP-1 fuel operation in Paper III, is a result of upset system operation, where significant fuel and char carryover from the FR to the AR is suspected to have caused significant alkali release in the AR. This case is further discussed later in this chapter. Aside from the two outliers, the data summary presented in Figure 13 shows no consistent correlation between the fuel alkali content and the measured gas-phase alkali emissions in the AR.

### *5.2.2 Distribution of Gas-phase Alkalis in a CLC system*

The distribution of gas-phase alkalis between the AR and FR is summarized in Table 7 for the experiments presented in Papers I-IV. Table 7 data are expressed as percentage of the total alkalis incoming with the fuel. As discussed in Section 5.1, since the speciation of alkali emissions in Papers I-IV was not known, alkali levels measured by the SID are presented as a range. The range minimum corresponds to the SID signal expressed in terms of KCl equivalents, and the range maximum corresponds to the SID signal expressed in terms of KOH equivalents.

***Table 7 – Relative alkali distribution in CLC operation (Papers I – IV)***

| | Paper I Ilmenite + CaMn (100 kW) | | Paper II Ilmenite (10 kW) | | Paper III Ilmenite (60 kW D-CFB) | | Paper III Braunite (60 kW D-CFB) | | Paper IV LD Slag (10 kW) | |
|---|---|---|---|---|---|---|---|---|---|---|
| **Fuel** | **FR** | **AR** | **FR** | **AR** | **FR** | **AR** | **FR** | **AR** | **FR** | **AR** |
| BP | 0.7-2.5% | 1.8-5.9% | 1.7-5.7% | 1.5-4.8% | | | | | 5.0-16.5% | 1.9-6.3% |
| WP | | | | | 0.9-3.1% | 0.3-1.1% | 1.8-5.8% | 0.5-1.8% | | |
| PFR | | | 0.7-2.3% | 0.6-2.0% | | | | | 0.8-2.6% | 0.3-0.9% |
| WC | | | | | 0.7-2.2% | 0.1-0.2% | 0.6-2.1% | 0.3-0.8% | | |
| SPM | 1.1-3.8% | 1.1-3.6% | 0.7-2.2% | 0.1-0.3% | | | | | | |
| SP-1 | | | | | | | 2.2-7.3% | 1.4-4.7% | | |
| SP-2 | | | | | | | | | 0.7-2.4% | 0.1-0.3% |

Table 7 shows that overall release of alkalis to the gas phase is in the range of 0.6-16.5% in the FR and 0.1-6.3% in the AR. For most of the tests in presented in Table 7 a lower percentage of fuel alkalis are detected in the gas-phase of the AR. Operation with BP fuel in Paper I results in higher alkali release measured in the AR than the FR. However, as mentioned prior, AR emissions in Paper I are subject to significant uncertainty since the SID sample dilution ratio was not precisely tracked. Several other cases, like BP and PFR fuel operation in Paper II, show that overall gas-phase alkali release is similar in the AR and the FR. Reviewing the actual measured gas-phase alkali concentrations measured in the flue gas by the SID (not shown here), shows that in all cases gas-phase alkali concentration is lower in the AR flue gas than in the FR flue gas. Thus, the driving force for release of alkalis to the gas phase is much lower in the AR. However, since the AR flue gas flow rate is 4 to 10 times higher than that of the FR, the overall net release of alkalis from the AR can in some cases equal that of the FR.

### *5.2.3 Origin of AR Alkali Emissions*

Further to relative comparison of AR and FR emissions, the measured levels of AR emissions are generally higher than expected. Since no fuel is fed into the AR during CLC operation, the alkalis released in the AR must be transported from the FR. Here, a few pathways are possible. One possibility is that some fraction of the biomass char is carried over to the AR along with the circulating OC bed material. Studies measuring release of alkalis from biomass report that only <10% of alkalis are typically released in the devolatilization stage of fuel decomposition [50,59]. After devolatilization, the temperature of the remaining char continues to rise towards the FR bed temperature, while steam gasification begins. As the temperature rises,

the primary gas-phase release of alkalis comes from evaporation of KCl, followed by decomposition of alkali carbonates and sulphates. Knudsen et al. [50] measured and modelled the high temperature dissociation reaction rates for potassium carbonates, sulphates, and silicates. Their work showed that carbonates begin to dissociate above 700 °C, sulphates above 900 °C, and silicates above 1200 °C. At the temperature of the FR, approximately 900-970 °C, the dissociation rate of KCl is fast, so release of KCl to the gas phase likely proceeds to completion. The dissociation rate of $K_2CO_3$ is slower, and very slow for $K_2SO_4$. Thus, with limited residence time in the FR, the unconverted char may carry over undissociated potassium carbonates and sulphates over to the AR. Another possibility for alkali carryover is that fuel ash that remains after char conversion can also be carried over to the AR by the bulk transport of the oxygen carrier. Fuel ash can contain alkalis such as silicates, but also possibly undecomposed carbonates and sulphates.

With either mode of transport, char-bound or ash-bound, condensed alkalis can continue their release to the gas phase in the AR. The bed temperature of the AR is typically 50 °C to 100 °C higher than that of the FR. Thus, the carried over ash is exposed to higher temperature in the AR than in the FR. This is also true for carried over char, although char readily burns in the AR and likely reaches local temperatures higher than that of the AR bed. In either case, the higher temperature may accelerate the dissociation of the carried over alkali compounds. The dissociation rate models from Knudsen et al. [50], show that for every 100 °C of temperature rise, potassium carbonate and sulphate dissociation rates increase roughly by a factor of 10.

Although in the presented experiments it was not possible to assess ash carryover, char slippage to the AR can be estimated by considering the carbon capture efficiency of the CLC systems. Average carbon capture performance for experiments conducted in Papers I-IV is presented in Table 8.

***Table 8 – Average carbon capture efficiency (Papers I – IV)***

| Fuel | Paper I Ilmenite & CaMn (100 kW) | Paper II Ilmenite (10 kW) | Paper III Ilmenite (60 kW D-CFB) | Paper III Braunite (60 kW D-CFB) | Paper IV LD Slag (10 kW) |
|---|---|---|---|---|---|
| **WP** | | | 74.0% | 87.1% | |
| **BP** | 99.4% | 99.0% | | | 98.5% |
| **WC** | | | 38.0% | 50.9% | |
| **PFR** | | 98.2% | | | 97.6% |
| **SWC** | | 95.4% | | | |
| **SPM** | 98.1% | 97.3% | | | |
| **SP-1** | | | | 79.4% | |
| **SP-2** | | | | | 97.1% |

Table 8 shows that carbon capture efficiency for experiments in Papers I, II, and IV was quite high. Experiments in Paper III achieved poor capture efficiency. Subtracting the carbon capture efficiency from 100% gives the approximate amount of the fuel's total carbon that was carried over from the FR to the AR. Converting this figure to the approximate share of char carryover requires making several assumptions.

The pilot reactors operated in experiments in Papers I, II, and IV use loop seals to avoid inter-reactor gas mixing, thus avoiding the slippage of fuel volatiles from the FR to the AR. The FR reactor designs of these pilots also allow for significant fuel residence time. In the 100 kW pilot in Paper I, significant fuel residence time is achieved by means of internal FR fuel re-circulation. In the 10 kW pilot in Papers II and IV, the large size of the bubbling fluidized regime FR assures significant fuel residence time. Due to the considerable fuel residence time, carryover of carbon from the FR to the AR likely occurs in the form of fully devolatilized char. Thus, for results from Papers I, II, and IV, char carryover can be estimated by recalculating the amount of total carried over carbon into fixed carbon equivalents.

The case in operation of the D-CFB pilot in Paper III is quite different. In this pilot unit, each reactor (AR and FR) is a circulating fluidized bed operated in the fast-fluidization regime. Since the FR in this system has no internal re-circulation, the fuel residence time was likely very short. Short fuel residence time gives rise to the possibility of carryover of either undevolatilized or partially devolatilized fuel. As such, for the results from Paper III, total char carryover is best estimated as a range. The range minimum corresponds to the char fraction in case of carryover of undevolatilized fuel (i.e., some of the carried over carbon can be volatile carbon). The range maximum represents the char fraction in case that all carried over carbon is fixed carbon. Char carryover estimates are presented in Table 9.

***Table 9 – Average estimated char carryover (Papers I – IV)***

| Fuel | Paper I<br>Ilmenite & CaMn<br>(100 kW) | Paper II<br>Ilmenite<br>(10 kW) | Paper III<br>Ilmenite<br>(60 kW D-CFB) | Paper III<br>Braunite<br>(60 kW D-CFB) | Paper IV<br>LD Slag<br>(10 kW) |
|---|---|---|---|---|---|
| **WP** | | | 3.6 - 89.0% | 1.8 - 44.2% | |
| **BP** | 1.6% | 2.7% | | | 4.0% |
| **WC** | | | 39.2 - 71.6% | 31.0 - 56.7% | |
| **PFR** | | 9.4% | | | 12.5% |
| **SWC** | | 4.9% | | | |
| **SPM** | 6.5% | 9.2% | | | |
| **SP-1** | | | | 3.5 - 52.0% | |
| **SP-2** | | | | | 7.7% |

Table 9 estimates indicate that moderate levels of char carryover likely occurred in operation of the pilot systems used in the experiments from Papers I,II, and IV. For D-CFB pilot operation in Paper III, the estimated char carryover was significant for the WC fuel, and potentially significant for the WP and SP-1 fuels. In all cases, it seems likely that char carryover is at least partially responsible for alkali release in the AR.

Finally, another possibility for the origin of AR emissions is that some alkali species may react with the oxygen carriers, forming condensed species that are stable in the reducing environment of the FR, but decompose to the gas phase in the oxidizing atmosphere of the AR. This carryover pathway was not evaluated in the work presented in this thesis and remains to be investigated.

### *5.2.4 Effect of Operating Temperature on AR and FR Alkali Emissions*

The effect of reactor temperature on alkali release was explored in Paper IV with experiments conducted at three reactor temperature levels. FR alkali emissions results vs. FR temperature are presented in Figure 14.

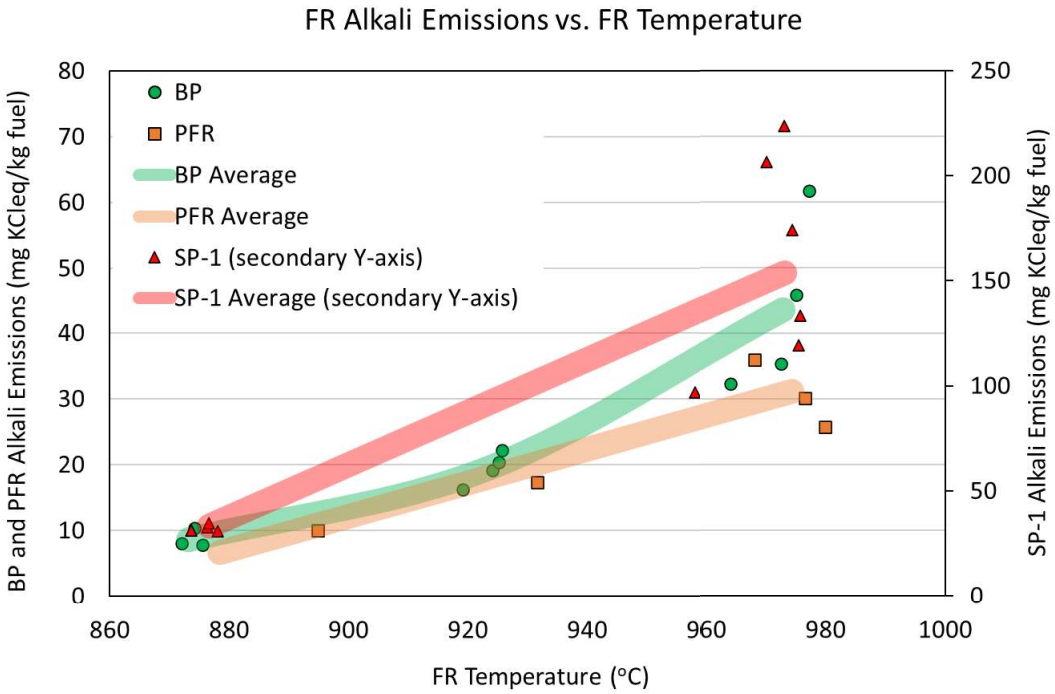


***Figure 14 – FR alkali emissions vs. FR Temperature (Study IV)*** *[88]*

In Figure 14, FR alkali emissions levels for tests with BP and PFR fuels are shown on the left Y-axis, while emissions levels for tests with SP-1 fuel are shown of the right Y-axis. Figure 14 clearly shows that FR emissions rise with FR temperature for all fuels. As mentioned in Section 2.4, the main mechanisms for volatilization of alkalis is the evaporation of KCl, followed by decomposition of potassium salts, such as $K_2CO_3$ and $K_2SO_4$. Both of these processes are accelerated at higher temperatures. KCl sublimation increases with temperature since the equilibrium vapor pressure of KCl rises sharply with temperature above temperatures of approx. 700 °C [50,59,61,64]. Decomposition of potassium salts to the gas phase is also accelerated at higher temperatures [50]. AR alkali emissions vs. AR temperature are shown in Figure 15.

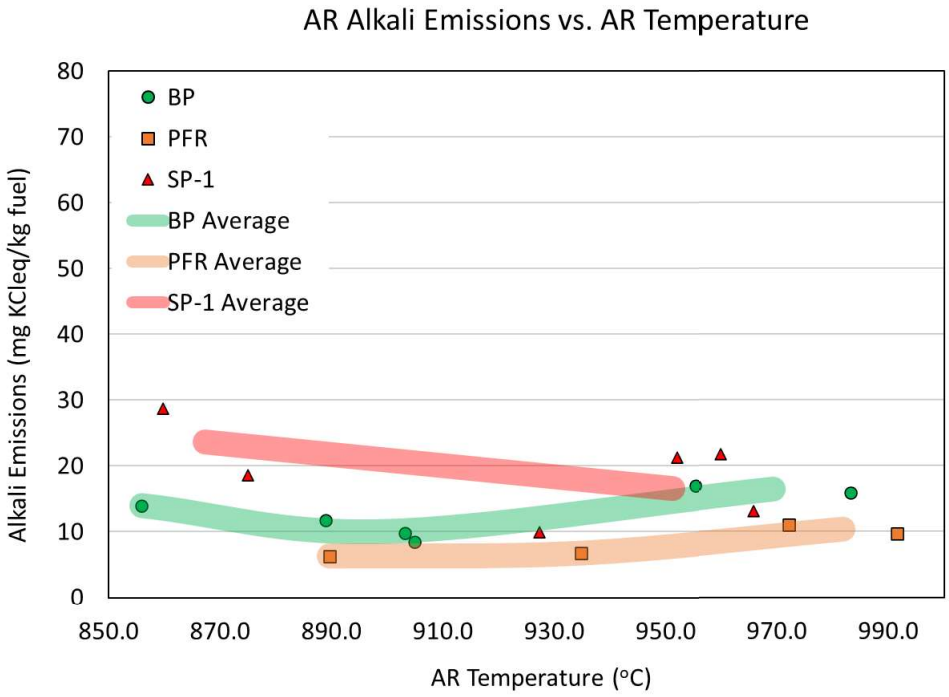


***Figure 15 – AR alkali emissions vs. AR Temperature (Study IV)*** *[88]*

Figure 15 shows that AR emissions do not show a consistent correlation with AR temperature. As mentioned earlier in this section, alkalis in the AR arise due to fuel char and/or ash carryover from the FR, or by absorption of alkalis by the OC in the FR followed by partial release of alkalis to the gas phase in the AR. For all these processes, higher temperature would likely increase the rate and driving force for volatilization of alkalis in the AR. On the other hand, higher AR temperature is associated with higher FR temperature and thus reduced char carryover and higher alkali release in the FR.

### *5.2.5 Effect of Chemical Looping Gasification (CLG) and Oxygen Carrier Aided Combustion (OCAC) Modes on Alkali Release*

Experiments in Papers III and IV explored the effect of different pilot operating modes on alkali emissions. CLC operation was compared to CLG operation in Paper IV. CLG operation can be established in a CLC pilot by decreasing the ratio of OC circulation to FR fuel feed such that only partial oxidation of the fuel of the OC occurs in the FR. The aim of CLG operation in Paper IV experiments was to produce an FR flue gas with a $CO:H_2:CO_2$ ratio of 1:1:1. This target gas quality was defined by a concurrent research project investigating chemical looping gasification performance. For investigation of alkali release, CLG operation presented an opportunity to evaluate how different FR atmospheres influence alkali release. Comparison of CLC and CLG operation for BP, PFR, and SP-2 fuels showed that alkali release in CLC and CLG modes is equivalent. Figure 16 shows an example of a transition from CLG operation to CLC operation for BP fuel.

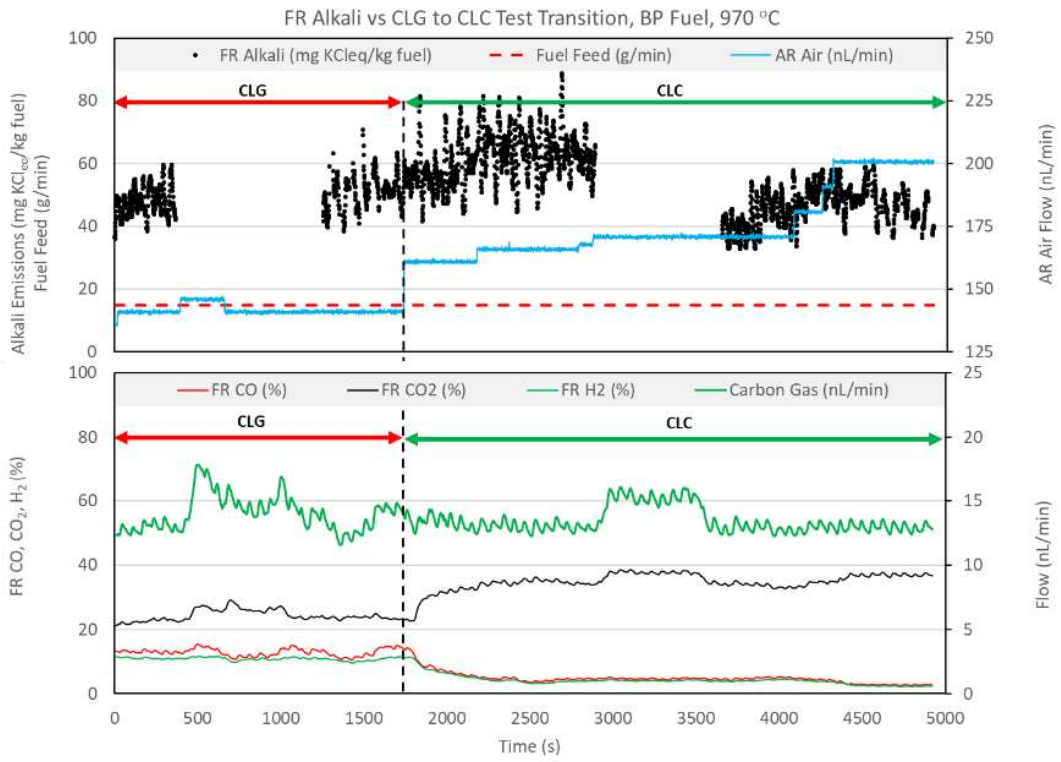


***Figure 16 - Effect of CLG vs CLC operation on FR alkali emissions (Paper IV)*** *[88]*

Figure 16 shows the FR alkali emissions, AR air flow rate, and BP fuel feed rate in the top plot section, and the corresponding gas concentrations in the bottom plot section. The transition from CLG to CLC operation is evident from the lowering of the CO and $H_2$ concentrations and the corresponding rise in $CO_2$ levels. The FR emissions initially increase slightly with the change to CLC operation, but then settle to the level similar to that in the preceding CLG period. Further analysis presented in Paper IV concluded that the majority of gaseous alkali release are associated with the extent of char conversion, which was determined to be similar for CLC and CLG operation of each of the fuels. Thus, the equivalent alkali emissions in CLC and CLG operation indicate that the more reducing atmosphere of CLG operation does not significantly influence net alkali release in the FR.

Experiments in Papers III and IV, compared alkali emissions in CLG operation vs OCAC operation. In OCAC operation, the FR is fluidized with air, instead of steam. This results essentially in conventional combustion operation, similar to that of a conventional CFB biomass boiler. The only difference is that unlike in a CFB boiler, the bed material is an oxygen carrier, which aids in buffering the oxygen concentration in the bed. Figure 17 shows an example of a test where OCAC operation with WC fuel and ilmenite OC is switched to CLC operation. Alkali emissions are plotted along with other key parameters.

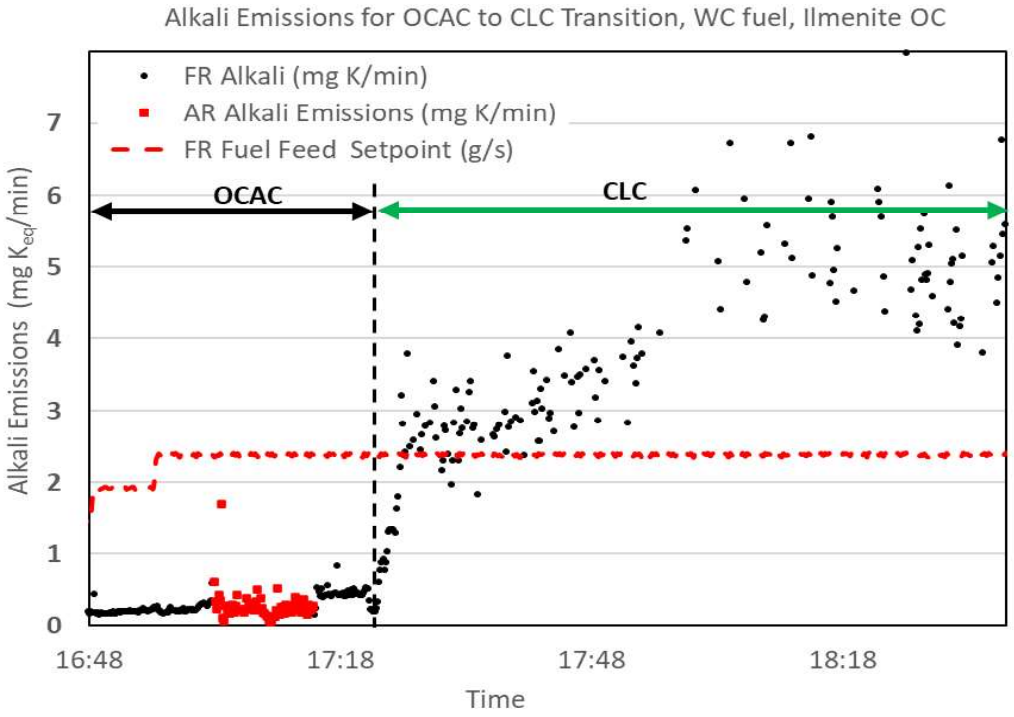


***Figure 17 - Alkali emissions for OCAC and CLC operation with WC fuel and ilmenite OC (Paper IV)*** *[78]*

Figure 17 clearly shows that a transition from OCAC to CLC operation results in a dramatic increase in FR alkali emissions. Figure 18 shows an example of a test where CLC operation with LD Slag OC and PFR fuel is transitioned to OCAC operation.

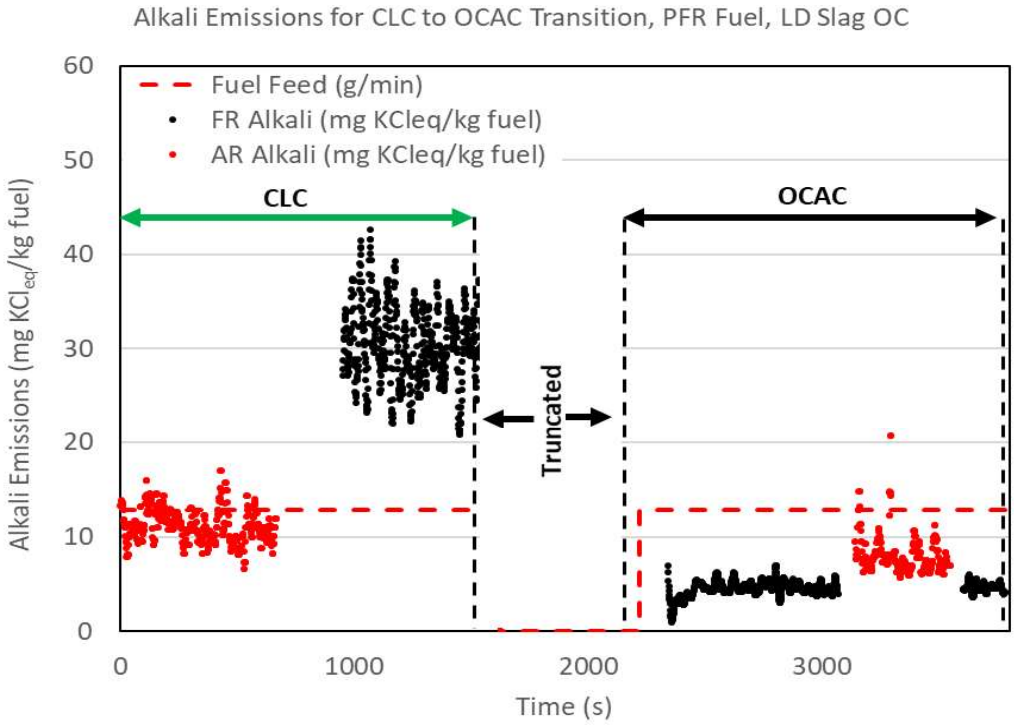


***Figure 18 - Alkali emissions for CLC and OCAC operation with PFR fuel and LD Slag OC (Paper IV)****[88]*

Figure 18 shows a dramatic drop in FR alkali emissions as operation is transitioned from CLC to OCAC operation. A comparison of average FR alkali emissions for all CLC-OCAC test pairs is summarized in Table 10.

***Table 10 – Average FR alkali emissions for OCAC-CLC test pairs (Papers III and IV)***

| | OC Material | Fuel | Fuel Alkali (mg K+Na/kg fuel) | OCAC FR Alkali Emissions (mg $KCl_{eq}$/kg fuel) | CLC FR Alkali Emissions (mg $KCl_{eq}$/kg fuel) | increase with CLC |
|---|---|---|---|---|---|---|
| **Paper III** | Ilmenite | WP | 648 | 3.7 | 11.7 | 217% |
| | | WC | 3344 | 4.3 | 46.6 | 983% |
| | Braunite | WP | 648 | 17.6 | 16.7 | -5% |
| | | WC | 3344 | 6.2 | 40.9 | 564% |
| | | SP-1 | 13853 | 37.1 | 583.1 | 1470% |
| **Paper IV** | LD Slag | BP | 510 | 6.9 | 19.4 | 181% |
| | | PFR | 2107 | 4.6 | 31.2 | 578% |
| | | SP-2 | 11260 | 32.0 | 153.7 | 380% |

With the exception of operation with braunite OC and WP fuel, all tests in Table 10 indicate that FR alkali emissions in CLC operation are much higher than in OCAC operation. Analysis of these results in Papers III and IV concluded that the CLC operation results in much higher emissions due to the presence of a steam-rich FR atmosphere in CLC operation. Specifically, after evaporation of alkalis in the form of KCl, the majority of the alkalis in the char conversion phase are thought to exist as $K_2CO_3$. Alkalis in the form of $K_2SO_4$ are less likely due to the low sulfur content of the fuels. In dry conditions, $K_2CO_3$ decomposes at temperatures approaching 900 $^oC$ via reactions R6 and R7[50].

$$K_3CO_3(s,l) \rightarrow CO_2(g) + K_2O(s,l) \quad \text{(R6)}$$

$$K_2O(s,l) \rightarrow K(g) + ½O_2(g) \quad \text{(R7)}$$

In contrast to this rather slow dry decomposition path, in wet conditions $K_2CO_3$ is known to undergo a much faster decomposition process by reacting with steam to form KOH(g) and $CO_2$(g) [50,59,89,90]. The wet decomposition path has been proposed to occur by a reaction of $K_2O$ with steam via reaction R8 [50] or as later proposed, by a direct reaction of $K_2CO_3$ with $H_2O$ via reaction R9[90].

$$K_2O(s,l) + H_2O(g) \rightarrow 2KOH(g) \quad \text{(R8)}$$

$$K_2CO_3(s,l) + H_2O(g) \rightarrow 2KOH(g)+CO_2(g) \quad \text{(R9)}$$

In competition with condensed-phase alkali retention via silicate formation, the faster wet decomposition of $K_2CO_3$ results in higher net release of alkalis to the gas phase. Furthermore, the onset of the wet decomposition process has been shown to occur at temperatures as low as 700 $^oC$, vs. the dry path only becoming significant at temperatures over 900 $^oC$ [50,89,90].

### *5.2.6 Effect of Steam on Alkali Release in CLC*

This hypothesis of steam enhanced alkali release was directly tested in experiments covered in Paper IV by observing the FR alkali emissions response to changes in the steam flow rate. In these tests, the total fluidizing flow was kept constant by balancing the steam flow rate with nitrogen. Figure 19 shows a steam reduction test conducted during CLC operation with BP fuel.

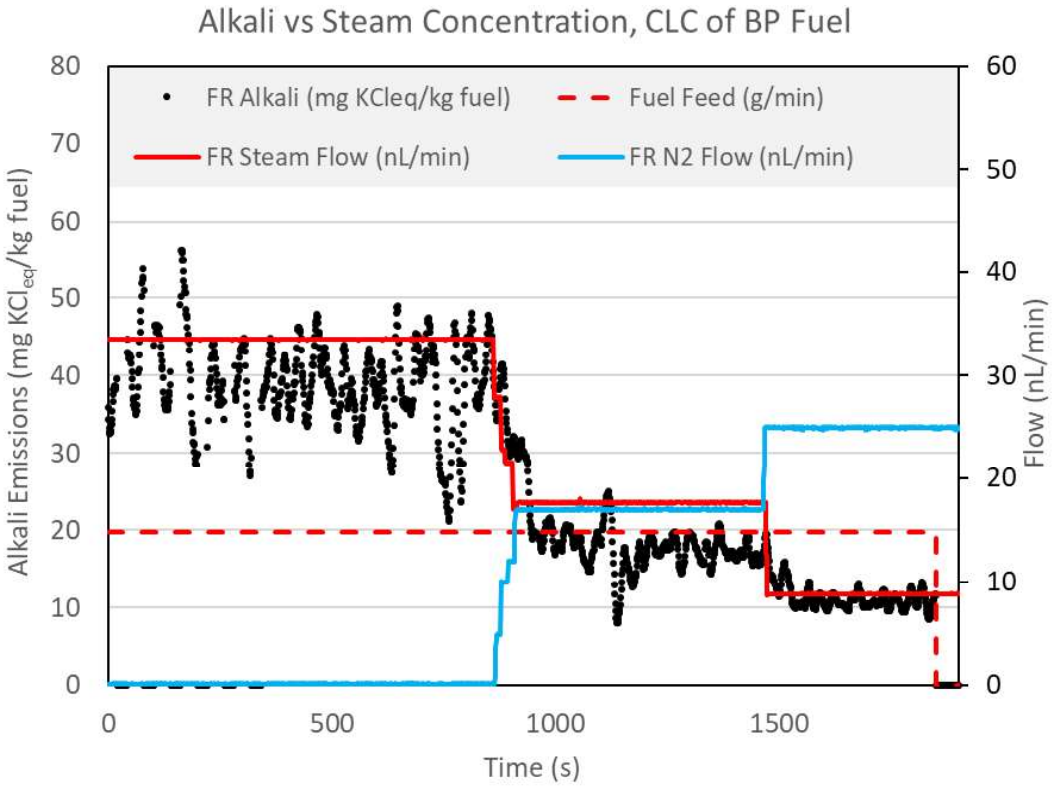


***Figure 19 - Effect of steam reduction on FR alkali emissions during CLC with BP fuel*** *[88]*

Figures 19 clearly shows that FR alkali emissions follow the reduction of steam concentration. Further experiments in Paper IV investigated whether steam directly accelerates alkali volatilization mechanisms or whether steam increases char conversion, thus influencing alkali release. The investigation concluded that the steam addition likely increases net gas-phase alkali release through steam-enhanced decomposition of $K_2CO_3$ during char conversion.

### *5.2.7 FR Alkali Emissions Speciation*

Alkali emissions in experiments presented in Papers I-IV were measured with the SID-based measurement system. The SID results allowed for approximate quantification of alkali release and determination of key release behavior, but could not provide information on which alkali species are formed. Alkali speciation was addressed in Paper V with a combination of thermodynamic modelling of fuel conversion and chemical analysis of alkali particles collected with a cascade impactor during CLC experiments performed in the 60 kW D-CFB pilot.

Thermodynamic modelling was performed in FactSage 7.2 software for two model cases:

**Fuel+$O_2$ Model:** model of fuel conversion without the influence of OC

**Fuel+OC Model:** model of fuel conversion in equilibrium with the OC

The Fuel+$O_2$ Model simulated fuel conversion in the atmosphere of the FR, but with some added oxygen to simulate the oxygen that would typically be supplied by the OC. This represents a hypothetical case which highlights the alkali speciation tendencies for fuel conversion without interaction with the OC, but at the reducing and steam-rich conditions of CLC. The Fuel+OC Model simulated fuel conversion in equilibrium with the OC material, in order to establish how fuel-OC interactions affect gas-phase alkali release. A more detailed explanation of the modelling approach is provided in Paper V. An example of the modelling results is presented in Figures 20-22 for the WP fuel. Figure 20 shows fuel conversion without OC interaction, with stable K species plotted against temperature. Figures 21 and 22 show a simulation of fuel conversion resulting from WP fuel reaction with ilmenite and braunite OC, respectively. In Figures 21 and 22, the equilibrium temperature is set to 800 °C, the approximate operating temperature of the D-CFB CLC pilot. K species are plotted vs. $R_{OC/F}$ - the mass ratio of the OC that is in equilibrium with the fuel. Gas conversion efficiency, $\eta_{g.c.}$, resulting from the equilibrium is also included in the figures to indicate the extent of fuel conversion.

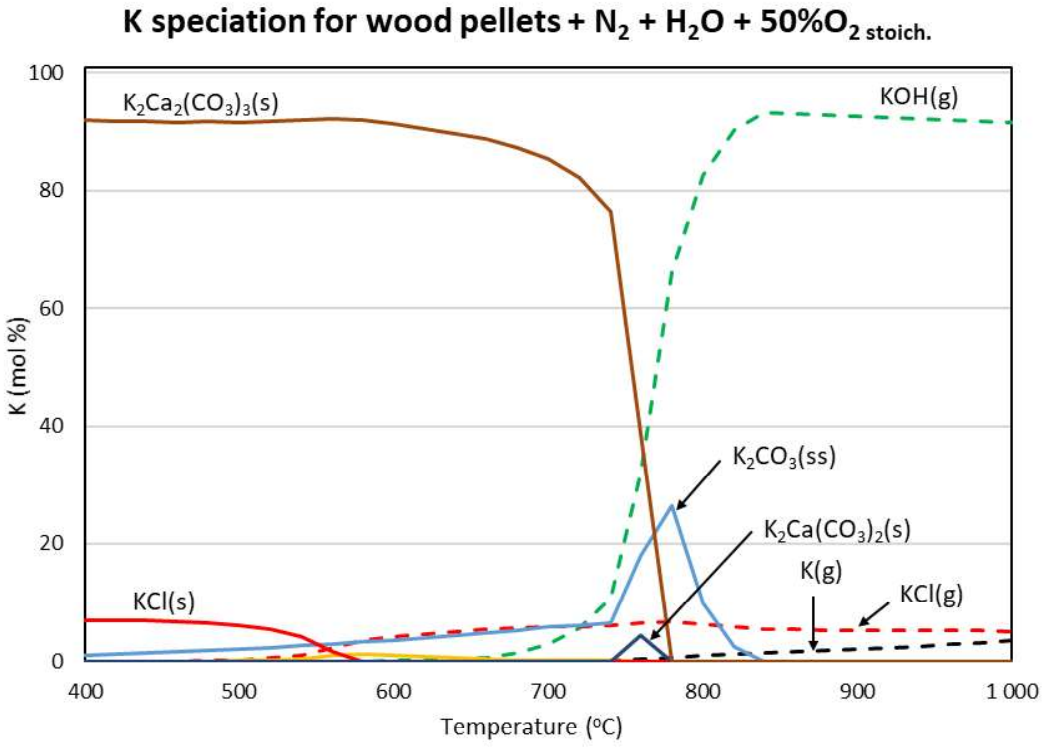


***Figure 20 – Equilibrium K-species for wood pellets reaction with FR atmosphere (Fuel+$O_2$ model)*** *[91]*

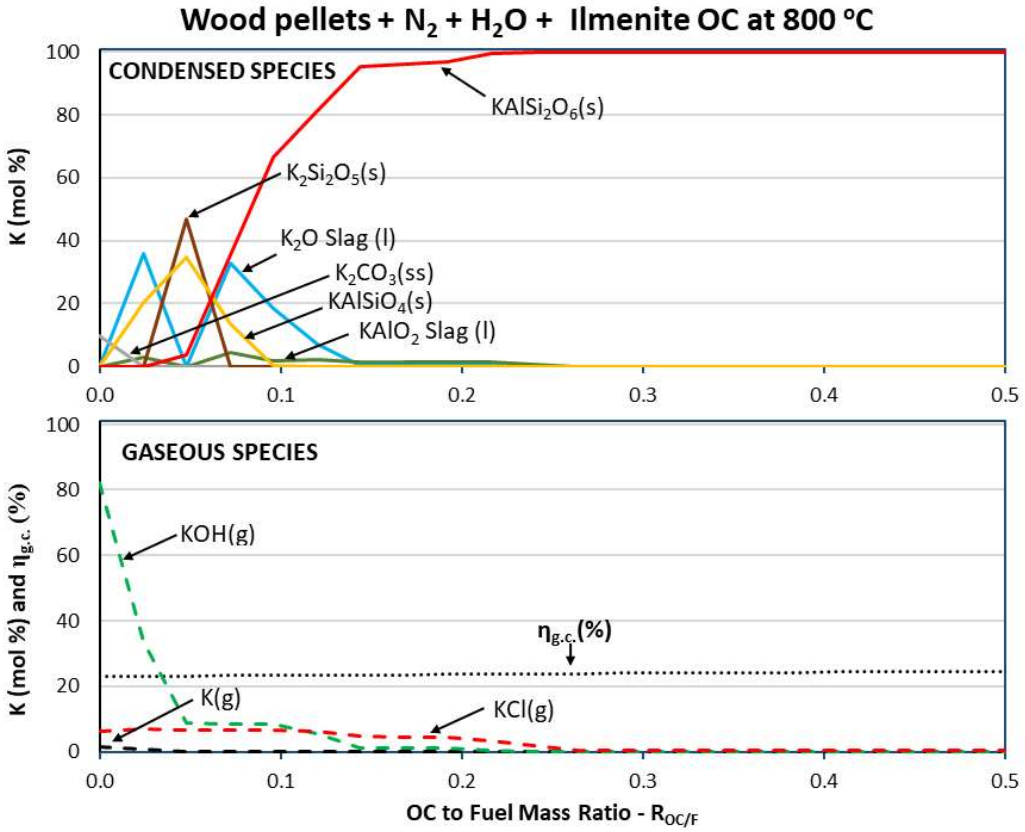


***Figure 21 – Equilibrium K-species for wood pellets reaction with ilmenite OC (Fuel+OC model)*** *[91]*

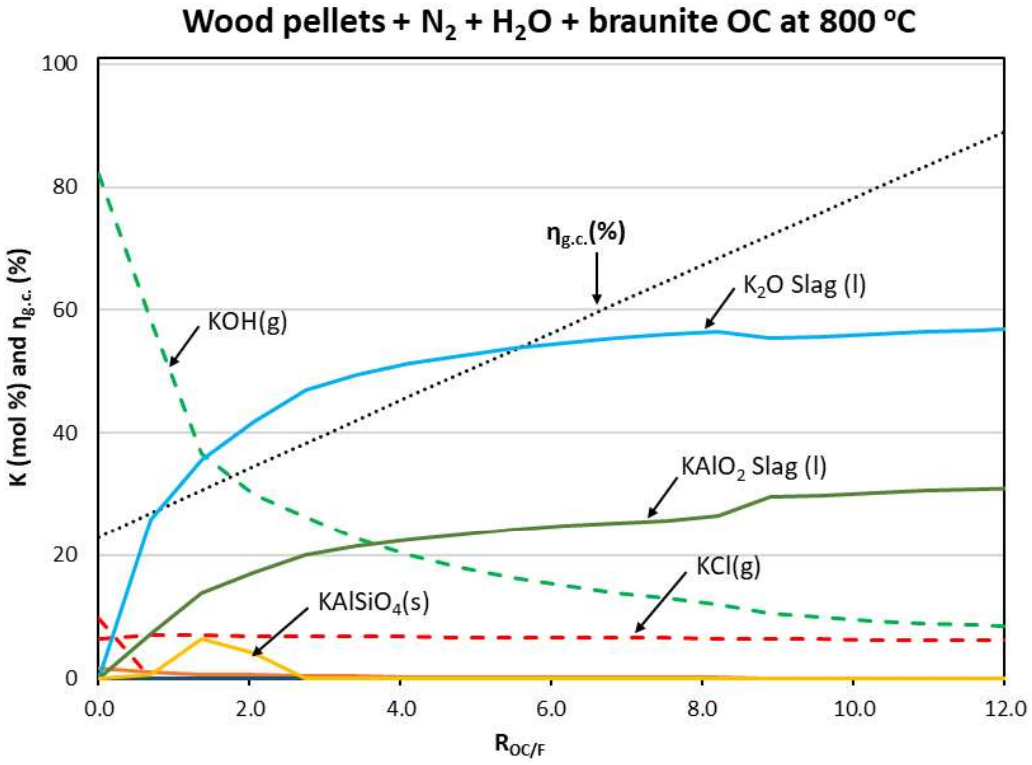


***Figure 22 – Equilibrium K-species for wood pellets reaction with braunite OC (Fuel+OC model)*** *[91]*

Modelling results in Figure 20 for WP fuel, and results for WC and SP-1 fuels (included in Fig. 6 and Fig. 7 of Paper V) suggest that below 500 °C most K is in a condensed form. For all three fuels the key condensed species are K-Ca-carbonates, $K_2CO_3$, and KCl. Additionally, $K_2Si_2O_5$ is predicted for the SP-1 fuel. These species are predicted by the FactSage model, but should not be confused with the actual species present in the virgin fuel. As mentioned in Chapter 2, K is known to be present in biomass in three main forms: organically-associated, salts, and excluded minerals. The organically-associated and salt forms are known to be releasable during thermal fuel conversion [22]. Alkali salts can account for up to 90% of alkalis in woody and herbaceous biomass [50–52]. The most common alkali salts found in biomass are phosphates, carbonates, sulphates, chlorides, and nitrates [53–56]. As such, KCl and $K_2CO_3$ predicted by the FactSage model make sense and are likely forms of K to be contained in the actual fuels. The K-Ca-carbonates, on the other hand, are not known to be originally present in biomass fuels. These species are rather products of secondary reactions that occur during the fuel decomposition process [57,86]. Thus, K that is included in the predicted K-Ca-carbonates exists in a different form in the virgin fuel, most likely as one of the salts mentioned above. For the SP-1 fuel, the silicates that are predicted to be stable below 500 °C are also not likely to occur in this form in the virgin fuel. While straw fuels are known to contain reactive organically-associated Si that can form alkali silicates [22], alkali silicate formation is known to be kinetically limited at temperatures below 800 °C [61]. Thus, the K that is predicted to exist in K-silicate form below 500 °C most likely exists in organically-associated form or as K-salt withing the virgin fuel.

As seen from the modelling results WP fuel in Figure 20, as well as in modelling results for WC and SP-1 fuel (included in Fig. 6 and Fig. 7 of Paper V), the FactSage model predicts that gaseous alkali species begin to become stable as the temperature rises beyond 500 °C. With increasing temperature, KCl(g) is the first gaseous species to become stable. The increased stability of KCl(g) is mirrored by a decreased stability of KCl(s), indicating that KCl(s) that is present in the virgin fuel, sublimates to the gas phase. This is in good agreement with literature. KCl sublimation is known to occur at pyrolysis, gasification, and combustion conditions [50,59,61,64], and thus should be relevant at the steam-rich reducing conditions of the CLC process. With further temperature increase, KOH(g) is predicted to become stable for WP fuel (Figure 20), as well as WC and SP-1 fuels (Fig. 6 and Fig. 7 of Paper V). KOH(g) release in biomass fuel conversion is known to arise from a reaction of $K_2CO_3$ with steam [50,59,89,90] or a reaction of steam with char-bound K at temperatures above 700-800 °C [50]. One notable result is that the FactSage model predicts that $K_2SO_4$ will not be stable in the FR flue gas. $K_2SO_4$ is a common form of alkalis in virgin biomass fuel and is also a common K-containing flue gas species in combustion and gasification of biomass. The modelling in Paper V concludes that at the experimental conditions of the D-CFB pilot, the overall availability of oxygen was too low for S to be associated as $K_2SO_4$. The model predicted that almost all S is stable as $H_2S$. The predicted $H_2S$ speciation is likely caused by the low reactor temperature (800 °C) and extremely oxygen deficient conditions experienced in the D-CFB experiments. Typically, CLC systems are operated at temperatures above 950 °C and with better oxygen availability from

the OC. In these conditions $SO_2$, rather than $H_2S$, is the dominant S species [92]. Even then, however, oxygen availability is likely not enough for alkali sulphate stability. Thus, in CLC operation, $K_2SO_4$ that may be present in the virgin fuels likely reacts with steam to yield KOH(g) that is seen in the model predictions. Lastly, for all three fuels, FactSage modelling predicts that K(g) gas can also be stable in the reducing environment of CLC systems.

Modelling the reaction of the fuels in equilibrium with the oxygen carriers shows that both OCs, ilmenite and braunite, affect the predicted stable gaseous K species. FactSage model results in Paper V show that ilmenite affects both KCl(g) and KOH(g) stability. This effect is quite strong since the stability of these species reduces greatly even at modest $R_{OC/F}$ ratios. An example of this is shown in Figure 21 for WP fuel. At the experimental conditions experienced in the D-CFB pilot experiments from Paper V, the model predicts only trace amounts of KCl(g) and KOH(g) to be stable in the gas phase. The reduced stability of KCl(g) and KOH(g) in equilibrium with ilmenite is mirrored by increased stability of condensed-phase K-bearing species, such as K-aluminosilicates.

For braunite, the effect on gaseous species stability is different from ilmenite. For all of the fuels, modelling predictions show that braunite affects KOH(g) stability, but does not seem to affect the stability of KCl(g). An example of this can be seen in Figure 22 for WP fuel, where the predicted levels of KOH are reduced with increased $R_{F/OC}$, but the KCl(g) level remains virtually unchanged. Modelling results also show that braunite's effect on KOH(g) stability is different for the three fuels considered in Paper V. As seen if Figure 22, KOH decays exponentially with increased $R_{F/OC}$. For WC fuel (see Fig. 12 in Paper V) KOH(g) is stable at lower $R_{OC/F}$ values and only decays slightly with further $R_{OC/F}$ increase. For SP-1 fuel (see Fig. 13 in Paper V) KOH(g) undergoes a slight continuous decay with increased $R_{OC/F}$. Further modelling in Paper V was performed to simulate the speciation for the individual cases for the alkali sampling periods conducted with the SID-based and the cascade impactor alkali sampling systems during CLC experiments conducted on the D-CFB reactor. These modelling cases are presented in Fig. 14 and 15 of Paper V and include K and Na species.

The modelling results, presented in Paper V and briefly summarized above, represent idealized cases, assuming perfect elemental mixing and no kinetic limitations. Also, FactSage 7.2 is known to have a lack of thermodynamic data to accurately characterize all the condensed phases that can accommodate alkalis. Thus, the modelling results in Paper V are only useful for high-level prediction of stable gaseous alkali species and for determining approximate global effects that OC's have on gaseous species. Nevertheless, the modelling results in Paper V, along with support from literature, highlight the following gas-phase alkali speciation trends in CLC:

- If Cl is available, K and Na prefer association as KCl and NaCl
- K and Na present in excess of Cl are associated as KOH and NaOH
- K and Na association with the $SO_4$ anion is unlikely

In Paper V, the trends established above were crucial for the interpreting the analysis results of the flue gas particulate samples collected from the D-CFB pilot unit with the cascade impactor system. The particles collected by the impactor were leached in water. The leachate was then analyzed for $K^+$ and $Na^+$ cations, and $Cl^-$ and $SO_4^-$ anions. The association of the alkalis was then determined using the trends established in the modelling predictions. The resulting speciation of four FR samples and one AR sample is shown in Figure 23. Figure 23 also shows what mass fraction of the total DLPI particle sample the detected alkali species constitute. The results in Figure 23 are separated by particle size class. Fine particles refer to the submicron particles, while coarse particles refer to particles between 1 and 10 microns in size.

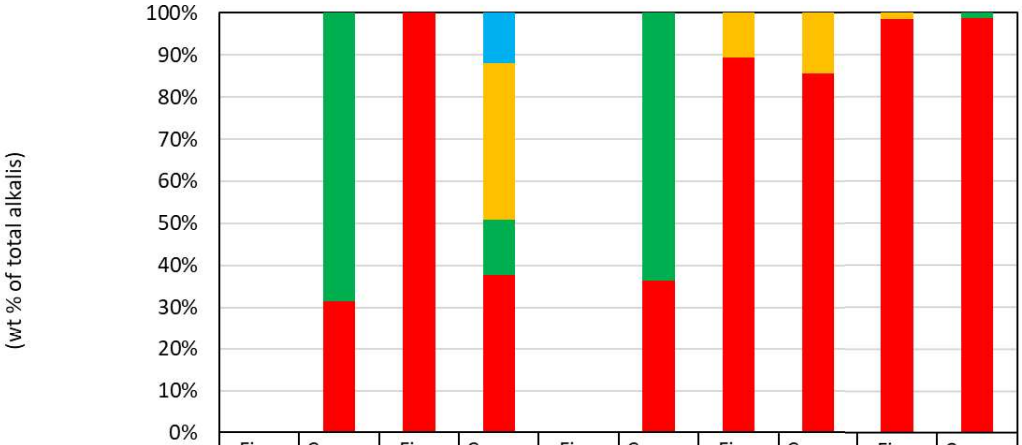


| | Fine | Coarse | Fine | Coarse | Fine | Coarse | Fine | Coarse | Fine | Coarse |
|---|---|---|---|---|---|---|---|---|---|---|
| | DLPI 2: WC+ilmenite (FR) | | DLPI 3: WP+braunite (FR) | | DLPI 4: WC+braunite (FR) | | DLPI 5: SP+braunite (FR) | | DLPI 6: SP+braunite (AR) | |
| NaOH (mg/Nm3 dry) | 0.00 | 0.00 | 0.00 | 0.03 | 0.00 | 0.00 | 0.00 | 0.00 | 0.00 | 0.00 |
| NaCl (mg/Nm3 dry) | 0.00 | 0.00 | 0.00 | 0.10 | 0.00 | 0.00 | 18.09 | 4.40 | 2.22 | 0.00 |
| KOH (mg/Nm3 dry) | 0.00 | 1.26 | 0.00 | 0.04 | 0.00 | 5.44 | 0.00 | 0.00 | 0.00 | 0.08 |
| KCl (mg/Nm3 dry) | 0.00 | 0.58 | 0.17 | 0.10 | 0.00 | 3.10 | 152.41 | 26.28 | 159.89 | 6.99 |
| wt% alkalis in sample | 0.0% | 0.4% | 1.9% | 0.1% | 0.0% | 0.5% | 58.5% | 5.7% | 74.7% | 4.5% |

***Figure 23 – Alkali speciation of impactor alkali measurements in the 60 kW D-CFB CLC pilot (Paper V)*** *[91]*

Figure 23 shows that alkali species in the flue gas are dominated by KCl, followed by KOH, NaCl and NaOH. For WP and WC fuels, the overall alkali concentration is quite low. Furthermore, most of the alkali mass occurs in the coarse particle fraction suggesting that alkalis heterogeneously condense onto coarse seed particles formed by refractory alkali species. For the straw fuel (SP-1), the overwhelming majority of the alkali mass appears in the fine particle mode, suggesting homogeneous nucleation of KCl particles.

Figure 23 includes one result for speciation of emissions samples collected from the AR during operation of SP-1 fuel with braunite oxygen carrier. Surprisingly the overall level of emissions is higher than FR emissions measured by the impactor prior to switching to the impactor to the AR. SID measurements collected in the same timeframe confirm this. The AR emissions sample is almost entirely composed of KCl. However, as determined in Paper V, the poor levels

of carbon capture efficiency of the pilot and the high levels of $CO_2$ detected in the AR atmosphere indicate that significant amounts of char and fuel carryover from the FR to the AR occurred during this sampling period. Thus, the AR emissions result in Figure 23 is not representative of stable CLC operation.

The only other evidence on AR alkali speciation was collected for SP-2 fuel experiments in Paper IV. There, AR fly ash trapped in AR flue gas filters was collected and analyzed for K and Cl content. The amount of detected Cl accounted for <1 wt.% of the fuel's Cl content. K was present in 70% molar excess to Cl. The collected AR fly ash particles were approximately 5-10 microns in size, and K and Cl made up approx. 10% of the ash particle mass. Thus, the detected K and Cl likely were condensed onto existing seed ash particles. The SID measurements collected during the time of this impactor sample period can also be used to estimate the maximum amount of KCl in the AR flue gas. This can be done by expressing the average SID signal in $KCl_{eq}$ units. For the SP-2 fuel tests in Paper IV, the SID measurements indicate that up to approx. 20 mg $KCl_{eq}$/kg fuel was detected in the AR flue gas. This corresponds to 0.6% of fuel Cl in the form of KCl(g), which is close to the estimate from the AR fly ash samples. Thus, the measurements suggest that KCl concentrations in the AR are very low. This is supported by the fact that KCl sublimation has been shown to begin at lower temperatures and to be several orders of magnitude faster than wet decomposition of $K_2CO_3$ [50]. Thus, with appreciable fuel residence time in the FR, KCl release should proceed to completion, or close to it. Consequently, as supported by some experimental evidence, AR flue gases should be nearly KCl-free.

### *5.2.8 Alkali Retention in Condensed Phases*

In CLC operation, alkalis that are not released to the gas phase are retained as condensed-phase alkali species. The fraction of such species can be estimated by subtracting the alkalis detected in the gas phase of the FR and AR from the alkalis introduced with the fuel. Estimates of condensed-phase alkalis are presented in Table 11 for experiments from Papers I-IV.

***Table 11 - Percentage of fuel alkalis retained in a condensed-phase (Papers I-IV)***

| Fuel | Paper I Ilmenite & CaMn (100 kW) | Paper II Ilmenite (10 kW) | Paper III Ilmenite (60 kW D-CFB) | Paper III Braunite (60 kW D-CFB) | Paper IV LD Slag (10 kW) |
|---|---|---|---|---|---|
| **WP** | | | >95.8% | >92.4% | |
| **BP** | >91.6% | >89.5% | | | >77.2% |
| **WC** | | | >97.6% | >97.1% | |
| **PFR** | | >95.7% | | | >96.5% |
| **SPM** | >92.6% | >97.5% | | | |
| **SP-1** | | | | >88.0% | |
| **SP-2** | | | | | >97.3% |

Estimates presented in Table 11 show that in all cases 77-98% of fuel alkalis remain in a condensed phase within the CLC systems. Condensed-phase alkalis can occur in different forms shown in Figure 24. One possibility is that alkalis bind to the oxygen carrier material

through interaction of the OC material with gaseous alkalis or with fuel ash. Another possibility is for alkalis to be present in a condensed form in fuel ash particles that are separate from the main OC fraction.

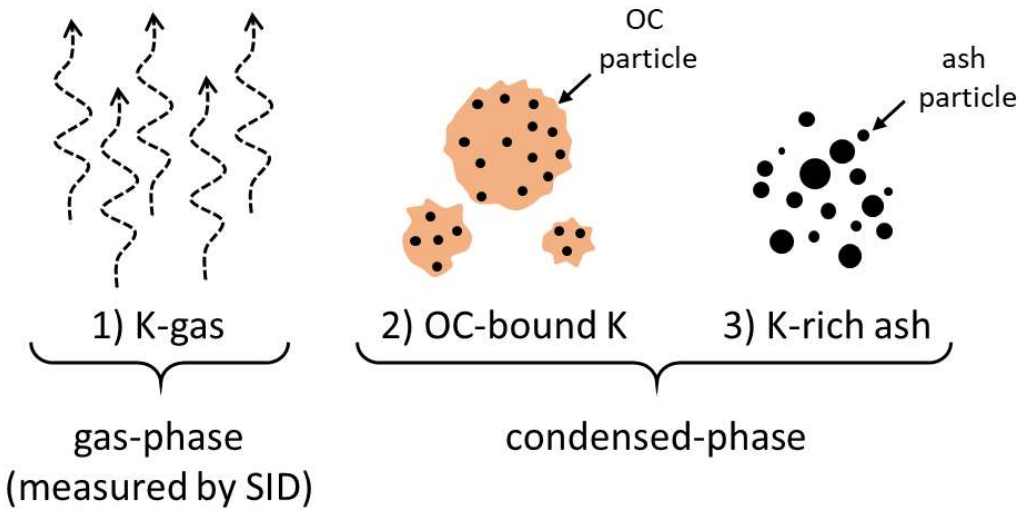


***Figure 24 – Forms of alkalis present in the reactor system (Paper IV)****[88]*

OC material before and after fueled CLC operation was analyzed for alkali content in experiments presented in Papers I-IV. In experiments presented in Papers I and II, where the bulk of the OC material was ilmenite, material analysis showed that the increase in alkali content of the OC material corresponds to approximately 98% of the alkali fed into the system with the fuel. This high absorption figure was attributed to ilmenite's known ability to capture K via formation of stable potassium titanate ($KTi_8O_{16}$) [62,71,93]. However, modelling work in Paper V suggested that retention of K also occurs via formation of K-Al-silicates in ilmenite. In Paper III experiments, the share of alkalis in the condensed phase was estimated to be in the range of 88-97%. OC analysis results, however, showed that the uptake of alkalis by braunite OC accounted for approximately 32% of the fuel alkalis. This uptake was determined to occur through formation of alkali manganates and silicates within the braunite OC. Beyond uptake by the OC, the remaining share of alkalis in the condensed phase were associated with formation of an ash fraction that is separate from the OC. This conclusion of Paper III led to a more rigorous analysis of the fate of condensed-phase alkalis in Paper IV. Experiments in Paper IV were performed with LD Slag OC, since it was expected to have limited interaction with alkalis in comparison to other oxygen carriers [94]. The limited interaction made it easier to investigate the fate of condensed-phase alkalis. During the experimental work conducted in Paper IV on the 10 kWth pilot, solids samples from the reactor system, the FR chimney and water seal system, and AR filter system were collected and analyzed for alkali content, leading to the development of a more detailed mass balance of condensed-phase alkalis in the system. Although such balances were performed for BP, PFR and SP-2 fuel tests, low estimate uncertainty was only achieved for the SP-2 fuel operation. For BP and PFR fuel operation, uptake of alkalis by the OC was too minor to be reliably measured by the ICP-OES method.

This analysis for SP-1 fuel established that from the condensed-phase alkalis present in the CLC pilot, approximately 33% are absorbed by the OC, 3-4% end up as AR fly ash, and the remaining 60-70% of the alkalis form alkali rich FR fly ash. The high proportion of alkalis that were determined to occur as ash particles that are not associated with the OC is supported by literature. Controlled experiments investigating gas phase alkali release at grate firing conditions report that approximately 20-40% of fuel alkalis are released for woody and annual biomass. The remaining 60-80% of the fuel alkalis are retained in ash that is left after fuel conversion [30,64]. In grate firing conditions fuel conversion occurs without interaction with extraneous material. This indicates that alkali retention can readily occur even without the influence of bed material.

## 5.3 Interdependence of CLC process performance and alkali release

The performance of a CLC system is typically measured by two key variables, carbon capture efficiency and fuel conversion. Optimization of these parameters can be addressed with the design of the CLC pilot system, and by manipulation of the CLC pilots operating parameters. With biomass fuels, control of alkali release in the CLC system can potentially introduce new design and operating constraints.

Carbon capture efficiency figures, estimated by the $\eta_{oo}$ parameter, for the different CLC test from experiments presented in Papers I-V were summarized in Table 8. In Table 8, there is clear divide in $\eta_{oo}$ values between the different pilot units. The $\eta_{oo}$ for the 60 kW D-CFB unit range from 38 to 87.1%. Such poor numbers are the result of the pilot arrangement, where the AR and the FR are both circulating fluidized beds operated in the fast-fluidization regime. As mentioned prior in Section 5.2.3, the fast-fluidized FR results in short fuel residence time, which limits fuel conversion and results in carryover of unconverted fuel and char to the AR. In experiments presented in Paper III this carryover is responsible for the high alkali emissions in the AR. The use of L-valves in the D-CFB unit can also contribute to the poor carbon capture efficiency, since L-valves are less effective than loop seals in preventing gas mixing between the two reactors.

In the 100 kW and 10 kW units, $\eta_{oo}$ >95% is achieved due to the longer residence time enabled by the FR designs in these CLC units. In the 10 kW unit the FR is a bubbling regime reactor with a large volume that provides long fuel residence time. In the 100 kW unit, long fuel residence time is achieved with the FR's internal re-circulation and with the carbon stripper which recycles unconverted char to the FR. The high $\eta_{oo}$ values achieved in these two pilot systems mean that char slip from the AR to the FR is low, limiting one of the probable pathways of alkali carryover to the AR. In summation, higher carbon capture efficiency is achieved mostly through improved reactor design and is desirable for better system performance and lower potential for AR alkali emissions.

Fuel conversion in a biomass CLC system is best reflected in the gas conversion efficiency parameter, $\eta_{g.c.}$. For a given oxygen carrier, $\eta_{g.c.}$ is controlled by two key process variables, the

FR temperature, and the solids circulation rate. The effect of FR temperature on gas conversion is shown in Figure 25 for experiments presented in Paper IV.

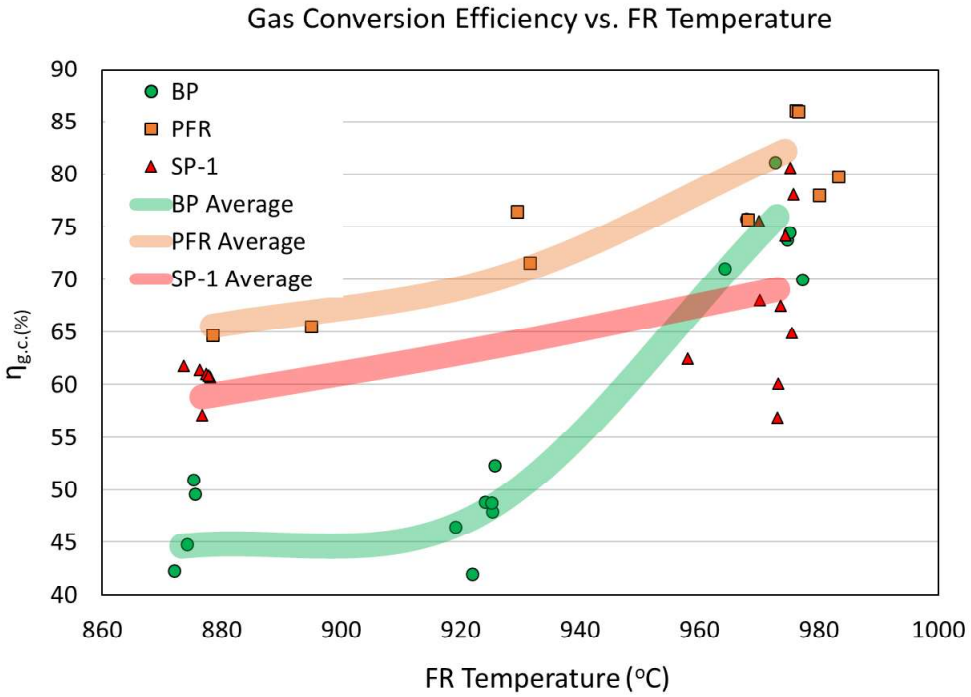


***Figure 25 – Gas conversion efficiency vs. FR temperature, 10 kW CLC pilot, LD Slag OC***

Figure 25 shows that higher FR temperature results in higher $\eta_{g.c.}$. This is explained by the fact that oxygen carrier reactivity increases with temperature [95–97]. With respect to alkali release, Section 5.2.4 established that higher operating temperature results in higher FR alkali release for all of the fuels tested in Paper IV experiments. Thus, there is a tradeoff between fuel conversion and alkali release that is moderated by the operating temperature.

The second key parameter, the solids circulation rate, is controlled by the flowrate of the AR air flow in the 10 kW and 100 kW pilot systems. The effect of solids circulation in the 10 kW CLC reactor system is shown in Figure 26, as replicated from Paper II.

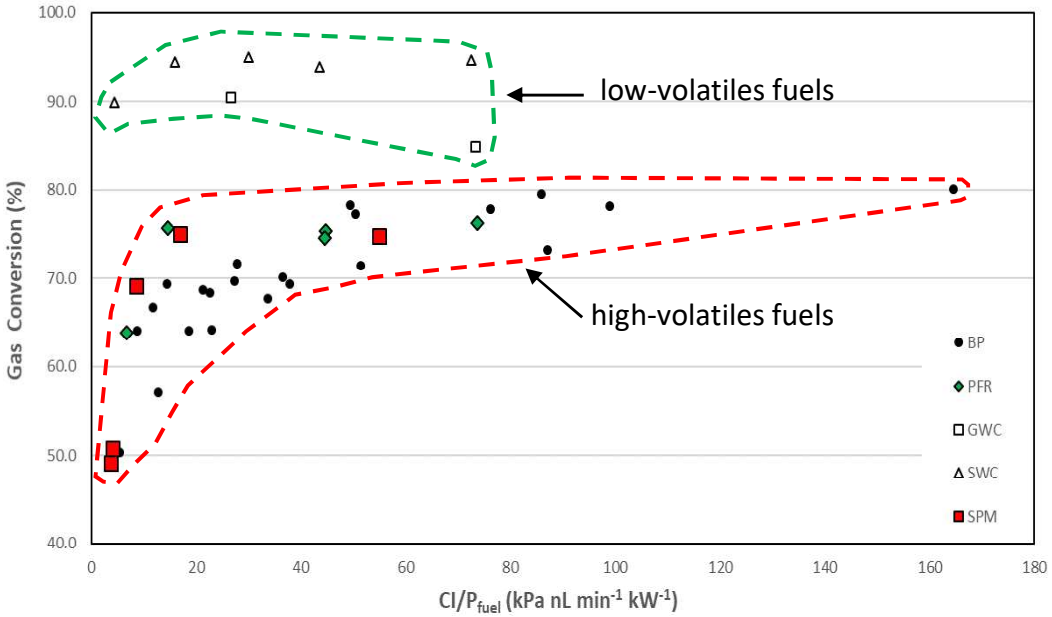


***Figure 26 – Gas conversion efficiency vs. power-specific circulation index, 10 kW CLC pilot, Ilmenite OC (Paper II)*** *[77]*

Figure 26 shows that increased solids circulation, represented here as power-specific circulation index ($CI/P_{fuel}$), improves $\eta_{g.c.}$ for high-volatiles biomass fuels. This effect is attributed to improved contact between the OC and the gaseous fuel components (volatiles + products of char gasification) and by higher OC reactivity that results from lower OC conversion in the FR. The low-volatiles char fuels, GWC and SWC, are not affected by be OC circulation rate since the release of their gaseous components (char gasification products) is limited by the slow char conversion process. With a slow release of gaseous fuel species, high gas conversion is achieved for a wide range of OC circulation rates. The effect of circulation rate on alkali release was investigated in experiments covered in Papers I and II. In these experiments, FR alkali concentration was compared to changes in AR flowrate, changes to system inventory, and to the calculated circulation index. No apparent effect of these parameters on the release of alkalis was found. The effect of circulation rate on AR alkali emissions was also investigated using operational and emissions data collected in Paper I-IV experiments. Unfortunately, the investigation was inconclusive due to significant noise in the AR emissions data and shortage of AR emissions measurements at different OC circulation rates. It is suspected that higher solids circulation may facilitate carryover of OC-bound alkalis, or of unconverted fuel or char from the FR to the AR. Further investigation is required to test this hypothesis.

CHAPTER 6

# 6. Discussion

The following chapter sections summarize the key findings and conclusions with respect to the key research questions of this thesis. For convenience, the main research questions are restated below:

*RQ1 - How are alkalis released/retained and distributed in the CLC process?*

*RQ2 - What is the interdependence between alkali release/retention and the key process control parameters in a CLC system?*

*RQ3 - What are the operational advantages and/or disadvantages of CLC technology for processing alkali-containing biomass?*

The chapter concludes with a discussion of key limitations of the conducted work as well as suggested topics for future research.

## 6.1 RQ1 – Alkali release and distribution in chemical looping

Review of literature on alkali release in thermal processing of biomass fuels and experimental observations from Papers I-V indicate that gas-phase release of alkalis in CLC of biomass occurs via the same mechanisms as alkali release in other biomass thermal conversion processes, such as pyrolysis, gasification, and combustion. These mechanisms and the distribution of alkalis in a CLC system are depicted in Figure 27.

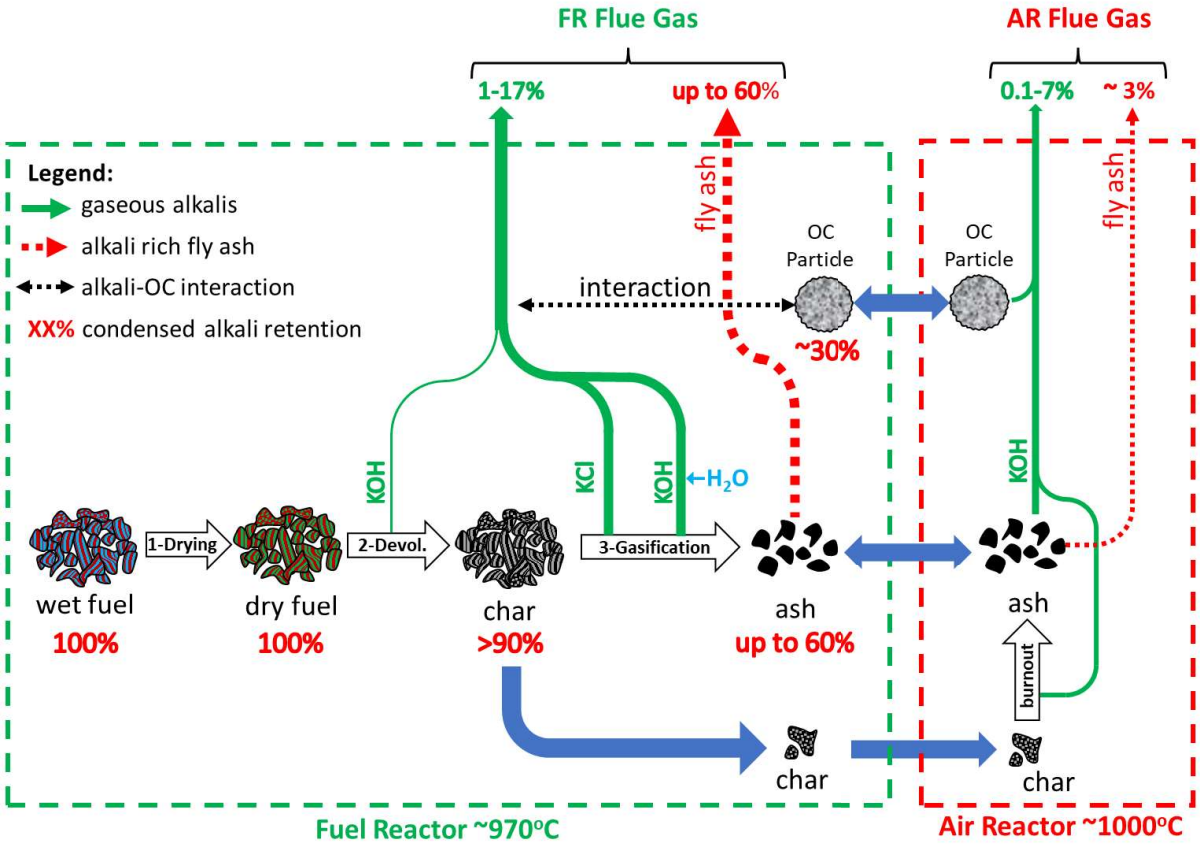


***Figure 27 – Illustration of the release and distribution of alkali compounds in CLC***

The release of alkalis in chemical looping combustion is thought to occur as follows. As the fuel particle enters the FR, it is heated and undergoes a staged conversion process consisting of drying, devolatilization, and char gasification. Just like in biomass pyrolysis, gasification, and combustion, gas-phase alkali release in CLC begins to occur during fuel devolatilization at temperatures <700 °C. Organically-associated K is released as KOH due to thermal decomposition of the organic fuel matrix [30,98,99]. As fuel particles in the FR are heated beyond 700 °C, gaseous alkali release starts to occur through sublimation of KCl(s) to KCl(g). Evidence of KCl sublimation in CLC was provided by thermodynamic modelling results and the impactor sample alkali speciation presented in Paper V. As in other biomass thermal conversion processes [50,61,65], the remaining gaseous release of alkalis in the FR is thought to occur through decomposition of alkali salts and release of char-bound K. Experimental findings from Papers III and IV suggest that release of K through decomposition of $K_2CO_3$ can be particularly important in CLC. In Paper III and IV experiments, K content of the tested fuels was present in stoichiometric excess to Cl and S, suggesting that a significant amount of K may be present as $K_2CO_3$ within the fuel. Furthermore, thermodynamic modelling in Paper V predicted that K may be present as or form K-carbonates within the fuel. Further evidence in Papers III and IV is provided in comparison of OCAC and CLC operation, and in experiments exploring the effect of steam on alkali release. As shown in several studies [50,59,89,90], the presence of steam greatly accelerates $K_2CO_3$ decomposition via a reaction of $K_2CO_3$ with steam

that yields KOH(g). Thus, the steam-enhanced alkali release observed in Paper III and IV experiments provides evidence that supports the steam enhanced $K_2CO_3$ decomposition alkali release mechanism. Moreover, thermodynamic modelling in Paper V predicts that KOH(g) is the second most abundant gaseous alkali specie in fuel conversion at CLC conditions.

The relative amounts of alkali release and retention, as determined in experiments presented in Papers I-IV , are also summarized in Figure 27. The gaseous alkalis measured in the FR flue gas by the SID-based system account for 1-17 % of the fuel alkalis. The majority of fuel alkalis were found to be retained as condensed species. As summarized in Table 11 and in Figure 27, condensed-phase alkalis account for more >77% of the fuel alkalis. A detailed balance on K distribution in the 10 kW pilot presented in Paper IV, estimates that from the condensed species, approximately 30% of the fuel K is absorbed by the oxygen carrier. The absorption is suspected to occur primarily through interaction of gaseous alkali species with the OC particles. Thus, the gaseous release of alkalis from the fuel, prior to interaction with the OC, should account for much more than the alkalis measured by the SID-based system. For alkali absorption by the OC, it should be noted that the 30% absorption figure is more valid for the LD Slag and braunite oxygen carriers. Alkali absorption by ilmenite was found to be much higher for ilmenite in Papers I and II, but the sampling method may not have accounted for presence of ash particles in the ilmenite sample. For the different OC materials tested in the experiments presented in Papers I-IV, several alkali absorption mechanisms were identified. The most ubiquitous mechanism is the formation of alkali silicates. Si is known to have high affinity for alkalis and is present in the naturally occurring OCs (ilmenite and braunite) as well as in the industrial waste product OC (LD Slag). Association of Si and K was confirmed for the LD Slag OC by EDX analysis covered in Paper IV. K-silicate formation for ilmenite and braunite was predicted by thermodynamic modelling in Paper V. Furthermore, alkali silicate formation in ilmenite has been reported in investigations by other researchers [100]. Other OC capture mechanisms include alkali manganate formation in braunite [101], and the well-established formation of alkali titanates in ilmenite [71,100]. Analytical techniques, such as SEM-EDX and XRD, were applied to the OC samples collected during the CLC pilot experiments, but were not effective in determining all forms of captured alkalis. Investigation of OC-alkali interaction is better addressed with lab scale studies where significant exposure of OC materials to different alkali components can be facilitated and studied.

Apart from absorption by the OC, the remainder of the condensed-phase alkalis were determined in Papers III and IV to be held by fuel ash particles. Depending on the system the fuel ash particles can remain in the reactor system or become fly ash that is carried out of reactor system. The K balance on the 10 kW in Paper IV estimates that approx. 3% of fuel alkalis end up being elutriated with the AR fly ash, while alkali-rich fly ash elutriated from the FR can account for up to 60-70% of the fuel alkalis. Here it is important to note that the 10 kW pilot used in Paper II and IV experiments is not equipped with a cyclone or a particle disengagement space at the FR flue gas chimney. As such, the elutriation of solids in this unit

is quite significant. In the 100 kW unit used in Paper I experiments, the elutriation of solids from the FR is significantly lower.

Gaseous alkali emissions in the AR flue gas accounted for 0.1-7% of the fuel alkalis. Gaseous alkalis in the AR are thought to originate from condensed alkalis carried over from the FR to the AR. Three possible mechanisms for such carryover were identified:

1) Carryover of alkali-rich char
2) Carryover of alkali-rich ash particles
3) Carryover of alkalis absorbed by the OC in the FR

With any of the carryover modes, it is hypothesized that the carried-over alkalis undergo release to the gas phase at the higher temperature oxidizing conditions of the AR. Carbon capture figures from experiments presented in Papers I, II and IV provide evidence that moderate amounts of char carryover occur in CLC operation. Experiments in Paper III show that significant carryover of char and unconverted fuel resulted in high AR emissions levels. The carryover of ash particles is weakly supported by the alkali-rich ash particles found in experiments in Paper IV. The carryover and release of alkalis by the oxygen carrier could not be investigated in the pilot CLC experiments.

In terms of alkali speciation, it is most important to establish the potential for the presence of KCl, the most aggressive alkali compound, in the AR. The alkali release mechanisms described above suggest that KCl release should occur in FR, since KCl sublimation is a process that is significantly faster than alkali salt decomposition [50]. Thus, gaseous AR alkalis likely originate from condensed species that are either stable at FR conditions or undergo a slower decomposition to the gas phase. Such species can include $K_2SO_4$ and K-silicates. In Paper IV experiments, analysis of the AR fly ash and estimation of the maximum KCl concentration in the AR indicates that only trace KCl amounts are found in the AR in operation with the highest Cl content fuel (SP-1 straw fuel). Thus, with the given theoretical background of alkali release and initial experimental evidence, it is concluded that the AR should be mostly free of KCl. This conclusion, however, can benefit from further experimental confirmation.

## 6.2 RQ2 – Interdependence of CLC performance and alkali release

The effects of key operating parameters on CLC system performance and the alkali emissions of a CLC system, as determined from experiments presented in Papers I-IV, are summarized in Table 12.

*Table 12 – Summary of interdependence of CLC performance and alkali release*

| Performance parameter | Controlling parameter | Effect on performance | Effect on AR alkali emissions | Effect on FR alkali emissions |
|---|---|---|---|---|
| Carbon Capture Efficiency ($\eta_{oo.}$) | **Reactor design:** Loop seal design, FR reactor design | Improved reactor design→ higher $\eta_{oo}$ | Higher $\eta_{oo}$ → lower alkali emissions | Higher $\eta_{oo}$ → no effect |
| Fuel gas conversion efficiency ($\eta_{g.c.}$) | **System solids (OC) circulation** | Higher circulation → higher $\eta_{g.c.}$ for high volatiles biomass | Higher circulation → no effect | Higher circulation → no effect |
| | **FR Temperature ($T_{FR}$):** | Higher $T_{FR}$ →higher $\eta_{g.c.}$ | Higher $T_{FR}$ → no effect | Higher $T_{FR}$ → higher alkali emissions |

Table 12 results shown that achieving higher carbon capture efficiency by means of improving pilot design is in line with lowering the potential of AR alkali emissions. Optimization of the solids circulation rate in order to maximize fuel gas conversion efficiency does not seem to influence alkali release in the AR or the FR. The only tradeoff in CLC performance vs. emissions occurs in selecting the reactor temperature. For a given OC material, higher operating temperature increases the gas conversion efficiency of high volatiles content biomass fuels. At the same time, higher operating temperature increases alkali emissions in the FR. This tradeoff is acceptable since release of alkalis in the FR is not detrimental to the process, as will be discussed in Section 6.3. In CLC operation, the alkali emissions in the AR are more important, since the main process heat exchangers extract heat from the AR flue gas. As discussed in Section 5.2.4, AR emissions levels are not affected by higher FR operating temperatures.

One variable that is not mentioned in Table 12, is the choice of the oxygen carrier used for the process. Experimental observations indicate that the different oxygen carriers tested in the conducted experiments clearly exhibit different extents and mechanisms of absorption of alkali species. However, long-term alkali uptake or the specific effects that alkali-OC interactions have on OC reactivity were not explored in experiments presented in Papers I-V. This is mostly due to the short operating times, and thus limited exposure of OC materials to alkalis in the conducted experiments. The lack of long-term effects of OC exposure to biomass alkalis is a known limitation of the work presented in this thesis. Recent investigations using ilmenite as a bed material in OCAC of biomass at industrial scale indicate long-term operation (>320 hours) does not significantly change ilmenite's reactivity [102,103]. Nonetheless, long-term reactivity of ilmenite and other OC's in CLC operation needs to be explored in more detail. With the exception of long-term reactivity effects, analysis of the operational data and alkali emissions collected in experiments presented in Papers I-IV indicate that alkali release does not significantly constrain the performance of CLC systems.

## 6.3 RQ3 – Advantages of CLC technology for processing biomass fuels

The alkali release behavior in CLC offers several advantages for processing of biomass fuels. In CLC systems the majority of the process heat is extracted from the AR flue gases. Since AR flue gases contain only minor amounts of alkalis with very little KCl, corrosion of heat exchange surfaces (steam tubes) should be largely avoided. With low fouling and corrosion, it should be possible to run higher steam temperatures in a CLC boiler than in conventional fluidized bed biomass boilers where steam temperatures are typically limited to <500 $^{o}$C in order to avoid corrosion issues. Higher steam temperatures would allow CLC boilers to reach higher thermodynamic efficiency than comparable fluidized bed biomass boilers.

In a full-scale CLC process, in addition to the main heat recovery in the AR, some heat recovery from the FR flue gas would also be included for better plant heat integration. The FR flue gas in contact with these surfaces would contain more alkalis than in a combustion process, as determined in the CLC vs. OCAC comparison. The FR flue gas would also hold almost all of the KCl. However, several strategies can assure that corrosion and fouling issues are manageable. Firstly, the FR heat exchangers can be run at temperatures which minimize fouling and corrosion. This strategy comes with a heavy efficiency penalty when applied to steam tubes in a boiler, but would not be a detrimental if applied to a minor heat recovery system such as in the FR. Furthermore, FR flue gas cleaning would be more manageable than in a comparable combustion system. This is because the FR flue gas has a much lower flowrate and a higher alkali concentration than a flue gas stream of a comparable combustion system, where the flue gas is diluted with nitrogen.

Further to advantages with respect to corrosion and fouling, the way that alkalis are released and partitioned the CLC system may also be more advantageous for minimizing bed agglomeration issues. As mentioned prior, fluidized bed biomass boilers with sand bed material struggle with bed material agglomeration which occurs due to in-bed formation of low melting point alkali silicate melts. In CLC, less agglomeration issues are expected for several reasons. Firstly, since CLC operation results in a higher overall gas-phase release of alkalis (vs. combustion), less alkali species will remain in the bed material. This should lower the agglomeration potential. Secondly, most OC materials used in CLC contain low amounts of Si (vs. silica sand used in conventional boilers), which should limit alkali silicate formation. Furthermore, OC materials are capable of absorbing alkalis through formation of benign species that do not cause agglomeration. An example of this is formation of alkali titanates in Ilmenite, formation of alkali manganites in braunite, and formation of high meting point alkali aluminosilicates in LD Slag. However, as mentioned prior, experiments in Papers I-IV did not specifically focus on investigation of bed material agglomeration since the OC exposure times to alkalis were relatively short.

## 6.4 Key limitations and remaining research gaps

The work presented in this thesis constitutes the first pilot-scale investigations with characterization of alkali emissions in CLC of biomass. Although pilot-scale experiments provide valuable information that is relevant for upscaling of the CLC process, some alkali release phenomena cannot be adequately explored in pilot operation. Thus, the work presented in this thesis is limited to establishing high-level trends with respect to alkali release. Key limitations of the pilot investigations presented in Papers I-V are summarized below.

### *6.4.1 AR Alkali Levels, Origin, and Speciation*

The SID alkali measurement system implemented in the pilot experiments was designed to measure one reactor at a time. Since most operational changes in the CLC pilots affect the FR unit first (e.g., fuel addition, change of fuel), alkali emissions measurement priority was given to FR alkali measurements. Periodic switching of the SID system to sample the AR emissions was carried out during experiments, but the AR sampling periods ended up being much shorter than for the FR. Since switching the SID system from one reactor to the next introduces a transient event for the sampling system, with short measurement periods the AR alkali emissions data contained considerable noise. The shortage and high noise levels of AR alkali emissions data limited the analysis of how different parameters affect AR emissions. Future work should consider experiments with full-time AR emissions measurement or operation of two SID instruments such that the FR and AR emissions can be measured simultaneously.

Beyond the limitations imposed by the SID measurement system, the nature of pilot experiments did not allow for determination of the exact carryover pathways for alkalis from the FR to the AR. Although evidence supporting alkali carryover by char slip from the FR to the AR was collected, there was no practical way to explore the ash-bound or OC-bound alkali carryover pathways. This type of determination is more appropriate for controlled lab-scale experiments in a batch fluidized bed reactor.

Lastly, the speciation of AR emissions was not fully addressed in the presented pilot experiments. AR alkali speciation in Paper V was compromised by unstable operation of the D-CFB unit. Future work should consider impactor measurements and speciation of AR alkali emissions.

### *6.4.2 Long-term Effects of Alkalis on OC Performance*

Each experimental campaign presented in Papers I-IV consisted of approximately 10-30 hours of CLC operation. Longer operating times are not practical due to limitations on experimental manpower, OC and fuel availability, and the occurrence of technical issues which require either a delay or stoppage of experiments. Considering that several fuels were typically tested in each experimental campaign, test durations for each fuel were quite short. Consequently,

the exposure of the OC materials to alkalis was quite limited. The limited alkali exposure prevented the investigation of the long-term exposure effects that alkalis can have on OC performance. These effects can include:

- Accumulation and eventual saturation of the OCs with alkalis
- Effects of alkali accumulation on OC reactivity
- Agglomeration performance of aged and alkali-saturated OCs
- Changes in net gas-phase alkali release due to diminished OC capacity for alkali absorption

Exploring these and other possible effects of long-term exposure of the OC material to biomass alkalis is more appropriate for lab-scale investigations, where more controlled and constant conditions can be established.

CHAPTER 7

# 7. Conclusions

Chemical looping combustion of biomass (bio-CLC) is a promising BECCs technology, capable of thermal conversion of biomass with net negative $CO_2$ emissions. The experimental work presented in this thesis was focused on resolving challenges to the development and implementation of biomass CLC. The primary focus was on investigating alkali-related issues in CLC. Specifically, the studies focused on determining how biomass alkalis are released in the CLC process. The alkali investigation was complemented with experimental evaluation of a new oxygen carrier materials and commissioning and evaluation of a new CLC pilot reactor. In total, four experimental CLC campaigns were conducted using three different CLC pilot systems, four different oxygen carriers, and nine different biomass fuels. A total of 70 hours of operation was conducted at CLC conditions.

A major effort for enabling investigation of alkali release in CLC pilot scale experiments was the development of a robust online alkali measurement system. This effort led to designing and constructing a surface ionization detector (SID), a sampling and dilution system, and a calibration system. Together these systems were built into a complete modular and transportable online alkali measurement system. The resulting alkali measurement system was successfully implemented in prototype form in experiments detailed in Paper I, and in completed form in experiments presented in Papers II-IV. The SID-based system was validated against an in-situ laser-based alkali measurement technique (Paper VI) and a gravimetric impactor-based alkali measurement technique (Paper V). Both validations indicated that the SID-based system has reasonable accuracy and high sensitivity to alkalis.

SID-based alkali emissions measurements for both the FR and the AR were conducted in experiments presented in Papers I-IV. Speciation of alkalis in the CLC process was investigated through capture and analysis of FR and AR flue gases with a cascade impactor sampling system. Thermodynamic modelling of alkali species formation and alkali-OC interactions were performed to augment the speciation analysis. The following key conclusions on alkali release in CLC systems were established from the work presented in Papers I-V:

- In CLC operation, majority of the gaseous alkali release occurs in the FR
- FR alkali emission are dominated with alkali chlorides and alkali hydroxides
- FR alkali emissions rise with alkali content of the virgin fuel and with operating temperature
- AR alkali emissions are lower than in the FR and do not depend on operating temperature
- AR gas-phase alkali emissions can occur due to carryover of unconverted char from the FR to the AR, and possibly by carryover of alkalis from the FR to the AR in the form of fuel ash, or through absorption of alkalis by the OC in the FR, followed by a re-release of alkalis in the AR
- Most of the fuel's KCl content is released in the FR, thus AR alkali emissions essentially KCl-free
- FR alkali emissions in CLC and CLG modes are equivalent due to the similar extent of char conversion of these two operating modes
- Alkali emissions in CLC are higher than in a comparable combustion operation (OCAC) due to enhanced decomposition of alkali salts facilitated by the steam-rich atmosphere of the FR
- Depending on the oxygen carriers used, 77-98% of fuel alkalis end up in the condensed phase within the CLC system
- Depending on the OC used, 30-98% of the fuel alkalis can be retained by the OC
- Up to 60-70% of fuel alkalis can be retained as ash, which either stays in the reactor system or is elutriated as fly ash
- CLC system performance, mainly carbon capture and gas conversion efficiency, is not constrained by alkali release behavior

The findings summarized above suggest that the general mechanisms of alkali release in CLC are similar to those in conventional combustion and gasification, but the distribution of the release within CLC's two reactor system offers some advantages in processing biomass fuels. In CLC, the majority of the process heat is extracted from the AR flue gas, where alkali emissions are low and should be almost free of KCl. Since KCl is the major cause of high temperature corrosion, but should be absent in the AR flue gas, biomass CLC systems have the potential to operate at higher steam temperatures and thus higher efficiencies than conventional biomass fluidized bed boilers. Further advantages include lower potential for bed material agglomeration due to lower availability of alkalis and Si in the bed material, as well as the ability of most OC materials to capture alkalis through formation of harmless stable alkali species. These advantages are contingent on stable long-term performance of oxygen carriers, which remains to be investigated.

The work and findings presented in this thesis and the associated publications establish a reliable methodology for investigation of alkali release in the CLC process, and outline the first comprehensive understanding of the release, retention, and effects of biomass alkalis in chemical looping combustion. Further to scientific contribution in alkali chemistry, the knowledge developed in this work contributes to the scale-up of CLC technology by identifying advantages of CLC technology in processing high-alkali biomass fuels.

# Nomenclature

| | |
|---|---|
| ***AR*** | *air reactor* |
| ***BECCS*** | *bioenergy with carbon capture and storage* |
| ***BP*** | *black pellets* |
| ***CFB*** | *circulating fluidized bed* |
| ***CLC*** | *chemical looping combustion* |
| ***CLOU*** | *chemical looping with oxygen uncoupling* |
| ***CPC*** | *condensation particle counter* |
| ***CR*** | *circulation riser* |
| ***CS*** | *carbon stripper* |
| ***D-CFB*** | *dual circulating fluidized bed* |
| ***ELIF*** | *laser induced fragmentation fluorescence* |
| ***FR*** | *fuel reactor* |
| ***GWC*** | *German wood char* |
| ***ICP-OES*** | *inductively-coupled plasma optical emission spectroscopy* |
| ***IPCC*** | *intergovernmental panel on climate change* |
| ***LLS*** | *lower loop seal* |
| ***LS*** | *loop seal* |
| ***MFC*** | *mass flow controller* |
| ***NETs*** | *negative emissions technologies* |
| ***OC*** | *oxygen carrier* |
| ***OCAC*** | *oxygen carrier aided combustion* |
| ***PFR*** | *pine forest residue* |
| ***SMPS*** | *scanning mobility particle sizer* |
| ***SPM*** | *straw pellet mixture* |
| ***SP*** | *straw pellets* |
| ***SID*** | *surface ionization detector* |
| ***SWC*** | *Swedish wood char* |
| ***TDLAS*** | *tunable diode laser absorption spectroscopy* |
| ***ULS*** | *upper loop seal* |
| ***VDC*** | *volts, direct current* |
| ***VTDMA*** | *volatility tandem mobility analysis* |
| ***WC*** | *wood char* |
| ***WP*** | *wood pellets* |

| | |
|---|---|
| $\boldsymbol{m_{oc,i}}$ | *mass of oxygen carrier in section $i$, in kg* |
| $\boldsymbol{\delta}$ | *perovskite oxygen deficiency factor* |
| $\boldsymbol{\Delta P_i}$ | *pressure drop over section $i$, in Pa* |
| $\boldsymbol{\dot{F}_{i,j}}$ | *flow of gas $i$ in section $j$, in mol/min* |
| $\boldsymbol{CI}$ | *dimensionless circulation index* |
| $\boldsymbol{\dot{Q}_{i,j}}$ | *flow of gas $i$ in section $j$, in $m^3_{normal}$/min* |
| $\boldsymbol{\eta_{oo}}$ | *oxide oxygen efficiency, in %* |
| $\boldsymbol{x_{i,j}}$ | *mole fraction of gas $i$ in reactor $j$* |
| $\boldsymbol{d}$ | *dimensionless nitrogen dilution ratio* |
| $\boldsymbol{\Omega_{OD}}$ | *oxygen demand, in %* |
| $\boldsymbol{\eta_{gas\ conv.}}$ | *gas conversion efficiency, in %* |
| $\boldsymbol{DR_j}$ | *dimensionless dilution ratio in reactor j* |
| $\boldsymbol{\Phi_o}$ | *ratio of moles of $O_2$/kg of fuel to moles of C/kg of fuel* |

# References


[1] Yongsung C, Davis SJ, Jackson RB, Lowe J, Rogner M, Kraxner F, et al. Biophysical and economic limits to negative CO2 emissions. Nat Clim Chang 2015;6:42–50. doi:10.1038/nclimate2870.

[2] H.-O. Pörtner, D.C. Roberts, M. Tignor, E.S. Poloczanska, K. Mintenbeck, A. Alegría, M. Craig, S. Langsdorf, S. Löschke, V. Möller, A. Okem BR (eds. . Climate Change 2022: Impacts, Adaptation, and Vulnerability. Contribution of Working Group II to the Sixth Assessment Report of the Intergovernmental Panel on Climate Change. Cambridge University Press; 2022.

[3] Lyngfelt A, Leckner B, Mattisson T. A fluidized-bed combustion process with inherent CO2 separation; Application of chemical-looping combustion. Chem Eng Sci 2001;56:3101–13. doi:10.1016/S0009-2509(01)00007-0.

[4] Kobayashi, N.; Fan L-S. Biomass direct chemical looping process: A perspective. Biomass and Bioenergy 2011:1252–62.

[5] Noorman S, van Sint Annaland M, Kuipers JAM. Experimental validation of packed bed chemical-looping combustion. Chem Eng Sci 2010;65:92–7. doi:10.1016/j.ces.2009.02.004.

[6] Iloeje CO, Zhao Z, Ghoniem AF. Design and techno-economic optimization of a rotary chemical looping combustion power plant with CO2 capture. Appl Energy 2018;231:1179–90. doi:10.1016/j.apenergy.2018.09.058.

[7] Mukherjee S, Kumar P, Yang A, Fennell P. Energy and exergy analysis of chemical looping combustion technology and comparison with pre-combustion and oxy-fuel combustion technologies for CO<inf>2</inf> capture. J Environ Chem Eng 2015;3:2104–14. doi:10.1016/j.jece.2015.07.018.

[8] Lyngfelt A, Leckner B. A 1000 MW th boiler for chemical-looping combustion of solid fuels – Discussion of design and costs. Appl Energy 2015;157:475–87. doi:10.1016/j.apenergy.2015.04.057.

[9] Zhu L, He Y, Li L, Wu P. Tech-economic assessment of second-generation CCS: Chemical looping combustion. Energy 2018;144:915–27. doi:10.1016/j.energy.2017.12.047.

[10] Keller M, Kaibe K, Hatano H, Otomo J. Techno-economic evaluation of BECCS via chemical looping combustion of Japanese woody biomass. Int J Greenh Gas Control 2019;83:69–82. doi:10.1016/j.ijggc.2019.01.019.

[11] Lyngfelt A, Brink A, Langørgen Ø, Mattisson T, Rydén M, Linderholm C. 11,000 h of chemical-looping combustion operation—Where are we and where do we want to go? Int J Greenh Gas Control 2019;88:38–56. doi:10.1016/j.ijggc.2019.05.023.

[12] Lyngfelt A, Linderholm C. Chemical-Looping Combustion of Solid Fuels - Status and Recent Progress. Energy Procedia 2017;114:371–86. doi:10.1016/j.egypro.2017.03.1179.

[13] Basu P. Biomass gasification, pyrolysis and torrefaction: Practical design and theory. 2018. doi:10.1016/C2016-0-04056-1.

[14] Gu H, Shen L, Xiao J, Zhang S, Song T. Chemical looping combustion of biomass/coal with natural iron ore as oxygen carrier in a continuous reactor. Energy and Fuels 2011;25:446–55. doi:10.1021/ef101318b.

[15] Gu H, Shen L, Zhong Z, Zhou Y, Liu W, Niu X, et al. Interaction between biomass ash and iron ore oxygen carrier during chemical looping combustion. Chem Eng J 2015;277:70–8. doi:10.1016/j.cej.2015.04.105.

[16] Adánez-Rubio I, Abad A, Gayán P, De Diego LF, García-Labiano F, Adánez J. Biomass combustion with CO2capture by chemical looping with oxygen uncoupling (CLOU). Fuel Process Technol 2014;124:104–14. doi:10.1016/j.fuproc.2014.02.019.

[17] Mendiara T, Abad A, de Diego LF, García-Labiano F, Gayán P, Adánez J. Biomass combustion in a CLC system using an iron ore as an oxygen carrier. Int J Greenh Gas Control 2013;19:322–30. doi:10.1016/j.ijggc.2013.09.012.

[18] Pikkarainen T, Hiltunen I. Chemical looping combustion of solid biomass–performance of ilmenite and braunite as oxygen carrier materials. 2017.

[19] Langørgen Ø, Saanum I. Chemical Looping Combustion of wood pellets in a 150 kW th CLC reactor. Proc. Int. Conf. Negat. CO2 Emiss., 2018, p. 1–10.

[20] Schmitz M, Linderholm C. Chemical looping combustion of biomass in 10- and 100-kW pilots – Analysis of conversion and lifetime using a sintered manganese ore. Fuel 2018;231:73–84. doi:10.1016/j.fuel.2018.05.071.

[21] Khan AA, de Jong W, Jansens PJ, Spliethoff H. Biomass combustion in fluidized bed boilers: Potential problems and remedies. Fuel Process Technol 2009;90:21–50. doi:10.1016/j.fuproc.2008.07.012.

[22] Zevenhoven M, Yrjas P, Hupa M. 4 Ash-Forming Matter and Ash-Related Problems n.d.

[23] Mikkanen P, Kauppinen EI, Pyykönen J, Jokiniemi JK, Aurela M, Vakkilainen EK, et al. Alkali Salt Ash Formation in Four Finnish Industrial Recovery Boilers 1999. doi:10.1021/ef980189o.

[24] Lind T, Valmari T, Kauppinen E, Nilsson K, Sfiris G, Maenhaut W. ASH formation mechanisms during combustion of wood in circulating fluidized beds. Proc Combust Inst 2000;28:2287–95. doi:10.1016/S0082-0784(00)80639-6.

[25] Lin W, Dam-Johansen K, Frandsen F. Agglomeration in bio-fuel fired fluidized bed combustors. Chem Eng J 2003;96:171–85. doi:10.1016/J.CEJ.2003.08.008.

[26] Zevenhoven-Onderwater M, Hman MO¨, Skrifvars B-J, Backman R, Nordin A, Hupa M. Bed Agglomeration Characteristics of Wood-Derived Fuels in FBC 2006. doi:10.1021/ef050349d.

[27] Hupa M, Karlström O, Vainio E. Biomass combustion technology development – It is all about chemical details. Proc Combust Inst 2017;36:113–34. doi:10.1016/J.PROCI.2016.06.152.

[28] Kleinhans U, Wieland C, Frandsen FJ, Spliethoff H. Ash formation and deposition in coal and biomass fired combustion systems: Progress and challenges in the field of ash particle sticking and rebound behavior. Prog Energy Combust Sci 2018;68:65–168. doi:10.1016/J.PECS.2018.02.001.

[29] Peters B, Smuła-Ostaszewska J. Simultaneous prediction of potassium chloride and sulphur dioxide emissions during combustion of switchgrass. Fuel 2012;96:29–42. doi:10.1016/j.fuel.2011.12.073.

[30] van Lith SC, Jensen PA, Frandsen FJ, Glarborg P. Release to the gas phase of inorganic elements during wood combustion. Part 2: Influence of fuel composition. Energy and Fuels 2008;22:1598–609. doi:10.1021/ef060613i.

[31] Cho P, Mattisson T, Lyngfelt A. Comparison of iron-, nickel-, copper- and manganese-based oxygen carriers for chemical-looping combustion. Fuel 2004;83:1215–25. doi:10.1016/j.fuel.2003.11.013.

[32] Hallberg P, Hanning M, Rydén M, Mattisson T, Lyngfelt A. International Journal of Greenhouse Gas Control Investigation of a calcium manganite as oxygen carrier during 99 h of operation of chemical-looping combustion in a 10 kW th reactor unit. Int J Greenh Gas Control 2016;53:222–9. doi:10.1016/j.ijggc.2016.08.006.

[33] Leion H, Mattisson T, Lyngfelt A. Solid fuels in chemical-looping combustion. Int J Greenh Gas Control 2008;2:180–93. doi:10.1016/S1750-5836(07)00117-X.

[34] TNO Biomass and Circular Technologies. 2020. Phyllis2, Database for (Treated) Biomass, Algae, Feedstocks for Biogas Production and Biochar. ECN Phyllis Classification. https://phyllis.nl/. n.d.

[35] Jenkins, B., Baxter, L., Miles, T. Jr., Miles T. Combustion properties of biomass, Fuel Processing Technology 54 1998:17–46.

[36] Keller M, Leion H, Mattisson T. Mechanisms of Solid Fuel Conversion by Chemical-Looping Combustion (CLC) using Manganese Ore: Catalytic Gasification by Potassium Compounds. Energy Technol 2013;1:273–82. doi:10.1002/ente.201200052.

[37] Mims CA, Pabst JK. Alkali-catalyzed carbon gasification kinetics: Unification of H2O, D2O, and CO2 reactivities. J Catal 1987;107:209–20. doi:10.1016/0021-9517(87)90286-7.

[38] Fennell P, Anthony B. Calcium and Chemical Looping Technology for Power Generation and Carbon Dioxide (CO2) Capture. Elsevier; 2015.

[39] Adánez J, De Diego LF, García-Labiano F, Gayán P, Abad A, Palacios JM. Selection of oxygen carriers for chemical-looping combustion. Energy and Fuels 2004;18:371–7. doi:10.1021/ef0301452.

[40] Johansson M, Mattisson T, Lyngfelt A. Comparison of oxygen carriers for chemical-looping combustion. Therm Sci 2006;10:93–107. doi:10.2298/tsci0603093j.

[41] Leion H, Mattisson T, Lyngfelt A. Energy Procedia Using chemical-looping with oxygen uncoupling ( CLOU ) for combustion of six different solid fuels. Energy Procedia 2009;1:447–53. doi:10.1016/j.egypro.2009.01.060.

[42] Arjmand M, Leion H, Mattisson T, Lyngfelt A. Investigation of different manganese ores as oxygen carriers in chemical- looping combustion ( CLC ) for solid fuels. Appl Energy 2014;113:1883–94. doi:10.1016/j.apenergy.2013.06.015.

[43] Sundqvist S, Khalilian N, Leion H, Mattisson T, Lyngfelt A. Manganese ores as oxygen carriers for chemical-looping combustion (CLC) and chemical-looping with oxygen uncoupling (CLOU). J Environ Chem Eng 2017;5:2552–63.

doi:10.1016/j.jece.2017.05.007.

[44] Mattisson T, Linderholm C, Jerndal E, Lyngfelt A. Enhanced performance of manganese ore as oxygen carrier for chemical-looping with oxygen uncoupling ( CLOU ) by combination with Ca ( OH ) 2 through spray-drying. Biochem Pharmacol 2016;4:3707–17. doi:10.1016/j.jece.2016.08.006.

[45] Obaidullah M, De Ruyck J, Obaidullah M, Bram S, Verma VK, De Ruyck J. A Review on Particle Emissions from Small Scale Biomass Combustion Process Integration and Intensification View project Erasmus Mundus External Cooperation Window (EMECW), European Commission View project A Review on Particle Emissions from Small Scale Bi. Int J Renew ENERGY Res M Obaidullah Al 2013;2.

[46] Johansson LS, Tullin C, Leckner B, Sjövall P. Particle emissions from biomass combustion in small combustors. Biomass and Bioenergy 2003;25:435–46. doi:10.1016/S0961-9534(03)00036-9.

[47] Valmari T, Kauppinen EI, Kurkela J, Jokiniemi JK, Sfiris G, Revitzer H. Fly ash formation and deposition during fluidized bed combustion of willow. J Aerosol Sci 1998;29:445–59. doi:10.1016/S0021-8502(97)10021-0.

[48] Wellinger M, Biollaz S, Wochele J, Ludwig C. Sampling and online analysis of alkalis in thermal process gases with a novel surface ionization detector. Energy and Fuels 2011;25:4163–71. doi:10.1021/ef200811q.

[49] Backman R, Skrifvars B-J, Nordin A, Öhman M, Hupa M. Bed Agglomeration Characteristics during Fluidized Bed Combustion of Biomass Fuels. Energy & Fuels 2002;14:169–78. doi:10.1021/ef990107b.

[50] Knudsen JN, Jensen PA, Dam-Johansen K. Transformation and release to the gas phase of Cl, K, and S during combustion of annual biomass. Energy and Fuels 2004;18:1385–99. doi:10.1021/ef049944q.

[51] Davidsson KO, Korsgren JG, Pettersson JBC, Jäglid U. The effects of fuel washing techniques on alkali release from biomass. Fuel 2002;81:137–42. doi:10.1016/S0016-2361(01)00132-6.

[52] Werkelin J, Skrifvars BJ, Zevenhoven M, Holmbom B, Hupa M. Chemical forms of ash-forming elements in woody biomass fuels. Fuel 2010;89:481–93. doi:10.1016/J.FUEL.2009.09.005.

[53] Vassilev S V., Baxter D, Andersen LK, Vassileva CG, Morgan TJ. An overview of the organic and inorganic phase composition of biomass. Fuel 2012;94:1–33. doi:10.1016/J.FUEL.2011.09.030.

[54] Vassilev S V., Baxter D, Andersen LK, Vassileva CG. An overview of the chemical composition of biomass. Fuel 2010;89:913–33. doi:10.1016/J.FUEL.2009.10.022.

[55] Westberg HM, Byström M, Leckner B. Distribution of Potassium, Chlorine, and Sulfur between Solid and Vapor Phases during Combustion of Wood Chips and Coal 2003. doi:10.1021/ef020060l.

[56] Jones JM, Darvell LI, Bridgeman TG, Pourkashanian M, Williams A. An investigation of the thermal and catalytic behaviour of potassium in biomass combustion. Proc Combust Inst 2007;31:1955–63. doi:10.1016/J.PROCI.2006.07.093.

[57] Boström D, Skoglund N, Grimm A, Boman C, Öhman M, Broström M, et al. Ash transformation chemistry during combustion of biomass. Energy and Fuels 2012;26:85–93. doi:10.1021/ef201205b.

[58] Fatehi H, He Y, Wang Z, Li ZS, Bai XS, Aldén M, et al. LIBS measurements and numerical studies of potassium release during biomass gasification. Proc Combust Inst 2015;35:2389–96. doi:10.1016/J.PROCI.2014.06.115.

[59] Johansen JM, Jakobsen JG, Frandsen FJ, Glarborg P. Release of K, Cl, and S during pyrolysis and combustion of high-chlorine biomass. Energy and Fuels 2011;25:4961–71. doi:10.1021/ef201098n.

[60] Johansen JM, Aho M, Paakkinen K, Taipale R, Egsgaard H, Jakobsen JG, et al. Release of K, Cl, and S during combustion and co-combustion with wood of high-chlorine biomass in bench and pilot scale fuel beds. Proc Combust Inst 2013;34:2363–72. doi:10.1016/J.PROCI.2012.07.025.

[61] Jensen PA, Frandsen FJ, Dam-Johansen K, Sander B. Experimental Investigation of the Transformation and Release to Gas Phase of Potassium and Chlorine during Straw Pyrolysis 2000. doi:10.1021/ef000104v.

[62] Wiinikka H, Grönberg C, Öhrman O, Boström D. Influence of TiO2 additive on vaporization of potassium during straw combustion. Energy and Fuels 2009;23:5367–74. doi:10.1021/ef900544z.

[63] Cao W, Li J, Lin L, Zhang X. Release of potassium in association with structural evolution during biomass combustion. Fuel 2021;287:119524. doi:10.1016/J.FUEL.2020.119524.

[64] Tchoffor PA, Davidsson KO, Thunman H. Transformation and Release of Potassium, Chlorine, and Sulfur from Wheat Straw under Conditions Relevant to Dual Fluidized Bed Gasification 2013. doi:10.1021/ef401703a.

[65] Johansen JM, Jakobsen JG, Frandsen FJ, Glarborg P. Release of K, Cl, and S during Pyrolysis and Combustion of High-Chlorine Biomass. Energy and Fuels 2011;25:4961–71. doi:10.1021/EF201098N.

[66] Fatehi H, Costa M, Bai XS. Numerical study on K/S/Cl release during devolatilization of pulverized biomass at high temperature. Proc Combust Inst 2021;38:3909–17. doi:10.1016/J.PROCI.2020.06.079.

[67] Eriksson J-E;, Zevenhoven M;, Yrjas P;, Brink A;, Hupa L, Eriksson J-E, et al. Corrosion of Heat Transfer Materials by Potassium-Contaminated Ilmenite Bed Particles in Chemical-Looping Combustion of Biomass. Energies 2022, Vol 15, Page 2740 2022;15:2740. doi:10.3390/EN15082740.

[68] Glazer MP, Khan NA, de Jong W, Spliethoff H, Schürmann H, Monkhouse P. Alkali Metals in Circulating Fluidized Bed Combustion of Biomass and Coal: Measurements and Chemical Equilibrium Analysis. Energy and Fuels 2005;19:1889–97. doi:10.1021/EF0500336.

[69] Davidsson KO, Elled A-L, Eskilsson D, Leckner B, Åmand L-E, Steenari B-M. Countermeasures against alkali-related problems during combustion of biomass in a circulating fluidized bed boiler. Chem Eng Sci 2008;63:5314–29. doi:10.1016/j.ces.2008.07.012.

[70] Gu H, Shen L, Xiao J, Zhang S, Song T. Chemical looping combustion of biomass/coal with natural iron ore as oxygen carrier in a continuous reactor. Energy and Fuels 2011;25:446–55. doi:10.1021/ef101318b.

[71] Corcoran A, Marinkovic J, Lind F, Thunman H, Knutsson P, Seemann M. Ash properties of ilmenite used as bed material for combustion of biomass in a circulating fluidized bed boiler. Energy and Fuels 2014;28:7672–9. doi:10.1021/ef501810u.

[72] Pushp M, Gall D, Davidsson K, Seemann M, Pettersson JBC. Influence of Bed Material, Additives, and Operational Conditions on Alkali Metal and Tar Concentrations in Fluidized Bed Gasification of Biomass. Energy and Fuels 2018;32:6797–806. doi:10.1021/acs.energyfuels.8b00159.

[73] Mattisson T, Keller M, Linderholm C, Moldenhauer P, Rydén M, Leion H, et al. Chemical-looping technologies using circulating fluidized bed systems: Status of development. Fuel Process Technol 2018;172:1–12. doi:10.1016/J.FUPROC.2017.11.016.

[74] Zhao X, Zhou H, Sikarwar VS, Zhao M, Park A-HA, Fennell PS, et al. Biomass-based chemical looping technologies: the good, the bad and the future. Energy Environ Sci 2017;10:1885–910. doi:10.1039/C6EE03718F.

[75] Markström P, Linderholm C, Lyngfelt A. Chemical-looping combustion of solid fuels - Design and operation of a 100kW unit with bituminous coal. Int J Greenh Gas Control 2013;15:150–62. doi:10.1016/j.ijggc.2013.01.048.

[76] Gogolev I, Linderholm C, Gall D, Schmitz M, Mattisson T, Pettersson JBC, et al. Chemical-looping combustion in a 100 kW unit using a mixture of synthetic and natural oxygen carriers – Operational results and fate of biomass fuel alkali. Int J Greenh Gas Control 2019;88:371–82. doi:10.1016/j.ijggc.2019.06.020.

[77] Gogolev I, Soleimanisalim AH, Linderholm C, Lyngfelt A. Commissioning, performance benchmarking, and investigation of alkali emissions in a 10 kWth solid fuel chemical looping combustion pilot. Fuel 2021;287:119530. doi:10.1016/j.fuel.2020.119530.

[78] Gogolev I, Pikkarainen T, Kauppinen J, Linderholm C, Steenari BM, Lyngfelt A. Investigation of biomass alkali release in a dual circulating fluidized bed chemical looping combustion system. Fuel 2021;297:120743. doi:10.1016/j.fuel.2021.120743.

[79] Erbel C, Mayerhofer M, Monkhouse P, Gaderer M, Spliethoff H. Continuous in situ measurements of alkali species in the gasification of biomass. Proc Combust Inst 2013;34:2331–8. doi:10.1016/j.proci.2012.06.037.

[80] Sepman A, Ögren Y, Qu Z, Wiinikka H, Schmidt FM. Real-time in situ multi-parameter TDLAS sensing in the reactor core of an entrained-flow biomass gasifier. Proc Combust Inst 2017;36:4541–8. doi:10.1016/j.proci.2016.07.011.

[81] Zhang Z, Liu J, Shen F, Yang Y, Liu F. On-line measurement and kinetic studies of sodium release during biomass gasification and pyrolysis. Fuel 2016;178:202–8. doi:10.1016/j.fuel.2016.03.067.

[82] Porbatzki D, Stemmler M, Müller M. Release of inorganic trace elements during gasification of wood, straw, and miscanthus. Biomass and Bioenergy 2011;35:S79–86. doi:10.1016/j.biombioe.2011.04.001.

[83] Gall D, Pushp M, Davidsson KO, Pettersson JBC. Online Measurements of Alkali and

Heavy Tar Components in Biomass Gasification. Energy and Fuels 2017;31:8152–61. doi:10.1021/acs.energyfuels.7b00474.

[84] Jäglid U, Olsson JG, Pettersson JBC. Detection of sodium and potassium salt particles using surface ionization at atmospheric pressure. J Aerosol Sci 1996;27:967–77. doi:10.1016/0021-8502(96)00025-0.

[85] Kent O. Davidsson, Klas Engvall †, Magnus Hagström, John G. Korsgren ‡, Benny Lönn and, Pettersson* JBC. A Surface Ionization Instrument for On-Line Measurements of Alkali Metal Components in Combustion: Instrument Description and Applications. Energy and Fuels 2002;16:1369–77. doi:10.1021/EF020020H.

[86] Hedayati A, Sefidari H, Boman C, Skoglund N, Kienzl N, Öhman M. Ash transformation during single-pellet gasification of agricultural biomass with focus on potassium and phosphorus. Fuel Process Technol 2021;217:106805. doi:10.1016/J.FUPROC.2021.106805.

[87] Gall D, Viljanen J, Gogolev I, Allgurén T, Andersson K. Alkali Monitoring of Industrial Process Gas by Surface Ionization–Calibration, Assessment, and Comparison to In Situ Laser Diagnostics. Energy & Fuels 2021;35:20160–71. doi:10.1021/ACS.ENERGYFUELS.1C03205.

[88] Gogolev I, Soleimanisalim AH, Mei D, Lyngfelt A. Effects of Temperature, Operation Mode, and Steam Concentration on Alkali Release in Chemical Looping Conversion of Biomass–Experimental Investigation in a 10 kWth Pilot. Energy & Fuels 2022:acs.energyfuels.1c04353. doi:10.1021/ACS.ENERGYFUELS.1C04353.

[89] Zhang ZH, Song Q, Yao Q, Yang RM. Influence of the Atmosphere on the Transformation of Alkali and Alkaline Earth Metallic Species during Rice Straw Thermal Conversion. Energy and Fuels 2012;26:1892–9. doi:10.1021/EF2011645.

[90] Zhao HB, Xu WT, Song Q, Zhuo JK, Yao Q. Effect of Steam and SiO2 on the Release and Transformation of K2CO3 and KCl during Biomass Thermal Conversion. Energy & Fuels 2018;32:9633–9. doi:10.1021/ACS.ENERGYFUELS.8B02269.

[91] Gogolev I, Pikkarainen T, Kauppinen J, Hurskainen M, Lyngfelt A. Alkali emissions characterization in chemical looping combustion of wood, wood char, and straw fuels. Fuel Process Technol 2022;237:107447. doi:10.1016/J.FUPROC.2022.107447.

[92] Linderholm C, Schmitz M, Biermann M, Hanning M, Lyngfelt A. Chemical-looping combustion of solid fuel in a 100 kW unit using sintered manganese ore as oxygen carrier. Int J Greenh Gas Control 2017;65:170–81. doi:10.1016/J.IJGGC.2017.07.017.

[93] Corcoran A, Knutsson P, Lind F, Thunman H. Mechanism for Migration and Layer Growth of Biomass Ash on Ilmenite Used for Oxygen Carrier Aided Combustion. Energy & Fuels 2018;32:8845–56. doi:10.1021/acs.energyfuels.8b01888.

[94] Störner F, Hildor F, Leion H, Zevenhoven M, Hupa L, Rydén M. Potassium Ash Interactions with Oxygen Carriers Steel Converter Slag and Iron Mill Scale in Chemical-Looping Combustion of Biomass—Experimental Evaluation Using Model Compounds. Energy & Fuels 2020;34:2304–14. doi:10.1021/ACS.ENERGYFUELS.9B03616.

[95] Abad A, Adánez J, Cuadrat A, García-Labiano F, Gayán P, de Diego LF. Kinetics of redox reactions of ilmenite for chemical-looping combustion. Chem Eng Sci 2011;66:689–702.

doi:10.1016/j.ces.2010.11.010.

[96] Abad A, García-Labiano F, de Diego LF, Gayán P, Adánez J. Reduction kinetics of Cu-, Ni-, and Fe-based oxygen carriers using syngas (CO + H2) for chemical-looping combustion. Energy and Fuels 2007;21:1843–53. doi:10.1021/EF070025K/ASSET/IMAGES/LARGE/EF070025KF00008.JPEG.

[97] Lin L, Liu D, Jin J, Cheng Q, Li W, Feng L. High Iron and Calcium Coal Ash As the Oxygen Carrier for Chemical Looping Combustion 2018. doi:10.1021/acs.iecr.8b01646.

[98] van Lith SC, Alonso-Ramírez V, Jensen PA, Frandsen FJ, Glarborg P. Release to the gas phase of inorganic elements during wood combustion. Part 1: Development and evaluation of quantification methods. Energy and Fuels 2006;20:964–78. doi:10.1021/ef050131r.

[99] Davidsson KO, Stojkova BJ, Pettersson JBC. Alkali emission from birchwood particles during rapid pyrolysis. Energy and Fuels 2002;16:1033–9. doi:10.1021/EF010257Y/ASSET/IMAGES/LARGE/EF010257YF00012.JPEG.

[100] Staničić I, Hanning M, Deniz R, Mattisson T, Backman R, Leion H. Interaction of oxygen carriers with common biomass ash components. Fuel Process Technol 2020;200:106313. doi:10.1016/J.FUPROC.2019.106313.

[101] Henrik Leion, Pavleta Knutsson B-MS. Experimental Evaluation of Interactions between K, Ca, And P And Mn/Si-Based Oxygen Carriers. Eur. Biomass Conf. Exhib. Proc. Vol. 2017, Issue 25th EUBCE, June 2017, 2017, p. 660–5.

[102] Lyngfelt A, Pallarès D, Linderholm C, Lind F, Thunman H, Leckner B. Achieving Adequate Circulation in Chemical Looping Combustion–Design Proposal for a 200 MWth Chemical Looping Combustion Circulating Fluidized Bed Boiler. Energy and Fuels 2021. doi:10.1021/ACS.ENERGYFUELS.1C03615/ASSET/IMAGES/LARGE/EF1C03615_0023.JPEG.

[103] Gyllén A, Knutsson P, Lind F, Thunman H. Magnetic separation of ilmenite used as oxygen carrier during combustion of biomass and the effect of ash layer buildup on its activity and mechanical strength. Fuel 2020;269:117470. doi:10.1016/J.FUEL.2020.117470.